NASA Technical Memorandum 81872

NASA-TM-81872 19800024834

CONCEPTUAL STUDY OF AN ADVANCED SUPERSONIC TECHNOLOGY TRANSPORT (AST-107) FOR TRANSPACIFIC RANGE USING LOW-BYPASS-RATIO TURBOFAN ENGINES

Shelby J. Morris, Jr., Willard E. Foss, Jr.
and Milton J. Neubauer, Jr.

September 1980

NASA
National Aeronautics and
Space Administration

Langley Research Center
Hampton, Virginia 23665

CONCEPTUAL STUDY OF AN ADVANCED SUPERSONIC TECHNOLOGY TRANSPORT (AST-107) FOR TRANSPACIFIC RANGE USING LOW-BYPASS-RATIO TURBOFAN ENGINES

By

Shelby J. Morris, Jr.; Willard E. Foss, Jr.;
and Milton J. Neubauer, Jr.

NASA Langley Research Center
Hampton, Virginia 23665

SUMMARY

A new advanced supersonic technology configuration concept designated the AST-107, using a low bypass-ratio-turbofan engine, is described and analyzed. The aircraft had provisions for 273 passengers arranged five abreast. The cruise Mach number was 2.62. The mission range for the AST-107 was 8.48 Mm (4576 n.mi.) and an average lift-drag ratio of 9.15 during cruise was achieved. The available lateral control was not sufficient for the required 15.4 m/s (30 kt) crosswind landing condition, and a crosswind landing gear or a significant reduction in dihedral effect would be necessary to meet this requirement. The lowest computed noise levels, including a mechanical suppressor noise reduction of 3 EPNdB at the flyover and sideline monitoring stations, were 110.3 EPNdB (sideline noise), 113.1 EPNdB (centerline noise) and 110.5 EPNdB (approach noise).

INTRODUCTION

Technology advances since 1972 have prompted several advanced supersonic technology vehicle integration studies (for example, refs. 1-3). Subsequent to these studies, a number of significant advances have occurred. These advances include the development of an expanded aerodynamic data base covering low-speed trim, longitudinal stability, and control (ref. 4) and low-speed lateral-directional stability and control (ref. 5); the development of techniques to size the wing area and thrust-weight ratio of supersonic cruise aircraft for optimum performance (ref. 6); and the development of techniques to compute airport noise for these configurations (refs. 7 and 8).

The objective of the present study is to apply this new technology to the conceptual design of an advanced supersonic transport for transpacific range (comparable to a San Francisco-Tokyo flight), and, then, to subject the concept to the latest analytical techniques for performance, noise, and economic evaluations. In addition, this detailed systems integration study has been used to support a recent noise-sensitivity study (ref. 9) by providing the system weight and performance used therein.

The configuration described in this report is very similar to that reported in reference 1 except for different engines. The engine used was a low-bypass-ratio turbofan incorporating both a mechanical suppressor in the outer exhaust jet and an inverted jet-velocity profile for coannular noise reduction. The

basic criteria used in this study are: the use of five abreast seating of 273 passengers in an all-tourist-class seating arrangement with a seat pitch of 0.864 m (34 in.); a range of 8.33 Mm (4500 n.mi.) at a cruise Mach number of 2.62 (8C above standard-day atmosphere); the ability to land and takeoff on existing runways with a tire footprint no greater than that of a DC-8-50; stability sufficient to trim for minimum trim-drag throughout the flight envelope with no significant pitch-up in the takeoff or landing modes; and satisfactory short-period characteristics at approach.

SYMBOLS

Computations in the course of this study were performed in U.S. Customary Units. Results were converted to the International System of Units (SI) by using conversion factors given in reference 10.

A	aspect ratio
b	wing span, m (ft)
$\bar{c}$	mean aerodynamic chord, m (ft)
$\bar{c}_{ref}$	reference mean aerodynamic chord, m (ft)
c.g.	center of gravity
C_D	drag coefficient, $\frac{\text{drag}}{qS}$
$C_{D_{p_o}}$	parasite drag coefficient associated with camber, protuberances, interference, and separated flow
C_{D_w}	wave-drag coefficient
C_L	lift coefficient, $\frac{\text{lift}}{qS}$
C_ℓ	rolling moment, $\frac{\text{rolling moment}}{qSb}$
C_{ℓ_β}	rolling moment coefficient due to sideslip, per degree
C_m	pitching moment coefficient, $\frac{\text{pitching moment}}{qSc}$
C_n	yawing moment coefficient, $\frac{\text{yawing moment}}{qSb}$

C_{n_β}	yawing moment coefficient due to sideslip, per degree
C_{Y_β}	side force coefficient due to sideslip, per degree
DOC	direct operating cost, cents/passenger km (cents/passenger statute mile)
EPNL	effective perceived noise level, EPNdB
g	acceleration due to gravity, m/s^2 (ft/s^2)
h	altitude, m (ft)
HSAS	hardened stability augmentation system
I_X, I_Y, I_Z	moments of inertia about X, Y, and Z body axes, respectively, $kg\text{-}m^2$ ($slug\text{-}ft^2$)
I_{XZ}	product of inertia, $kg\text{-}m^2$ ($slug\text{-}ft^2$)
K_1	directional-control flexibility factor
L_α	lift per unit angle of attack per unit momentum (qs/aircraft momentum) $\frac{\partial C_L}{\partial \alpha}$, per second
L/D	lift-drag ratio
M	Mach number
n	load factor
P	pressure, Pa (lbf/ft^2)
P_{sp}	period of longitudinal short-period oscillation, s
P_d	period of Dutch roll oscillation
PR	pilot rating
P_{ph}	period of longitudinal phugoid oscillation
q	dynamic pressure, Pa (lbf/ft^2)
S	wing area, m^2 (ft^2)
S_{ref}	wing reference area, m^2 (ft^2)
S_{an}	static normal acceleration gust sensitivity, g/(m/s), (g/(ft/s)
SCAS	stability and control augmentation system

t_2	time to double amplitude, s
$t_{1/2}$	time to damp to one-half amplitude, s
$t_{\phi=30^o}$	time required to roll 30^o, s
TOC	total operating cost, cents/seat km (cents/seat statute mile)
V	airspeed, m/s (ft/s)
V_1	aircraft velocity at engine failure for balanced field length, m/s (ft/s)
V_2	aircraft velocity at obstacle, m/s (ft/s)
V_R	aircraft velocity at rotation, m/s (ft/sec)
$\overline{V}$	tail-volume coefficient
x	longitudinal coordinate, m (ft)
y	lateral coordinate, m (ft)
z	vertical coordinate, m (ft)
α	angle of attack (deg or rad, as noted)
α_{wrp}	angle of attack of wing reference plane, deg
β	angle of sideslip, deg
ΔP_{max}	maximum sonic boom overpressure, Pa (lbf/ft^2)
δ_a	aileron deflection, positive for right-roll command, deg
δ_i	deflection of ith flap (see fig. 6 for definition of i) deg
δ_r	rudder deflection, deg
δ_t	horizontal-tail deflection, positive when leading-edge is deflected up, deg
$\dot{\delta}_a$	aileron deflection rate, positive for right-roll command, deg/s

$\dot{\delta}$	aileron deflection rate, positive for right-roll command, deg/s
$\dot{\delta}_i$	deflection rate of ith flap (see fig. 6 for definition of i), deg/s
$\dot{\delta}_r$	rudder deflection rate, deg/s
$\dot{\delta}_t$	horizontal tail deflection rate, positive when leading-edge is deflected up, deg/s
ζ_d	Dutch roll damping ratio
ζ_{ph}	longitudinal phugoid mode damping ratio
ζ_{sp}	longitudinal short-period mode damping ratio
ζ_ϕ	damping ratio of numerator quadratic of a transfer function
θ	pitch angle, deg
$\dot{\theta}$	pitch rate, deg/s
$\ddot{\theta}$	pitch acceleration, rad/s^2
ϕ	roll angle, deg
$\dot{\phi}$	roll rate, deg/s
$\dot{\phi}_1$, $\dot{\phi}_2$	rolling angular velocities at the first and second peaks of a roll rate oscillation, deg/s
$\ddot{\phi}$	roll acceleration, rad/s^2
ψ	yaw angle, deg
$\dot{\psi}$	yaw rate, deg/s
$\ddot{\psi}$	yaw acceleration, rad/s^2
τ_R	time constant of roll mode, s
ω_d	undamped natural frequency of Dutch roll mode, rad/s

ω_{sp} longitudinal short-period undamped natural frequency, rad/s

ω_{ph} undamped natural frequency of phugoid mode, rad/s

ω_{ϕ} undamped natural frequency appearing in numerator quadratic of ϕ/δ_a transfer function, rad/s

Subscripts:

app	approach
c.g.	center of gravity
elastic	elastic airplane
f	friction
LG	landing gear
max	maximum
min	minimum
r	roughness
rigid	rigid airplane
req	required
ss	steady state
trim	trimmed condition

RESULTS AND DISCUSSION

CONFIGURATION

The present AST-107 (fig. 1) is geometrically similar to the concept of reference 1. Geometric characteristics are defined in Table I. The fuselage length is 92.96 m (305 ft) with provisions for 273 passengers arranged five abreast at 0.86 m (34 in.) pitch. Passenger baggage and cargo volume is provided under the floor forward of the wing structural box. Figure 2 shows the inboard profile of the configuration. Fuel tanks are located in the wing, under the fuselage floor in the center-wing carry-through structure, and in the rear of the fuselage. The fuselage tank provides for aircraft balance control and fuel reserve. The tank arrangement and capacities are shown in figure 3.

The arrow-wing planform is retained from the configuration of reference 1; however, the wing area was modified to obtain a wing loading of 4.07 kPA (85 psf) at a design gross weight of 3.15 MN (709,000 lbm). The wing thickness-ratio varies from approximately 3 percent at the root to 2.5 percent at the tip

(fig. 4). Contours of wing thickness are shown in figure 5. Wing control surfaces (fig. 6) are geometrically similar to those of reference 1 except for adjustments for the difference in wing area.

The aircraft is powered by four General Electric GE21/J10-B5 low bypass-ratio turbofan engines. The nacelle shape is based on a Boeing configuration sized to the appropriate engine thrust level. The inlet used is a mixed compression axisymmetric design designated as the NASA "P" Inlet. The nacelles are mounted under the wing at the trailing edge with the nozzles and thrust reversers sufficiently rearward to provide for clearance.

The main landing gear is a two-strut arrangement with 12 wheels per strut and retracts forward into the wing. Wheels are 0.80 m x 0.28 m size with the appropriate ply rating to satisfy the equivalent single-wheel load and the 0.61 m (24 in.) flexible pavement thickness flotation criteria. The strut location provides for a 13^{o} flare angle from the static ground line and a 14.5^{o} flare angle with the gear fully extended. These flare angles provide a maximum of 0.30 m (12 in.) clearance for the engine nacelle, wing tip, and horizontal tail under normal takeoff-and-landing conditions.

The nose landing gear is a single-strut, two-wheel arrangement and retracts rearward into the fuselage. Wheel size is 0.69 m x 0.19 m at the required ply rating to satisfy loading and floatation requirements.

Flight crew provisions and the visor nose are the same as those in reference 1. With the visor nose in the downward position, sufficient clearance is available for a ground handling tractor.

The normal area distribution of the AST-107 is presented in figure 7. The utilization of aircraft volume for subsystem and accommodations is also shown in this figure.

AERODYNAMIC CHARACTERISTICS

Low Speed

The low speed aerodynamic characteristics are based on the wind tunnel data of reference 4. Since the data of reference 4 are unaffected by Reynolds number above that achieved at tunnel dynamic pressures of approximately 527 Pa (11 lbf/ft^2), the data for these higher Reynolds number were used directly. The friction drag from the wind tunnel tests was adjusted to full scale using the Somers and Short T' method (ref. 11) assuming flat-plate fully turbulent boundary-layer flow. Form drag corrections, which depend on thickness-chord ratio for surfaces and the fineness ratio for bodies, were applied. An additional three percent of friction drag was added for roughness, and 5 percent of friction drag was added for gaps and irregularities. Trim drag was obtained from reference 4 with appropriate corrections for tail-size and wing-reference-area differences. Flap increments to lift and drag were obtained from reference 4. The landing-gear drag coefficient increments (ref. 12) are shown in figure 8. Ground effect was estimated using the procedure of reference 2. The resulting lift curves and drag polars are shown in figures 9 and 10. The corresponding lift-drag ratios are shown in figure 11.

High Speed

Method of analysis - The procedure used to establish the high-speed drag values parallels the techniques used in references 1, 2, and 3. The common data base used for each of those analyses was also used for the present configuration. The drag buildup consists of computing the wave drag, skin friction and roughness drag, and parasite drag; each at zero lift, and then adding the induced drag and the trim drag (for the appropriate lift coefficient and pitching moment) to this value.

Wave drag - Zero-lift wave drag coefficients for the AST-107 were computed using the supersonic area-rule technique of reference 13. The Mach 2.62 equivalent area distributions developed by the area rule for both the fuselage and complete configuration are shown in figure 12. Wave drag as a function of Mach number for the overall configuration is presented in figure 13.

Skin friction and roughness drag - Skin friction drag has been computed using the T' method described in reference 11. The friction drag for a given Mach number-altitude combination was computed by representing the various configuration components as appropriate wetted areas and reference lengths. Smooth flat-plate, adiabatic wall, fully turbulent boundary layer conditions were assumed. Configuration components such as the wing or tail, which may exhibit significant variations in reference lengths, were further subdivided into strips for a more accurate determination of the friction drag. In addition to the skin friction drag, a separation-drag component was estimated for subsonic Mach numbers using an empirical method (ref. 14). A subsonic form-drag factor relating the skin friction on an airfoil or fusiform body to the flat plate skin friction was determined for each configuration component and used to obtain the subsonic form drag.

The configuration roughness-drag increment was assumed to be 6 percent of the friction drag for the Mach 2.62 cruise condition. For other Mach numbers, the ratios of roughness drag to skin friction previously developed in reference 2 were used.

A summary of the configuration wetted areas is presented is Table II. Skin friction and roughness-drag coefficients are shown in figure 14 as a function of Mach number. The altitude corresponding to each Mach number is defined by the nominal climb schedule of the aircraft.

Parasite drag - The parasite drag coefficient was derived from the analysis of reference 2 and is shown in figure 15. Parasite drag includes camber drag, interference drag, excrescences, locally separated flow, and other miscellaneous zero-lift drag contributions.

Trim drag - The incremental drag-due-to-lift values for the AST-107 horizontal tail were obtained by correcting the values of reference 1 for differences in wing and tail areas. These prior results were obtained from a detailed analysis of the horizontal-tail incidence required for maximum configuration performance.

Total drag - The various drag components discussed above were combined to obtain the overall drag characteristics of the AST-107. Figure 16 presents the

variation in minimum drag coefficient across the Mach number range. Figure 17 presents typical polars at Mach numbers of 0.6, 1.2, and 2.62. Figure 18 presents $(L/D)_{max}$ as a function of Mach number.

PROPULSION

Engine

A General Electric advanced, augmented, low bypass-ratio turbofan engine, GE21/J10-B5, was selected for this study. This engine was designed for cruise at a Mach number of 2.55 and an altitude of 18.3 km (60,000 ft) on a standard day. For the present study, the engine was sized to meet a sea-level-static installed thrust-weight ratio of 0.268 at temperatures 8C above standard. The resulting sea-level-static maximum airflow was 298.4 kg (657.8 lbm). The General Electric GE21/J10-B5 has a sea-level-static dry thrust of 211 kN (47,504 lbf). The engine has a design overall pressure ratio of 16.3 and a bypass ratio of 0.30. The technology required for this engine is projected to be available in 1985. The engine has a low-temperature (1,533 K) augmentor. The exhaust system consists of an annular, translating, plug nozzle with a thrust reverser and a mechanical sound suppressor installed in the outer stream of the nozzle. The mechanical sound suppressor furnishes an estimated incremental noise suppression of 3 EPNdB at maximum power and is assumed to weigh 2.22 kN (500 lbf) per engine.

The engine weight was determined by scaling the baseline-engine weight as the 1.2 power of thrust. The length and diameter of the engine was assumed to scale as the square root the thrust. The external configuration and envelope of the engine are shown in figure 19. The weight of the engine is 55.55 kN (11,590 lbf) including the engine, nozzle, thrust reverser, and mechanical noise suppressor.

Nacelle and Inlet

The nacelle housing the scaled GE21/J10-B5 engine is shown in figure 20. The fixed downward cant of the nozzle (8^{o}) is provided so that the thrust line of the engine will pass through the airplane rearmost center-of-gravity during takeoff and landing conditions. Location of the nacelles on the aircraft is shown schematically in figure 21.

The inlet is the NASA-Ames "P" inlet (ref. 15). It is a axisymmetric, mixed compression design with a translating centerbody sized for supersonic cruise conditions. Allowance was made in the inlet design to provide 2 percent of the inlet-system airflow for nacelle cooling and ventilation. Inlet performance is presented in figure 22.

Performance

The installed engine performance is based on the 1962 U.S. standard atmosphere using the inlet total-pressure recovery of reference 15 and a fuel lower heating value of 42.8 MJ/kg (18,400 BTU/lbm). An engine bleed of 0.906 kg/s (2 lbm/s) per engine below 6.1 km (20,000 ft) and 0.459 kg/sec (1 lbm/s) per engine above 6.1 km (20,000 ft) was used to account for required cooling air. A power extraction of 149 kW (200 HP) per engine was also included.

The installed engine performance presented in this report includes the effect of inlet pressure recovery, compressor bleed air, power extraction, the nozzle velocity coefficient (with the mechanical noise suppressor), as well as boattail drag from the engine nozzle-nacelle connection point rearward (stations D through G of figure 20). At all engine operating conditions, engine performance has also been corrected for the effects of inlet spillage, bleed, and bypass drag. The nacelle skin friction, interference, and wave drags are accounted for in the aircraft drag polars. The resulting engine performance data for maximum climb, maximum cruise, and part-power throttle setting is shown in figure 23 through 25.

Mechanical Noise Suppressor

The mechanical noise suppressor used on the AST-107 is a 40 shallow-chute outer-stream design which is assumed to weigh an additional 2.22 kN (500 lbf) per engine and to supply 3 EPNdB of noise suppression at the sideline and fly-over noise stations. The nozzle velocity coefficient was estimated to be 0.92 when the suppressor was deployed because of the flow losses associated with the suppressor.

MASS CHARACTERISTICS

Method of Analysis

Configuration selection and sizing of the AST-107 was accomplished through the use of the techniques described in reference 6 and in accordance with the mission requirements specified in section entitled "Mission Analysis." The mass-properties prediction technique of reference 6 is based on data from previous similar configurations and shows good correlation with data generated by airframe manufacturers.

The sizing and configuration selection was performed within the computer program of reference 6 by producing a matrix of conceptual aircraft with an array of design gross weights ranging from 3.05 to 3.67 MN (685,000 to 825,000 lbf); with sea-level installed thrust-weight ratio varying from 0.20 to 0.44; and wing loading varying from 3.4 to 4.8 kPa (70 to 100 lbf/ft^2). These conceptual aircraft were then subjected to mission performance evaluations. The results of the evaluation were used to generate plots referred to as "thumbprints" (fig. 26). The aircraft configuration selected for more detailed analysis has a design gross weight of 3.15 MN (709,000 lbf), a wing loading of 4.07 kPa (85 lbf/ft^2), and a sea-level-static thrust-weight ratio of 0.268.

The aircraft primary structure was assumed to be all titanium. Special design features included: stressed-skin titanium skin and core sandwich for all wing and other aerodynamic surfaces; skin, stringer, and frame fuselage construction of titanium; and landing gear of high-strength steel-alloy construction.

Weight and Balance

After the design gross weight, wing loading, and aircraft thrust-weight ratio were determined, an estimate of the weight and location of the different aircraft components was made using data from previous designs and the standard scaling techniques described in reference 6. The result of this analysis is presented in Table III.

The aircraft components were located, their individual weights were estimated, and an analysis of the balance characteristics of the aircraft was made. The desired center-of-gravity limits for this aircraft, as determined in a later section of this paper (Stability and Control), were a forward center-of-gravity limit of 42.55 percent of $\bar{c}_{ref}$ and an rearward limit of 60.01 percent of $\bar{c}_{ref}$. For minimum trim drag, it was desirable to maintain the center of gravity at about 50 percent $\bar{c}_{ref}$..

Combinations of different fuel usage and fuel-transfer sequencing were investigated to determine attainable center-of-gravity boundaries. These boundaries, together with the desired center-of-gravity trace during a typical mission, are presented in figure 27. It was determined that, if the wing apex was located at fuselage station 15.24 m (50 ft), all points along the center-of-gravity path would lie within the required boundaries, provided that proper fuel management was utilized. It should be noted that the attainable rearward center-of-gravity exceeds the stability limit defined by 60.1 percent $\bar{c}_{ref}$. For center-of-gravity locations behind this point, the aircraft would not stable with the current tail size.

Inertial Characteristics

Inertial characteristics were computed for maximum gross weight and for normal landing weight. The inertias of the individual components were computed about their respective centroids and then translated to the aircraft's center-of-gravity location for both conditions. The inertia information is summarized in Table IV.

STABILITY AND CONTROL

Requirements

Longitudinal - The requirements for longitudinal stability and control during takeoff were that the forward center-of-gravity limits should be set at the position of neutral stability, and the center-of-gravity range during takeoff should be at least 66 cm (26 in.). It was also required that the main landing gear struts be located at least 6 percent of $\bar{c}_{ref}$ behind the rear center-of-

limit. Furthermore, it must be possible to maintain control within the above center-of-gravity limits at takeoff, both in and out of ground effect, with no significant pitch-up.

The requirement for longitudinal stability and control during landing was that the rear center-of-gravity limit be set to provide a nose-down pitching acceleration of 0.08 rad/s^2 at minimum demonstrated flight speed and normal landing weight. It was also required that acceptable dynamic short-period characteristics be achieved at approach speeds with an operations hardened stability augmentation system, (HSAS), and that no significant pitch-up be present under these conditions.

Lateral-directional - For all cases, it was required that a negative roll result from the occurrence of positive sideslip (positive dihedral effect). During takeoff, control power sufficient to maintain directional control in a 15 m/s (30-knot) crosswind at 90^o was required. Directional control should also be sufficient to counteract the yaw caused by the loss of an outboard engine at takeoff. A 30^o roll response in 2.5 seconds after initiation of a rapid full-control input at, or above, normal approach speeds was also required. Control power must be adequate to trim the aircraft at $\alpha = 0^o$ in a 15 m/s (30-knots), 90^o crosswind using not more than 75 percent of full lateral control. Furthermore, the aircraft should possess inherent Dutch-roll stability with acceptable levels of undamped natural frequency ($\omega_d \geq 0.4$ rad/sec). At supersonic cruise, the yawing moment due to sideslip must be greater than, or equal to, zero for a 2.5 g manuever.

Data Base

Low-speed, high-lift, longitudinal stability and control data were obtained from reference 4. Transonic and supersonic longitudinal data were obtained from references 16 and 17. Low-speed, high-lift, lateral-directional stability and control data were taken from reference 5 and from recent unpublished wind-tunnel test results. Supersonic lateral-directional data were taken from reference 6. All data were corrected for tail-volume differences from the configuration of reference 2.

Wing flexibility associated with lateral control deflections was estimated using the results of reference 18. Fuselage transverse bending due to vertical tail deflection was taken from reference 19.

High-Lift Devices and Controls

The high-lift devices include two-segment leading-edge flaps at the wing apex and outboard Krueger flaps near the wing tips. The trailing-edge flaps consist of an inner flap between the fuselage and the inboard engine, a flap between the inboard and outboard engine, and another flap between the outboard engine and the aileron at the outermost trailing edge. The high-lift devices and nomenclature are given in figure 6. The present high-lift configuration is defined by the two leading edge inner flaps (labeled 9 and 10) deflected 30^o;

the two outer leading-edge Krueger flaps (labeled 13 and 14) deflected 45°; the two outer trailing edge flaps (labeled 5 and 6); and the ailerons (labeled 7 and 8) deflected 5°. Longitudinal control is an all-movable horizontal tail with a geared elevator, and directional control is an all-movable vertical tail. Table V presents the mass and dimensional characteristics of the aircraft, and the maximum control-surface deflections and the deflection rates assumed for the present analysis.

Control Power

Longitudinal - Longitudinal control power was established by the use of data from reference 3. Based on the assumed gearing between tail incidence and elevator deflection for the configuration of reference 3 (fig. 28), longitudinal control capability was determined for the horizontal-tail-volume coefficient $\overline{V}$ of reference 4.

For takeoff and approach, the maximum lift-drag ratio was achieved with 20° of trailing-edge flap deflection (fig. 11). The rearmost center-of-gravity limit was chosen to be 60.1 percent of $\bar{c}_{ref}$, enabling the aircraft to achieve an angle of attack of 8.6° at the 158 knot approach speed. The tail area was chosen to be 83 m^2 (893 ft^2) in order to achieve a nose-down pitch acceleration of 0.08 rad/s^2 (ref. 20) at minimum approach speed. With the landing gear located at 66.1 percent $\bar{c}_{ref}$ (6 percent behind 60.1 percent $\bar{c}_{ref}$), the minimum nose-wheel lift-off speed is approximately 77 m/s (150 knots). This speed can be compared with the 103 m/s (200 knot) nose-wheel lift-off speed required for takeoff.

Lateral - Lateral control power was determined using the wind-tunnel data of reference 5. Lateral-control flexibility factors for each surface (fig. 29) were established from the results of reference 18 for a stiffness-sized (flutter-free) wing design.

The steady-state sideslip, bank angle, rudder deflection, and lateral control required for approaches with sideslip at an airspeed of 81 m/s (158 knots) are shown in figure 30. It can be seen that 75 percent of the available lateral control is required for a crosswind component of approximately 12 m/s (22.5 knots) rather than the 15 m/s (30 knots) required by the criteria. It would require a reduction of about 20 percent in dihedral effect to achieve 15 m/s (30 knot) crosswind capability.

Acceptable crosswind landing capability could be achieved by the use of a crosswind landing gear or by a substantial reduction in dihedral effect. Geometric anhedral (ref. 21) would reduce positive dihedral effect. The models of references 4 and 5 were tested in the high-lift configuration with the wing shape of the flexible wing at supersonic cruise. Reference 18 indicates that aeroelastic effects would result in comparatively greater anhedral at low speeds. The increased anhedral would alleviate the low-speed crosswind problem but might necessitate longer main landing-gear struts.

Directional - The piloted simulator study of reference 20 was conducted on a configuration similar to the present AST-107. The vertical tail size was

chosen as 32.9 m^2 (354 ft^2) to provide the increased directional control in crosswinds recommended by reference 20. The directional-control flexibility factor presented in figure 31 is based on the data of reference 19.

The directional trim required during takeoff ground-roll in a 90^o crosswind is shown in figure 32. For a 12 m/s (22.5 knot) crosswind, directional control cannot be maintained at ground speeds less than approximately 44 m/s (85 knots). For lower speeds or higher crosswinds, nose-wheel steering or differential thrust would be required.

Static Stability

Longitudinal - The low-speed longitudinal static-stability analysis was based on wind-tunnel tests (ref. 4) of the configuration of reference 2. Figures 33 to 36 present the calculated trim and stability results without ground effect for trailing-edge flap deflections of 0, 10, 20, and 30 degrees. The horizontal tail was assumed to produce maximum lift-drag ratio (tail upload) for climb, acceleration to cruise, deceleration, and descent from cruise. From figure 35, it can be seen that the trimmable center-of-gravity range with trailing-edge flap deflections of 20^o for flaps 1, 2, 3, and 4 (of fig. 6) is from 42.55 to 60.10 percent of $\bar{c}_{ref}$.

Supersonic longitudinal static stability was estimated from the aerodynamic center data of reference 3. The resulting flexible-airplane aerodynamic-center location is shown in figure 37.

Lateral-directional - The low-speed lateral-directional static-stability analyses were based on the wind-tunnel results of reference 5. Supersonic-cruise lateral-directional static-stability characteristics (estimated from ref. 3) for the flexible AST-107 are presented in figure 38. Figure 38 shows that there is barely sufficient directional stability to meet the criterion of $C_{n_\beta} \geq 0$ in a 2.5 g pull-up maneuver.

Dynamic Stability and Handling Qualities

Extensive simulator studies (ref. 12) have been conducted on the configuration of reference 3 which was equipped with a Hardened Stability Augmentation System (HSAS) and a Stability and Control Augmentation System (SCAS). Details of these systems and the associated autothrottle are given in reference 12. Similar studies, including pilot ratings, have not been conducted on the present configuration; however, the stability, control, and handling qualities may be inferred by a comparsion with the results of reference 12.

The dynamic stability characteristics of the AST-107 are presented in Table VI and the control response characteristics are given in Table VII. The location of the AST-107 with respect to the short-period frequency requirements of reference 22 is compared with the results of reference 12 in figure 39(a).

A similar comparison using the criteria of reference 23 is shown in figure 39(b). The low-speed pitch time-history is compared with the requirement of reference

24 in figure 40. In all cases, the aircraft is indicated to be at least "acceptable" based on these criteria.

Roll control is compared with the criteria of reference 22 in figure 41(a) and with the criterion of reference 25 in figure 41(b). Provision of greater control power would markedly improve the lateral handling qualities of the AST-107.

AIRPORT NOISE

The jet-only noise characteristics of the AST-107 were calculated for selected takeoff and approach profiles (using the methods of refs. 7 and 8) at the three measuring stations prescribed in reference 26. The relative location of these stations on the airport runway is shown in figure 42. The flight trajectories used for the noise calculations were required to meet the balanced field-length and climb-gradient requirements of the federal safety regulations.

Computed jet-only noise for the trajectories described as case numbers 1 through 3 of Table VIII and figure 43 are summarized in Table IX. Case 1 did not use any power cutback and the normal takeoff-power setting was used throughout the takeoff and climbout. Case 2 used the normal takeoff-power setting in takeoff and climbout until the aircraft reached 5.94 km (19,500 ft) from brake release, at which point the throttle was cut back to 62.6 percent of normal takeoff power. In case 3, the takeoff power was set such that the takeoff Federal-Aviation-Regulation field-length was 3.81 km (12,500 ft). This throttle setting (approximately 93 percent of normal) was used throughout the takeoff and until the aircraft reached an altitude of 213 m (700 ft) (which occurred at 6.4 km (20,995 ft) from brake release). At that point, the power setting was further reduced to about 65.2 percent for the remainder of the climbout.

The takeoff of case 1 (Table IX) resulted in a maximum sideline noise level of 113.8 EPNdB and a centerline noise level of 119.4 EPNdB. The takeoff of case 2 resulted in a maximum sideline noise level of 113.3 EPNdB and a centerline noise of 116.1 EPNdB. The takeoff of case 3 resulted in a maximum sideline noise of 113.4 EPNdB and a centerline noise of 120.7 EPNdB. All of these levels should be reduced by an estimated 3 EPNdB to account for the mechanical jet-noise noise suppressor. Of the trajectories considered, case 2 produced the least noise, which, including the increment for the mechanical suppressor, resulted in a maximum sideline noise of 110.3 EPNdB and a centerline noise of 113.1 EPNdB. The mechanical-suppressor noise increment is only an estimate and should be considered with caution. Approach noise, using a standard 3° glide slope at an approach speed of 158 knots was 110.5 EPNdB.

Jet-noise-only contours for case 1 and case 2 are shown in figures 44 and 45. The results of the jet-noise-only calculations for the three cases are summarized in figure 46.

SONIC BOOM

Equivalent area distributions due to volume and lift which are required for the sonic boom analysis were computed by the use of method described in reference 13. These methods were modified prior to their use in references 1 and 3, and in the present study, to include the effect of angle of attack. The resulting equivalent areas and the procedures of references 27 and 28 were employed to define near-field pressure signatures below the aircraft for three different fuselage lengths. These near-field pressure signatures were extrapolated to ground level using the methods described in reference 29 which include the effects of variations in atmospheric properties, of aircraft acceleration, and the variation in aircraft flight path angle. A reflection factor of 1.9 was used through the analysis.

Sonic boom signatures were computed for a series of Mach numbers from transonic climb through supersonic cruise. The maximum overpressure (Δp_{max}) was then computed as a function of Mach number (fig. 47) for the aircraft trajectory. The maximum sonic-boom overpressure (Δp_{max}) is about 130 Pa (2.7 lbf/ft^2). Based on figure 47 and information from previous analyses, a focused boom (ref. 30) could occur on the ground as a result of the acceleration during the transonic climb phase of the flight (about M = 1.10). This focused boom effect can be positioned well offshore (about 160 km (88 n.mi.) from brake release) of any land mass for many of the airports to be used by a supersonic transport.

MISSION ANALYSIS

Mission Requirements

The design objective was to optimize a supersonic transport aircraft concept for the minimum weight required to achieve the mission goals. Mission analysis was required to establish the weight of the aircraft required to meet these goals.

The objective of the study was an aircraft concept which could cruise at a Mach number of 2.62 (at standard day plus 8C temperature) for 8.33 Mm (4,500 n.mi.) carrying a payload of 273 passengers and their baggage (a total payload weight of 253.8 kN (57,057 lbf). The balanced field length for takeoff was not to exceed 3.81 km (12,500 ft) (at standard day plus 10C temperature). The approach speed was not to exceed 81.3 m (158 knots).

The fuel requirement included that required to complete the base mission plus reserve fuel sufficient to overcome the effect of headwinds (5 percent of trip fuel); the fuel required for 30 minutes in a holding pattern at 3.05 km (10,000 ft); the fuel required for one missed approach and the necessary "go-around"; and the fuel required for cruise to an alternate airport 463 km (250 n.mi.) away (using the best cruise Mach number and altitude). The fuel reserves described above are based on the recommendations of reference 31.

Method of Analysis

The methods of reference 6 were used to establish the configuration of the aircraft and to determine its size. An array of candidate aircraft was studied by varying the thrust-weight ratio and wing loading. This resulted in a matrix of aircraft of different gross weights. The takeoff field length, approach speed, fuel volume, and climb acceleration margin were included as constraints on the designs. Data generated for this matrix of related aircraft were plotted to establish the "thumbprint" sizing plot shown on figure 26.

Since the study objective was to determine the minimum weight of the aircraft required to fly a given payload at fixed range with the above constraints, the presentation of figure 26 is in the form of constant takeoff-gross-weight contours as a function of thrust-weight ratio and wing loading. From this thumbprint plot, a candidate aircraft having the minimum gross weight within the required constraints was selected. This aircraft had an estimated takeoff gross weight of 3.15 MN (709,000 lbf) with an installed thrust-to-weight ratio of 0.268 and a design wing loading of 4.07 kPa (85 lbf/ft^2).

This configuration was then subjected to a more detailed analysis to determine pertinent performance characteristics and to evaluate its compliance with mission goals. The conceptual aircraft was "flown" within the computer program (ref. 6) in accordance with the selected mission profile. For each segment of the profile, the program determined enroute details such as thrust and fuel required, altitude, speed, and the end point time of each segments. The profile used in this study (fig. 48) was composed of the following segments: a 10-minute warmup and taxi-out fuel allowance; a takeoff of one minute at full takeoff thrust a climb and acceleration using the climb schedule shown in figure 49, where the flaps are deflected 30^{o} below 213 m (700 ft.) altitude and are retracted above 213 m (700 ft.) altitude; a cruise at either optimum Brequet range factor or at climb ceiling; a descent in accordance with figure 49.

Design Mission Performance

Results of the mission performance evaluation are summarized in Table X. Cruise lift-drag ratio, an indicator of aerodynamic efficiency, averaged 9.15. Additional evaluations were performed for reduced payload conditions to produce the payload-range characteristics shown in figure 50.

Off-Design Operation

The aircraft was also investigated while performing subsonic off-design missions. The trade between the length of the subsonic (M = 0.9) and length of the supersonic (M = 2.62) flight segments for passenger load factors of 60 percent and 100 percent is shown in figure 51. Figure 51 indicates that at 60 percent load factor the all-subsonic range is about 7.60 Mm (4200 n.mi.) and the all-supersonic range is about 9.50 Mm (5200 n.mi.).

Sensitivity Analysis

The sensitivity of the design range to changes in total drag coefficient, engine specific fuel consumption, and structural weight was also investigated. The results of this sensitivity analysis are presented in figure 25.

ECONOMIC EVALUATION

An airline, as a potential purchaser and user of transport aircraft, must consider the profit-making potential of any aircraft which it might introduce into its fleet. Parameters important in determining the productivity, and thus, in effect, the profit-making capability of any aircraft, include the direct and total operating costs of the aircraft. The fuel burned per mission also is important because of the current difficulty in predicting the future cost of fuel. Block fuel and seat miles per gallon are used to evaluate the fuel efficiency of the aircraft.

The direct operating cost was computed as described in the Air Transport Association model of reference 32. The indirect operating cost and the total operating cost (sum of direct operating cost and indirect operating cost) was computed as described in reference 33. Monetary values were in terms of constant 1976 dollars. The ticket price was computed with a return-on-investment of 15 percent. Analyses were performed for both 60 and 100 percent passenger load factors at subsonic (M = 0.90) and supersonic (M = 2.62) cruise for various ranges. At 1976 dollars, the AST-107 is economically viable producing 15 percent return-on-investment with 60 percent load factor and an average ticket price of approximately 300 dollars per passenger at a range comparable to a flight from San Francisco to Tokyo or 200 dollars per passenger for a New York to London flight.

The direct operating cost, total operating cost and ticket price are presented in figures 53 to 55. From the comparison of ticket prices, it is apparent that operation of the AST-107 in the subsonic cruise mode would impose a significant burden on the fare-paying passenger. The fuel cost used in the foregoing calculations was 10.25 cents per liter (38.7 cents per gallon). The block fuel and passenger statute miles per gallon are shown in figures 56 and 57. The AST-107 obtains about 14.5 passenger kilometers per liter (34.3 passenger statute-miles per gallon) at reduced ranges (fig. 57). The effect of varying the fuel cost and the hours of utilization per year on the total operating cost of the vehicle is shown in figures 58 and 59. The fuel cost and hours of utilization sensitivities shown in figures 58 and 59 are for cruise at a Mach number of 2.62 and a range of between 4500 and 4600 nautical miles.

CONCLUSIONS

A new advanced supersonic technology configuration designated the AST-107 using a low bypass-ratio turbofan has been described and analyzed. The results of this study indicate that:

1. Mission range for the AST-107 was 8.48 Mm (4576 n.mi.). The average lift-drag ratio during cruise was 9.15.

2. The available lateral control is not sufficient for the 15.4 m/sec (30 kt) crosswind requirement. A crosswind landing gear or a significant reduction in dihedral effect would be required to meet this criteria.

3. Centerline and maximum sideline noise (jet only) were computed to be 110.3 EPNdB (sideline noise) and 113.1 EPNdB (centerline noise) including a 3 EPNdB benefit for a mechanical noise suppressor. The approach noise was estimated to be 110.5 EPNdB.

4. Off-design operation of the AST-107 in the subsonic cruise mode would not be economically attractive because of the poor subsonic specific fuel consumption of this particular engine.

5. The AST-107 obtains as much as 14.5 seat-kilometers per liter (34.3 seat-miles per gallon) at reduced ranges.

6. At 1976 dollars, the AST-107 is economically viable producing 15 percent return on investments with 60 percent load factor and an average ticket price of approximately 300 dollars per passenger at a range comparable to a flight from San Francisco to Tokoyo or 200 dollars per passenger for a New York to London flight.

REFERENCES

1. Baber, Hal T., Jr.: Characteristics of the Advanced Supersonic Technology AST-105-1 Configured for Transpacific Range With Pratt and Whitney Aircraft Variable Stream Control Engines. NASA TM-78818, March 1979.

2. Advanced Supersonic Technology Concept Study, Reference Characteristics. NASA CR-132374, 1973.

3. Baber, Hal T., Jr.; and Swanson, E. E.: Advanced Supersonic Technology Concept AST-100 Characteristics Developed in a Baseline - Update Study. NASA TM X-72815, 1976.

4. Smith, Paul M.: Low-Speed Aerodynamic Characteristics From Wind-Tunnel Tests of a Large-Scale Advanced Arrow-Wing Supersonic-Cruise Transport Concept. NASA CR-14580, 1980.

5. Coe, Paul L., Jr.; Smith, Paul M.; and Parlett, Lysle P.: Low-Speed Wind Tunnel Investigation of an Advanced Supersonic Cruise Arrow-Wing Configuration. NASA TM-74043, 1977.

6. Fetterman, David E., Jr.: Preliminary Sizing and Performance Evaluation of Supersonic Cruise Aircraft. NASA TM X-73936, 1976.

7. Foss, Willard E., Jr.: A Computer Program for Detail Analysis of the Takeoff and Approach Performance Capabilities of Transport Category Aircraft. NASA TM-8012, June 1979.

8. Raney, John P.: Noise Prediction Technology for CTOL Aircraft. NASA TM-78700, 1978.

9. Staff of the Langley Research Center: Preliminary Noise Tradeoff Study of a Mach 2.7 Cruise Aircraft. NASA TM-78732, April 1979.

10. Mechtly, E.A.: The INternational System of Units - Physical Constants and Conversion Factors (Second Revision) NASA SP-7012, 1973.

11. Sommer, Simon C.; and Short, Barbara, J.: Free Flight Measurements of Turbulent Boundary Layer Skin Friction in the Presence of Severe Aerodynamic Heating at Mach Numbers From 2.8 to 7.0. NACA TN 3391, 1955.

12. Grantham, William D.; Nguyen, Luat T.; Deal, Perry L.; Neubauer, Milton, J., Jr.; Smith, Paul M.; and Gregory, Frderick D.: Ground-Based and In-Flight Simulator Studies of Low-Speed Handling Characteristics of Two Supersonic Cruise Transport Concepts. NASA TP-1240, July 1978.

13. Harris, Roy V., Jr.: An Analysis Correlation of Aircraft Wave Drag. NASA TM X-947, 1964.

14. Hoerner, S. F.: Fluid-Dynamic Drag. Hoerner Fluid Dynamics (Bricktown, N.J.), c. 1965.

15. Koncsek, J.L.; and Syberg, J.: Transonic and Supersonic Test of a Mach 2.65 Mixed Compression Axisymmetric Intake. NASA CR-1977, March 1972.

16. Decker, John P.; and Jacobs, Peter F.: Stability and Performance Characteristics of a Fixed Arrow-Wing Supersonic Transport Configuration (SCAT 15F-9898) at Mach Numbers From 0.60 to 1.20. NASA TM-78726, June 1978.

17. Morris, Odell A.; Fuller, Dennis E.; and Watson, Carolyn B.: The Aerodynamic Characteristics of a Fixed Arrow-Wing Supersonic Cruise Aircraft Configuration at Mach Numbers of 2.30, 2.70, and 2.95. NASA TM-78706, June 1978.

18. Wrenn, G. A.; McCullers, L. A.; and Newsom, R., Jr.: Structural and Aeroelastic Studies of a Supersonic Arrow Wing Configuration. NASA CR-145325, 1977.

19. Douglas Aircraft Company: Studies of the Impact of Advanced Technologies Applied to Supersonic Transport Aircraft. MDC J-4394, 1973.

20. Grantham, William D.; Nguyen, Luat T.; Neubauer, M. J., Jr.; and Smith, Paul M.: Simulator Study of the Low-Speed Handling Qualities of a Supersonic Cruise Arrow-Wing Transport Configuration During Approach and Landing. NASA CP-001, Part 1, 1976, pp. 215-248.

21. Lockwood, Vernard E.: Effect of Leading-edge Contour and Vertical-Tail Configuration on the Low-Speed Stability Characteristics of a Supersonic Transport Model Having a Highly Swept Arrow-Wing. NASA TM-78683, 1978.

22. Anon: Flying Qualities of Piloted Airplanes. Military Specification NIL-F-8785 B(ASG), 1969.

23. Shomber, H. A.; and Gertsen, W.M.; Longitudinal Handling Qualities Criteria: An Evaluation. Journal of Aircraft, Vol. 4. No. 4, July-August 1967.

24. Suddreth, Robert W.; Bohn, Jeff G.; Caniff, Martin A.; and Bennett Gregory R.: Development of Longitudinal Handling Qualities and Criteria For Large Advanced Supersonic Aircraft. NASA CR-137635, 1975.

25. Anon: Aerospace Recommended Practice - Design Objectives for Flying Qualities of Civil Transport Aircraft. ARAP 842, SAR, 1964.

26. DOT/FAA Noise Standards: Aircraft Type and Airworthiness Certification. FAR Part 36, June 1074.

27. Carlson, Harry W.: Correlation of Sonic Boom Theory With Wind Tunnel and Flight Measurements. NASA TRR-213, 1964.

28. Middleton, Wilbur D.; and Carlson, Harry W.: A Numerical Method for Calculating Near-Field Sonic Boom Pressure Signatures. NASA TN D-3982, 1965.

29. Thomas, Charles L.: Extrapolation of Sonic Boom Pressure Signatures by the Wave Form Parameter Method. NASA TN D-6832, 1972.

30. Haglund, George T.; and Kane, Edward J.: Effect of SST Operational Maneuvers on Sonic Boom. Journal of Aircraft. Vol. 9, No. 8, August 1972, pp. 563-568.

31. Anon.: An Airline's View of Reserve Fuel Requirements for the Supersonic Transport. Lockheed-California LR 26133, 1973.

32. Anon.: Standard Method of Estimating Comparative Direct Operating Costs of Turbine Powered Transport Airplanes. Air Transport Assoc. of America, 1967.

33. Anon.: Indirect Operating Expense Coefficients, Years 1963 Through 1979. Lockheed-California Company AA/2917, June 1980.

TABLE I.- AST 107 GEOMETRIC CHARACTERISTICS

Geometry		Wing	Horizontal tail	Vertical tail	Wing fin
Geometric area	m^2 (ft^2)	853.96 (9192)	82.96 (893)	32.84 (354)	18.12 (195)
Mean Aerodynamic chord, c	m (ft)	31.19 (102.32)	8.97 (29.43)	8.90 (29.20)	7.19 (23.58)
Wing reference area S_{ref}	m^2 (ft^2)	774.16 (8333)			
Reference mean aerodynamic chord, c_{ref}	m (ft)	26.82 (87.99)			
Exposed area	m^2 (ft^2)		57.60 (620)	32.89 (354)	18.12 (195)
Span, b	m (ft)	38.39 (125.97)	10.54 (34.57)	4.16 (13.66)	2.99 (9.83)
Aspect ratio based on above geometric area		1.721	1.338	.527	.495
Aspect ratio based on wing reference area		1.904			
Leading edge sweep	Deg	74 70.84 60	55	68.2	73.42
Root chord	m (ft)	51.02 (167.38)	12.96 (42.53)	12.77 (41.90)	10.64 (34.91)
Tip chord	m (ft)	4.92 (16.13)	2.79 (9.14)	3.03 (9.93)	1.45 (4.75)
Root thickness/chord	%		3.000	2.996	2.996
Tip thickness/chord	%		3.000	2.996	2.996
Taper ratio			.215	.237	.136
Dihedral	Deg		-15		
Vol. coeff. (gross), $\bar{V}$	*		.113	.041	.012 (each)
Vol. coeff. (ref.), $\bar{V}$	**		.146	.046	.014 (each)

*Based on gross wing characteristics
**Based on reference wing characteristics

TABLE II.- WETTED AREA SUMMARY

Component	Wetted area m^2 (ft^2)
Wing	1400.71 (15077.09)
Fuselage	733.63 (7896.77)
Nacelles (4)	204.53 (2201.52)
Wing fins (2)	72.78 (783.42)
Vertical tail	66.11 (711.65)
Horizontal tail	119.73 (1288.72)
Total	2597.49 (27959.15)

TABLE III.- GROUP WEIGHT SUMMARY

	kN	lbf
Wing	336.850	75727
Horizontal tail	29.394	6608
Vertical tail	17.962	4038
Vertical fin	9.461	2127
Canard	0.0	0
Fuselage	226.935	51017
Landing gear	122.268	27487
Nacelle	47.200	10611
Structural total	(790.070)	(177615)
Engines	206.220	46360
Thrust reversers	0.0	0
Miscellaneous systems	7.918	1780
Fuel system - tanks and plumbing	32.681	7347
- insulation	0.0	0
Propulsion total	(246.819)	(55487)
Surface controls	41.311	9287
Auxiliary power	0.0	0
Instruments	7.811	1756
Hydraulics	25.898	5822
Electrical	22.321	5018
Avionics	12.273	2759
Furnishings and equipment	88.048	19794
Air conditioning	38.553	8667
Anti-icing	0.934	210
Systems and equipment total	(237.149)	(53313)
Weight empty	1274.038	286415
Crew and baggage - flight, 3	3.003	675
- cabin, 9	6.606	1485
Unusable fuel	8.972	2017
Engine oil	2.180	490
Passenger service	36.760	8264
Cargo containers, 6	11.921	2680
Operating weight	1343.480	302026
Passengers, 273	200.370	45045
Passenger baggage	53.432	12012
Cargo	0.0	0
Zero fuel weight	1597.282	359083
Mission fuel	1556.508	349917
Takeoff gross weight	3153.790	709000

TABLE IV.- INERTIA SUMMARY

	Condition	
	Takeoff gross weight	Normal landing weight
Weight, kN , lbf	3153.790 709000	1827.153 410500
Horizontal c.g., m , in	52.923 2083.58	52.645 2072.65
Percent of $\bar{c}_{ref}$	60.00	58.97
Roll inertia, I_x, $Gg\text{-}m^2$, $slug\text{-}ft^2$	11.089 8.179×10^6	6.081 4.485×10^6
Pitch inertia, I_y, $Gg\text{-}m^2$, $slug\text{-}ft^2$	77.904 57.459×10^6	73.808 54.438×10^6
Yaw inertia, I_z, $Gg\text{-}m^2$, $slug\text{-}ft^2$	86.565 63.847×10^6	77.721 57.423×10^6
Product of inertia, I_{xz}, $Gg\text{-}m^2$, $slug\text{-}ft^2$	-2.562 -1.890×10^6	-2.259 -1.666×10^6
Principle axis angle of inclination, rad , deg	-0.0338 -1.94	-0.0316 -1.81

TABLE V.- MASS AND DIMENSIONAL CHARACTERISTICS OF THE AST-107

Reference wing area, m^2 (ft^2)	774.16 (8333)
Wing span, m (ft)	38.39 (125.964)
Wing leading-edge sweep, deg (see fig. 1)	74.00/70.84/60.00
Reference mean aerodynamic chord, m (ft)	26.82 (87.985)
Center-of-gravity location, percent $\bar{c}_{ref}$	60.10
Static margin, percent	-3.7
Takeoff weight, mN (lbf)	3.154 (709,000)
I_x, kg-m^2 (slug-ft^2)	11,089,230 (8,179,000)
I_y, kg-m^2 (slug-ft^2)	77,903,940 (57,459,000)
I_z, kg-m^2 (slug-ft^2)	86,564,910 (63,847,000)
I_{xz}, kg-m^2 (slug-ft^2)	-2,562,500 (-1,890,000)
Landing weight, mN (lbf)	1.827 (410,500)
I_x, kg-m^2 (slug-ft^2)	6,080,840 (4,485,000)
I_y, kg-m^2 (slug-ft^2)	73,808,020 (54,438,000)
I_z, kg-m^2 (slug-ft^2)	77,720,910 (57,324,000)
I_{xz}, kg-m^2 (slug-ft^2)	-2,258,790 (-1,666,000)
Maximum control surface deflections in degrees:	
Horizontal tail (δ_t)	±20
Flap (δ_1 and δ_2)	0 to 30
Aileron (δ_7 and δ_8)	±25
Outboard flaperon (δ_5 and δ_6)	±30
Inboard flaperon (δ_3 and δ_4)	±10
Rudder (δ_r)	±25
Maximum control surface deflection rates in degrees per second	
Horizontal tail	±50
Flap	±10
Aileron	±70
Outboard flaperon	±40
Inboard flaperon	±40
Rudder	±50

TABLE VI.- DYNAMIC STABILITY CHARACTERISTICS OF AST-107

(158 knots approach speed)

Parameters	Augmentation				Satisfactory criterion	Acceptable criterion
	None	HSAS	SCAS	Modified SCAS		
Short-period mode						
ω_{sp}, rad/s	.167	.704	1.394	1.394	See fig. 39	See fig. 39
P_{sp}, s	44.88	12.63	24.63	24.63	- - -	- - -
δ_{sp}	.542	.708	.983	.983	0.35 to 1.30	0.25 to 2.00
L_α/ω_{sp}	2.91	.688	.348	.348	See fig. 39	See fig. 39
n/α, g units/rad	4.02	4.02	4.02	4.02	See fig. 39	See fig. 39
Long-period (aperiodic) mode						
t_2, s	5.32	∞	∞	∞	- - -	>5
Long-period (periodic) mode						
ω_{ph}, rad/s	- - -	.089	.087	.087	- - -	- - -
P_{ph}, s	- - -	84.98	89.74	89.74	- - -	- - -
δ_{ph}	- - -	.555	.597	.597	$\geq$0.04	$\geq$0
Roll mode						
t_R	1.536	.282	.321	.117	$\leq$1.4	$\geq$3.0
Spiral mode						
$t_{1/2}$, s	32.46	50.26	∞	∞	- - -	- - -
Dutch roll mode						
ω_d, rad/s	.937	.541	1.117	.740	$\geq$0.4	$\geq$0.4
δ_d	.109	.359	.220	.229	$\geq$0.08	$\geq$0.02
$\delta_d\omega_d$, rad/s	.102	.194	.243	.169	$\geq$0.15	$\geq$0.05
P_d, s	6.75	12.43	5.77	8.72	- - -	- -
ϕ/p	2.81	2.68	.78	.78	- - -	- -
Roll-control parameters						
ω_ϕ/ω_d	.638	1.106	1.017	1.006	0.80 to 1.15	0.65 to 1.35
δ_ϕ/δ_d	1.90	.636	1.202	1.004	- - -	- - -

TABLE VII.- CONTROL RESPONSE CHARACTERISTICS OF AST-107

(158 knots approach speed)

Parameters	Augmentation				Satisfactory criterion	Acceptable criterion
	None	HSAS[a]	SCAS[a]	Modified SCAS[a]		
Longitudinal						
$\ddot{\phi}_{max}$, rad/s^2	b-.070	b-.049	b-.070	Same as SCAS[a]	b-0.08	b-0.0
$\dot{\phi}/\dot{\phi}_{ss}$	- - -	- - -	See fig. 40		See fig. 40	
Lateral						
$\ddot{\phi}_{max}$, rad/s^2	.248	.209	.194	.20	See fig. 41	See fig. 41
$\dot{\phi}_{max}$, deg/s	16.57	10.51	23.25	21.10	See fig. 41	See fig. 41
$t_{\phi} = 30^{o}$, s	2.90	3.80	2.82	2.86	≤2.5	≤3.2

[a]Autothrottle on

[b]Minimum demonstrated speed of 129 knots

TABLE VIII.- SUMMARY OF TAKEOFF PARAMETERS

Case number	1	2	3	4
Takeoff performance				
Rotational velocity, m/s (kts)	100.3 (195)	100.3 (195)	97.7 (190)	100.3 (195)
Liftoff velocity, m/s (kts)	107.3 (208.5)	107.3 (208.5)	104.3 (202.7)	107.3 (208.5)
Velocity at obstacle, m/s (kts)	110.8 (215.4)	110.8 (215.4)	108.3 (210.5)	110.8 (215.4)
Engine out (V_1), m/s (kts)	91.2 (177.2)	91.2 (177.2)	88.4 (171.8)	91.2 (177.2)
Engine out (V_2), m/s (kts)	107.0 (208.0)	107.0 (208.0)	106.2 (206.4)	107.0 (208.0)
Engine out balanced field length, m (ft)	3518 (11544)	3518 (11544)	3739 (12270)	3518 (11544)
FAR field length, m (ft)	3568 (11706)	3568 (11706)	3810 (12500)	3568 (11706)
Cutback performance				
Altitude at cutback, m (ft)		250 (822	213 (700)	235 (773)
Distance to cutback, m (ft)	No	5944 (19500)	6399 (20995)	5944 (19500)
Velocity at cutback, m/s (kts)	Cutback	125.5 (244)	122.4 (238)	121.7 (236.5)
C_L at cutback		.424	.436	.445
L/D at cutback		8.5	8.2	8.1
Percent thrust, after cutback		.626	.641	.652
6.49 km (3.5 n.mi.) flyover point Altitude, m (ft)	307 (1008)	273 (897)	217 (712)	259 (851)

Above data assumes 20 degree flap deflection.

TABLE IX.- EFFECTIVE PERCEIVED NOISE LEVELS

		Jet EPNdB
Case 1	Takeoff, normal throttle setting, accelerating climb, no power cutback:	
	maximum sideline noise	113.8
	centerline noise	119.4
Case 2	Takeoff, normal throttle setting, accelerating climb, power cutback 5944 m (19,400 ft):	
	maximum sideline noise	113.3
	centerline noise	116.1
Case 3	Takeoff, reduced throttle setting*, accelerating climb, power cutback limited by altitude 213 m (700 ft), cutback at 6399 m (20995 ft)	
	maximum sideline noise	113.4
	centerline noise	120.7
Case 4	Takeoff, normal throttle setting, cutback at obstacle to 93 percent power setting, accelerating climb	
	maximum sideline noise	113.6
	centerline noise	117.4
	Approach, standard 3 degree glide slope, constant speed 813 m/sec (158 kt):	
	centerline noise	110.5

Values listed are jet only data and the suppression increment is not yet removed from these EPNdB values. Text assumes that an increment will be removed.

*A throttle setting of 93 percent was used for the initial portion of Case 3.

TABLE X.- MISSION PERFORMANCE

Mission: Supersonic cruise at Mach 2.62

Aircraft characteristics:

Design gross weight	kN (lbf)	3153.790	(709000)
Operating weight empty	kN (lbf)	1343.480	(302026)
Payload - Passengers, 273	kN (lbf)	200.370	(45045)
- Passenger, baggage	kN (lbf)	53.432	(12012)
Total payload weight	kN (lbf)	253.802	(57057)
Wing area - reference	m^2 (ft^2)	774.161	(8333)
- gross	m^2 (ft^2)	853.965	(9192)
GE21/J10-B5 engines (4); sea level static (std. +8°C day) installed thrust per engine, N (lbf)		211.304	(47503)
Initial installed thrust to weight ratio		.268	.268
Initial wing loading - reference kPa, (lbf/ft^2)		4.074	(85.08)
- gross kPa, (lbf/ft^2)		3.693	(77.13)

Mission segment or condition	Operating Weights kN	lbf	Fuel kN	lbf	Range km	n.mi.	Time min.
Ramp gross weight	3153.790	(709000)					
Warm-up & taxi-out			14.946	(3360)	0	0	10.0
Takeoff gross weight	3138.843	(705640)					
Takeoff run			21.280	(4784)	6	(3)	1.4
Begin ascent	3117.563	(700856)					
Climb & accelerate			379.656	(85350)	970	(524)	36.4
Begin cruise	2737.907	(615506)					
Cruise segment			893.928	(200963)	6932	(3743)	146.7
End cruise	1843.979	(414543)					
Descent & decelerate			18.042	(4056)	572	(309)	28.6
End descent	1825.937	(410487)					
Landing & taxi-in			0	0	0	0	0
End mission	1825.937	(410487)					
Trip fuel, range & time			1312.906	(295153)	8474	(4576)	213.1
Block fuel, range & time			1327.852	(298513)	8480	(4579)	223.1

TABLE XI.- BASELINE DATA FOR DIRECT OPERATING COST ANALYSIS

(Monetary values in constant 1976 dollars)

Gross takeoff weight, kN (lbf)	3153.8	(709,000)
Range, km (n.mi.)	8480.8	(4579)
Cruise speed, Mach number	2.62	
Number of engines	4	
Thrust per engine, kN (lbf)	211.3	(47503)
Seats (passengers)	273	
Load factor, %	100	
Fuel cost, cents/liter (cents/gal)	10.25	(38.7)
Insurance rate, % of purchase price (average value)	0.5	(1.0)
Year dollars	1976	
Depreciation period, years	16	
Residual value, %	10	
Utilization rate, hrs/yr block (flight)	4000	(3820)
Crew	3	
Purchase price:		
Aircraft, complete millions of dollars	88.52	
Airframe, millions of dollars	72.02	
Engines, millions of dollars	16.5	
Spares, millions of dollars	9.27	
Crew pay relative to subsonic, %	117	
Down payment (5%/6 month intervals)	20%	
Return on investment	15%	
Interest rate	10%	
Salvage value	10%	
Tax rate	48%	
Economic lifetime	16 yr	

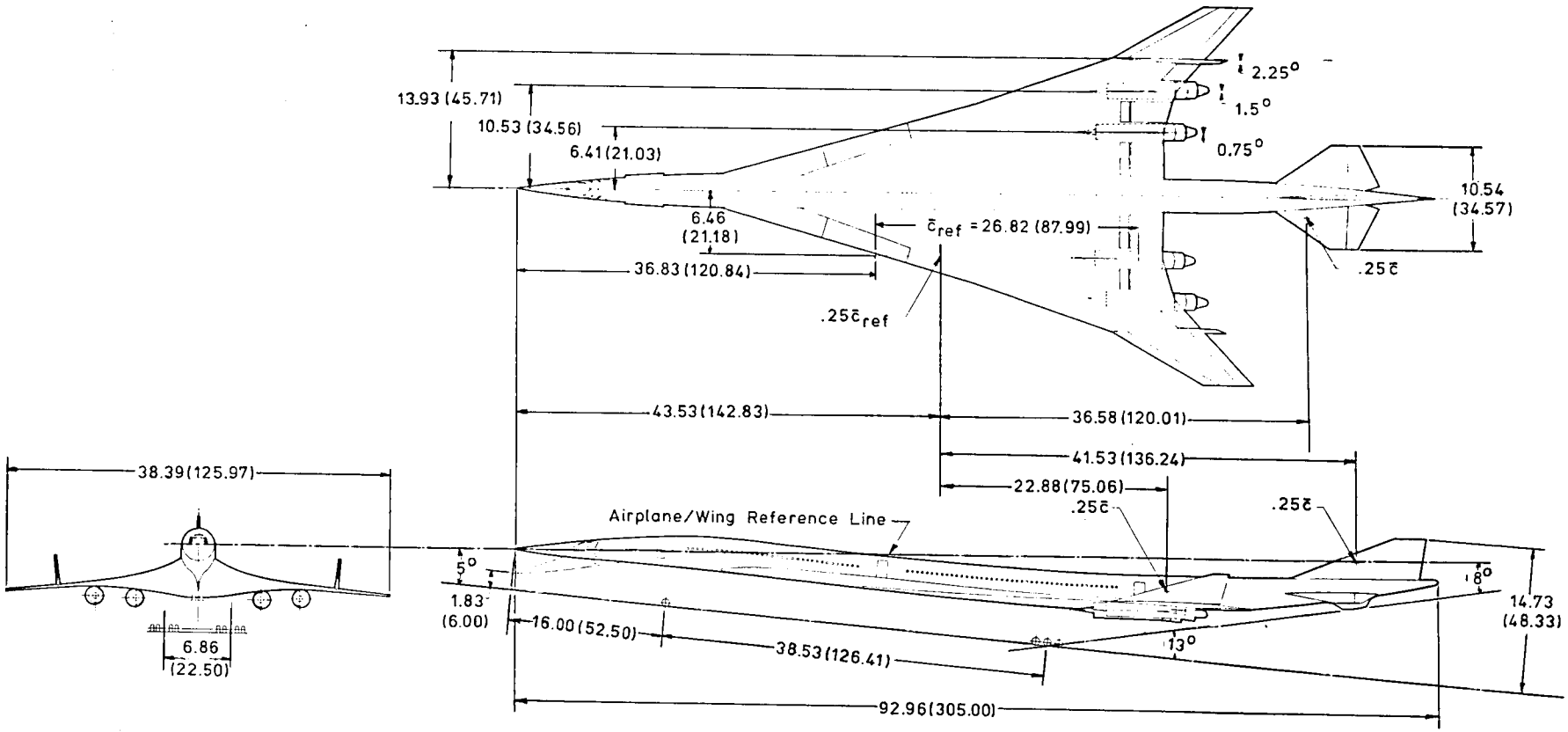

Figure 1.- General arrangement.

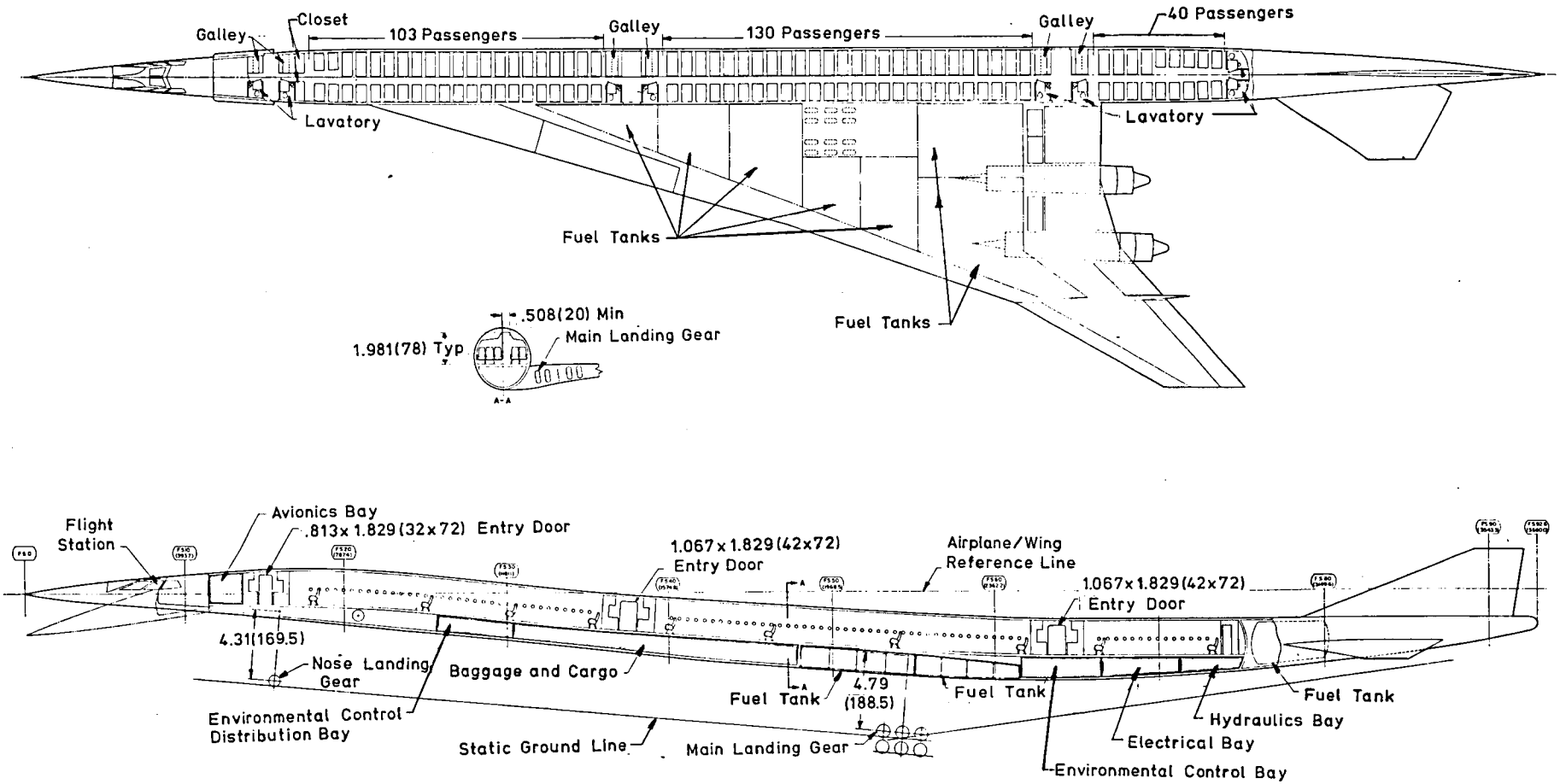

Figure 2.- Inboard profile.

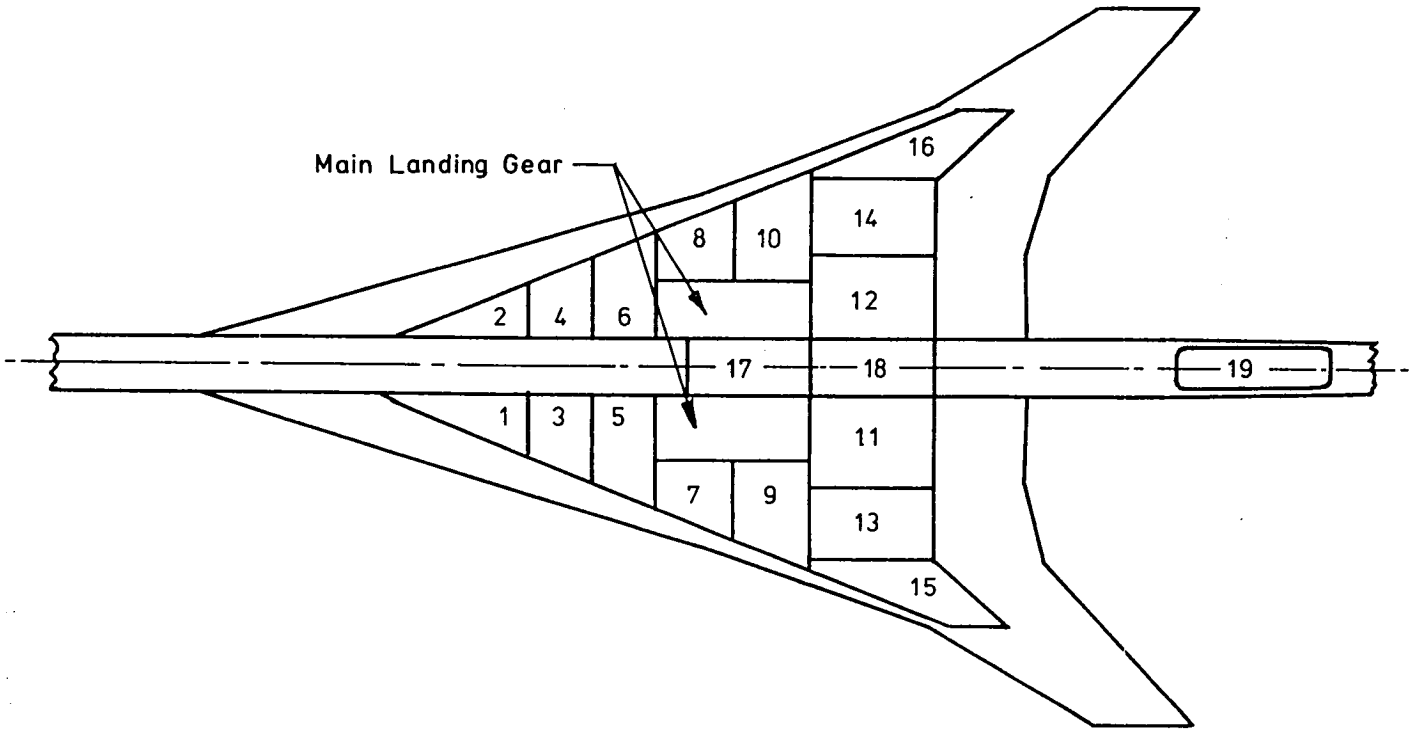

Tank Number	Fuel Weight Per Tank	
	kN	lbf
1 - 2	84.525	19002
3 - 4	97.251	21863
5 - 6	129.377	29085
7 - 8	75.900	17063
9 - 10	98.110	22056
11 - 12	158.054	35532
13 - 14	92.719	20844
15 - 16	38.811	8725
17	200.535	45082
18	134.123	30152
19	119.212	26800
Total	2003.364	450 374

Figure 3. - Fuel tank locations and capacities.

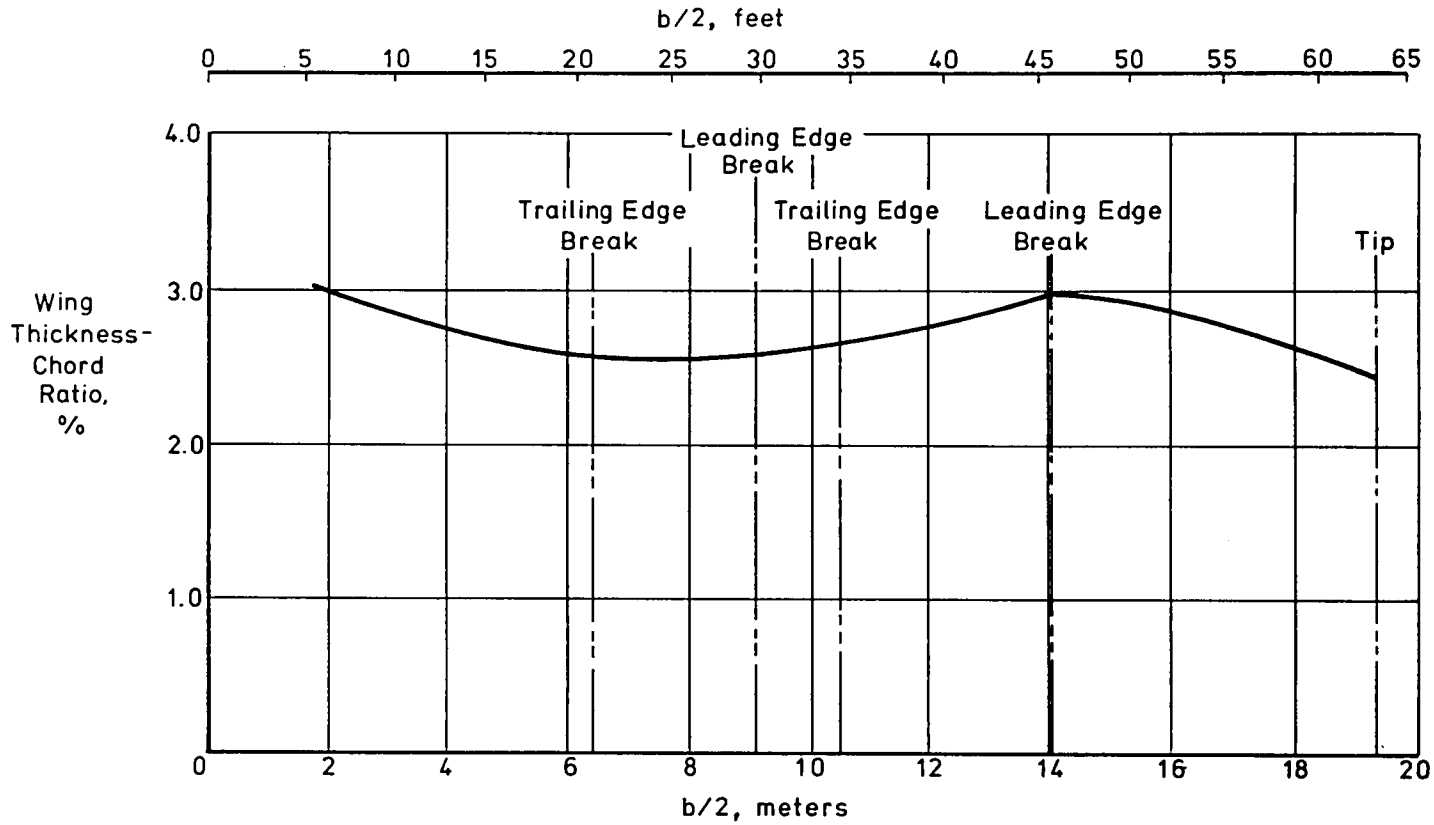

Figure 4.- Spanwise thickness distribution.

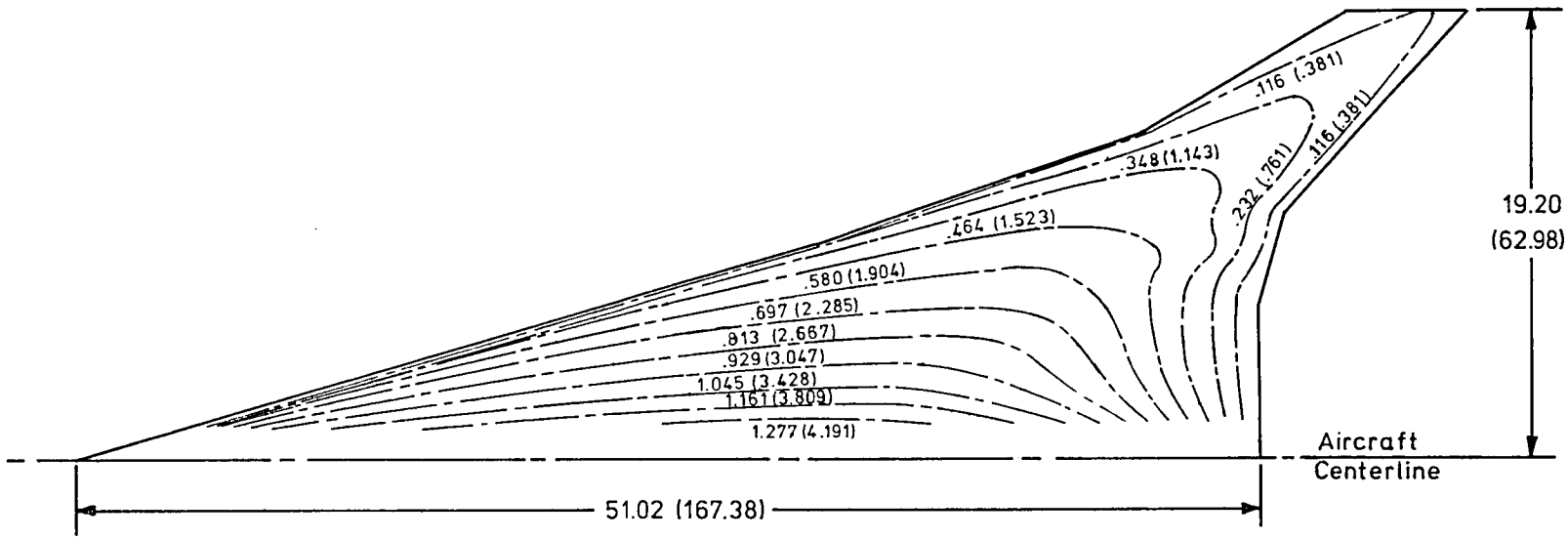

Figure 5.- Contours of wing thickness, dimensions in meters (ft.).

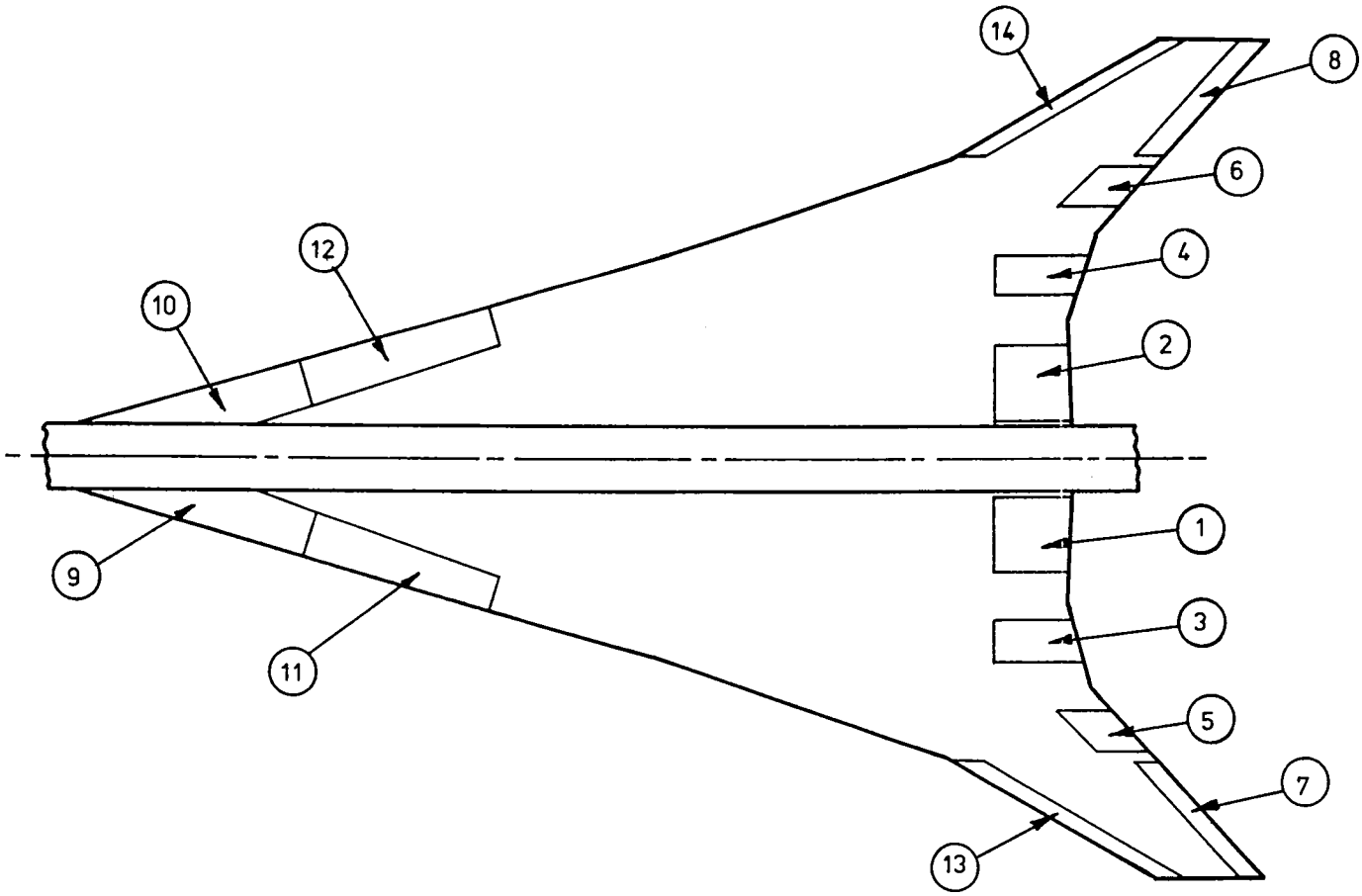

Flap Number	Area, m^2 (ft^2) Each	
1 - 2	11.687	(125.8)
3 - 4	8.070	(86.9)
5 - 6	4.673	(50.3)
7 - 8	7.634	(82.2)
9 - 10	15.379	(165.5)
11 - 12	16.332	(175.8)
13 - 14	8.421	(90.6)

Figure 6.- Wing control surface geometry and flap definition.

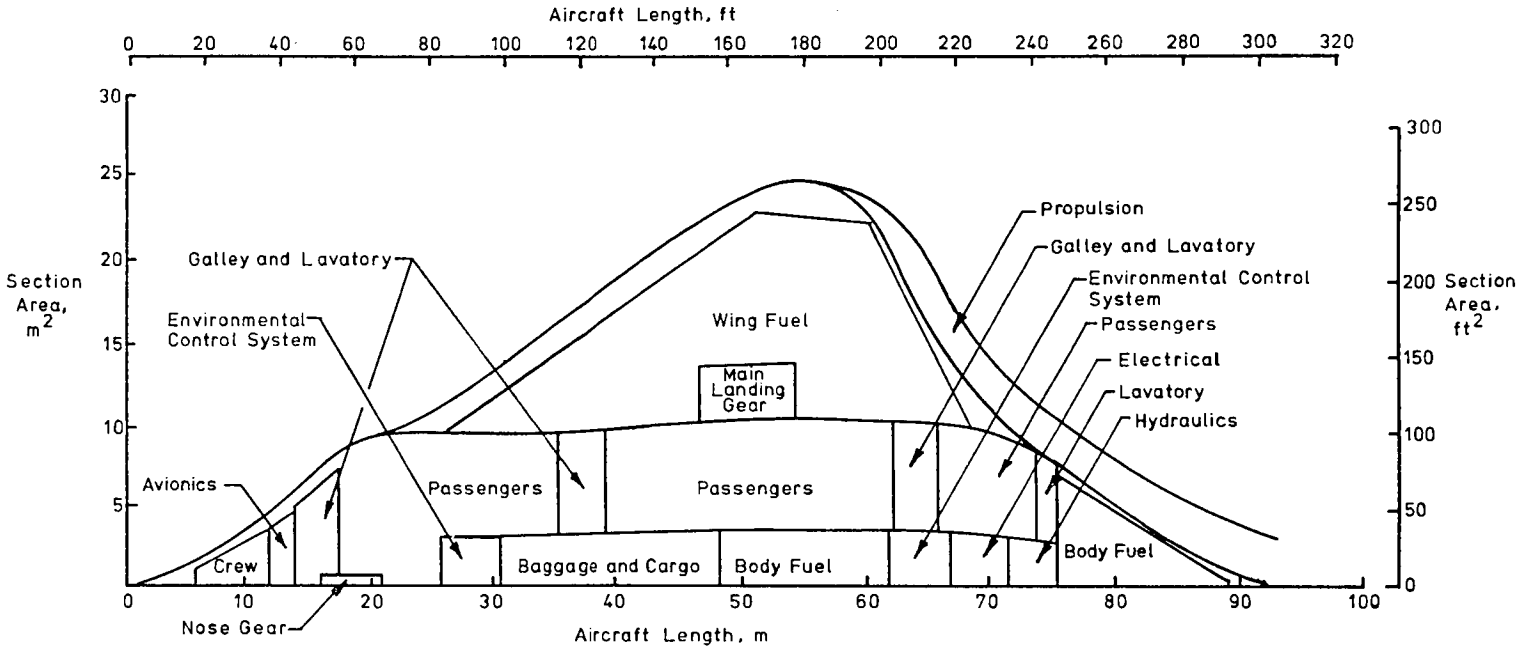

Figure 7.- Volume utilization of configuration.

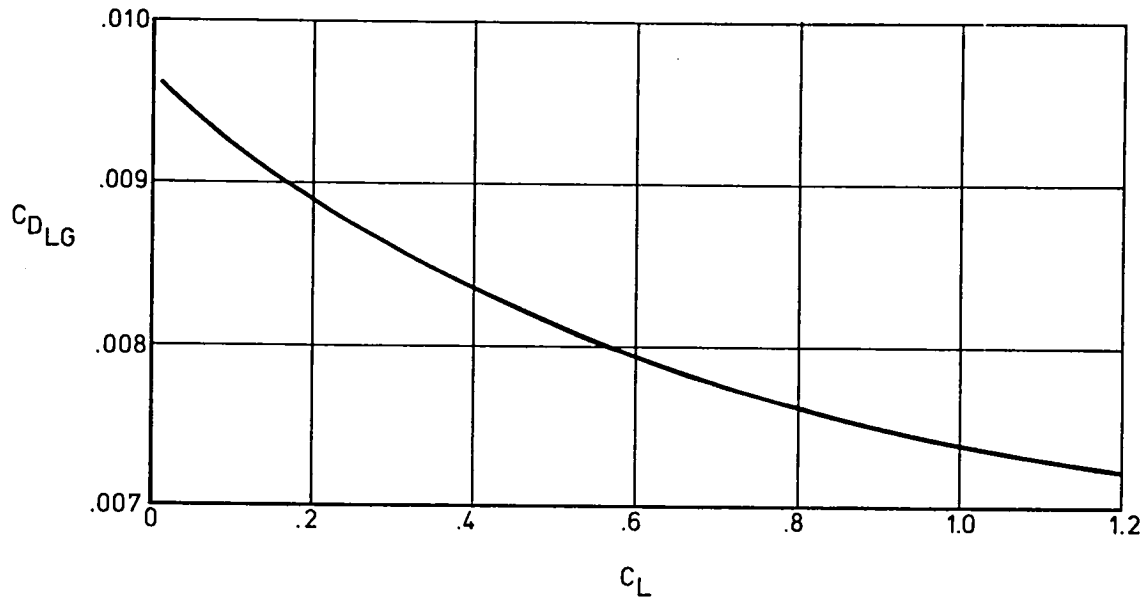

Figure 8.- Landing gear incremental drag coefficient as a function of C_L-in or out of ground effect.

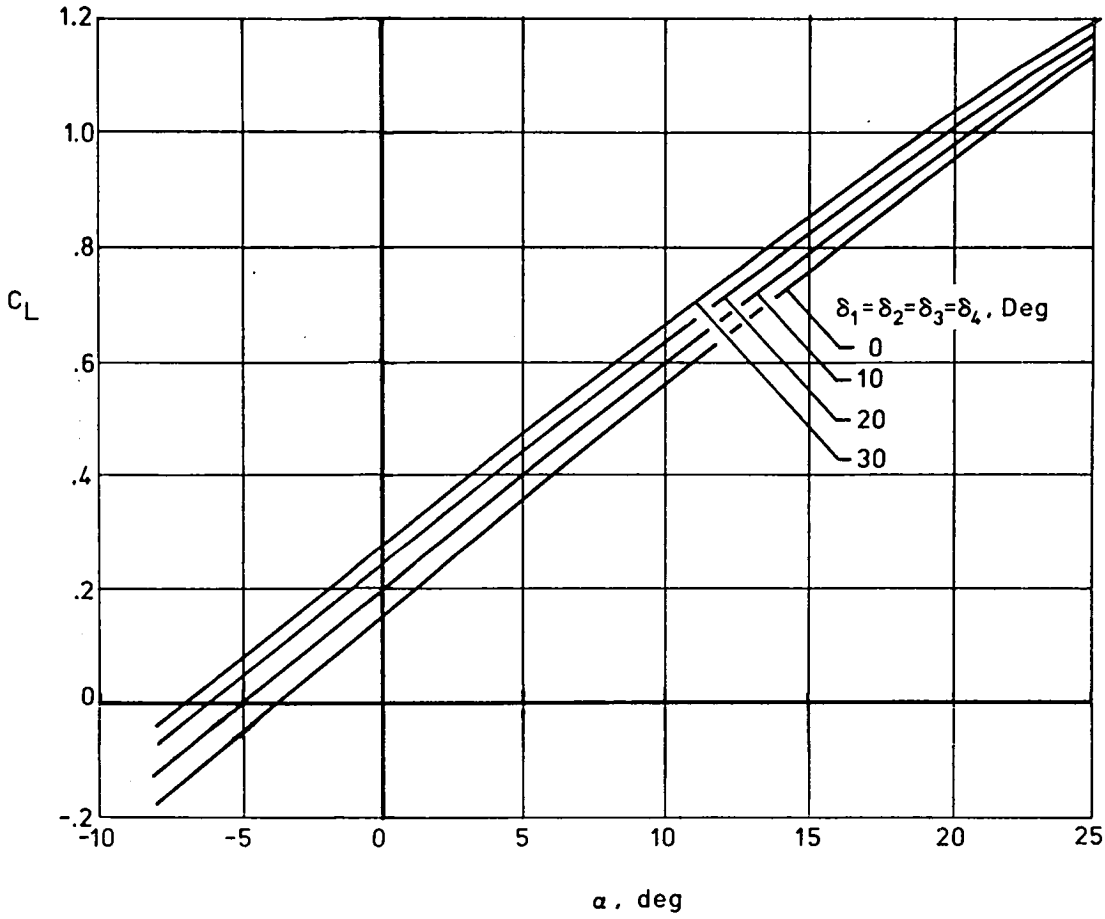

Figure 9.- Trimmed lift curves (out of ground effect), $\delta_9 = \delta_{10} = \delta_{11} = \delta_{12} = 30^o$, $\delta_{13} = \delta_{14} = 45^o$, $\delta_5, \delta_6, \delta_7, \delta_8 = 5^o$, center of gravity of 60.1 percent of $\bar{c}_{ref}$.

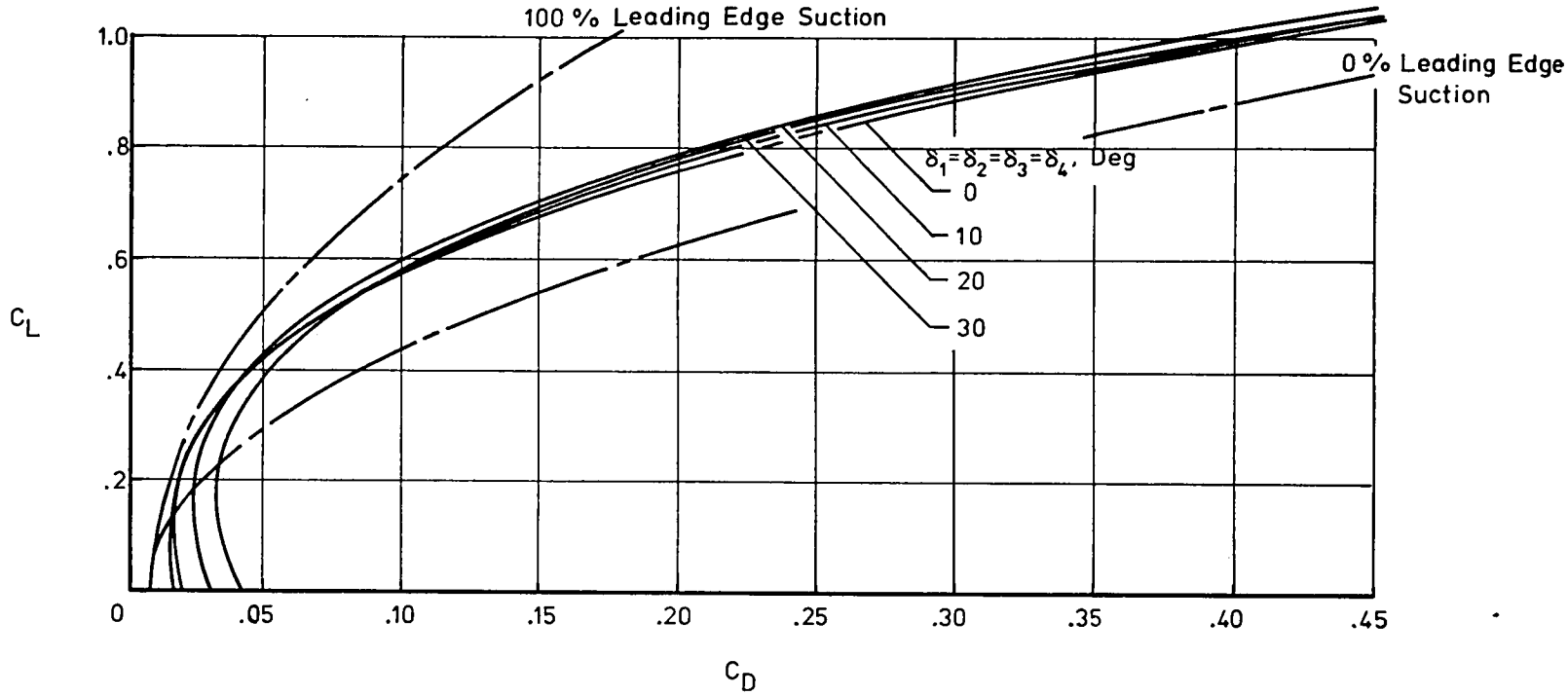

Figure 10.- Trimmed drag polar (out of ground effect), landing gear retracted, center of gravity at 60.1 percent mean aerodynamic chord, $\delta_9 = \delta_{10} = \delta_{11} = \delta_{12} = 30^0$, $\delta_{13} = \delta_{14} = 45^0$, $\delta_5 = \delta_6 = \delta_7 = \delta_8 = 5^0$.

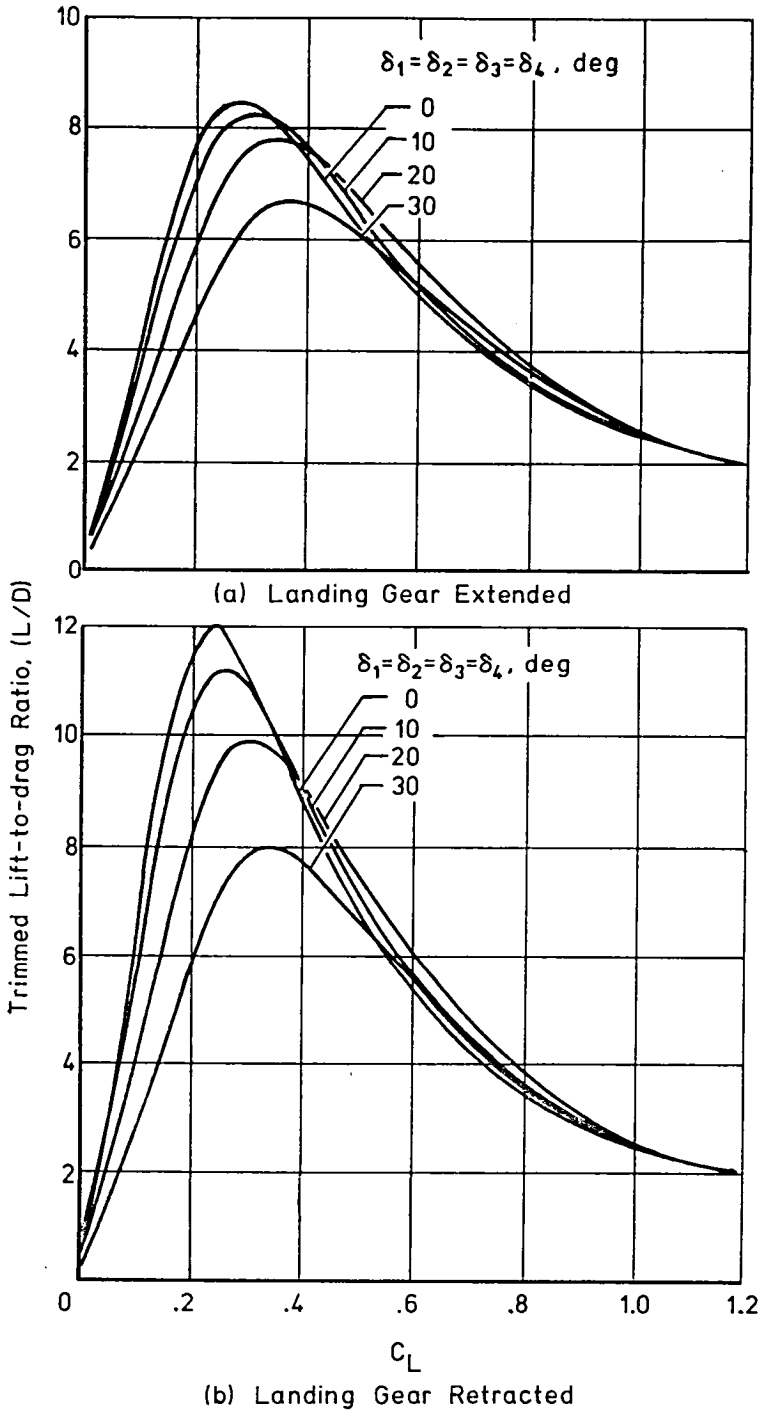

Figure 11.- High-lift configuration aerodynamic performance (out of ground effect), center of gravity at 60.1 percent, of $\bar{c}_{ref}$. $\delta_9 = \delta_{10} = \delta_{11} = \delta_{12} = 30^o$, $\delta_{13} = \delta_{14} = 45^o$, $\delta_5 = \delta_6 = \delta_7 = \delta_8 = 5^o$.

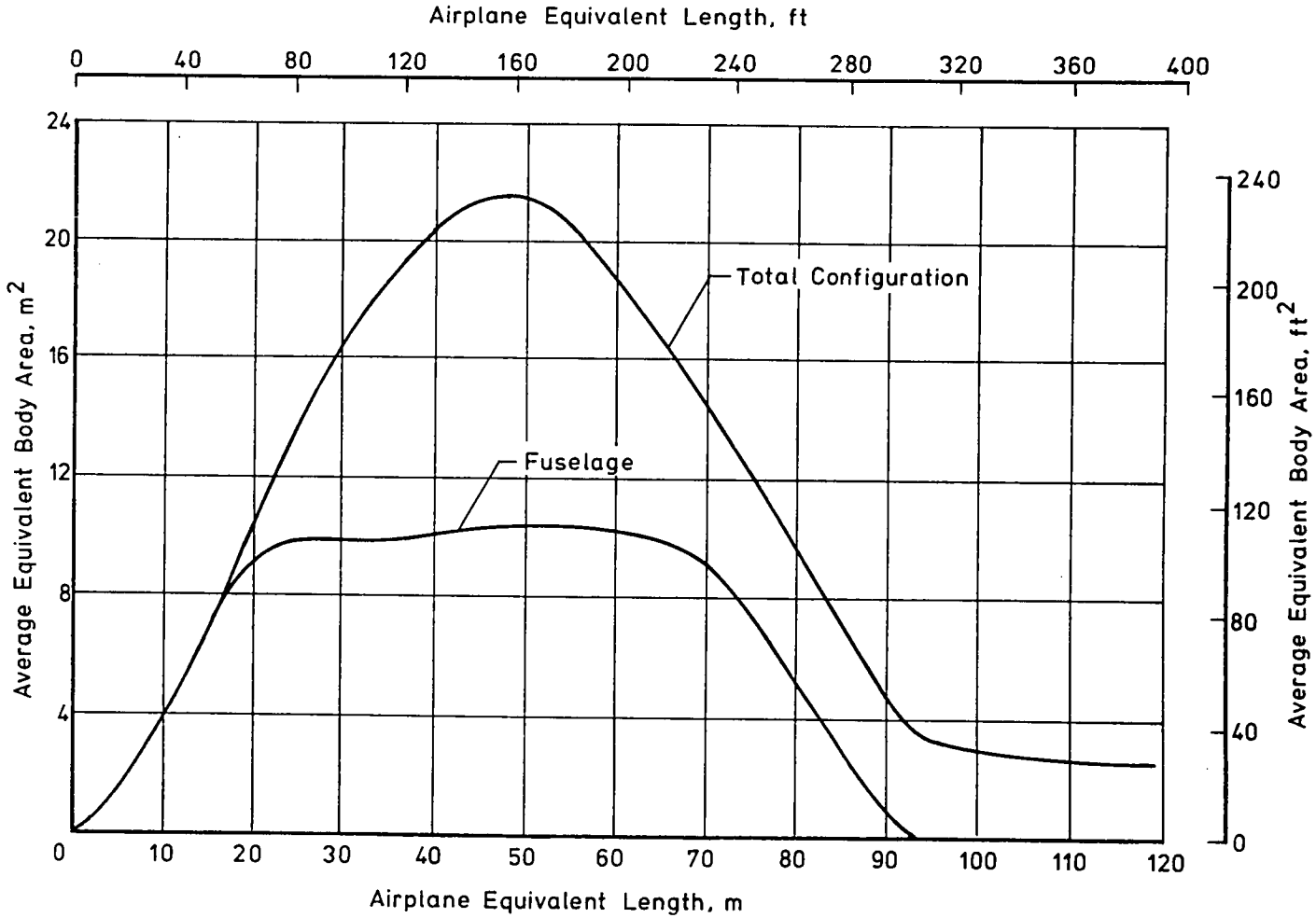

Figure 12.- Equivalent area distribution, M = 2.62.

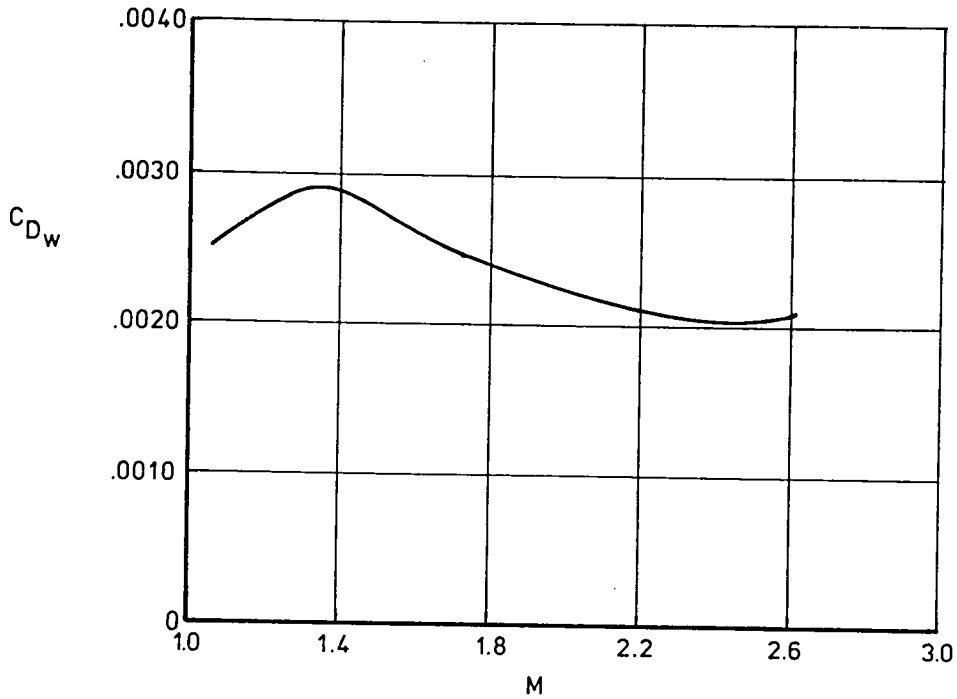

Figure 13.- Wave drag coefficient as a function of Mach number.

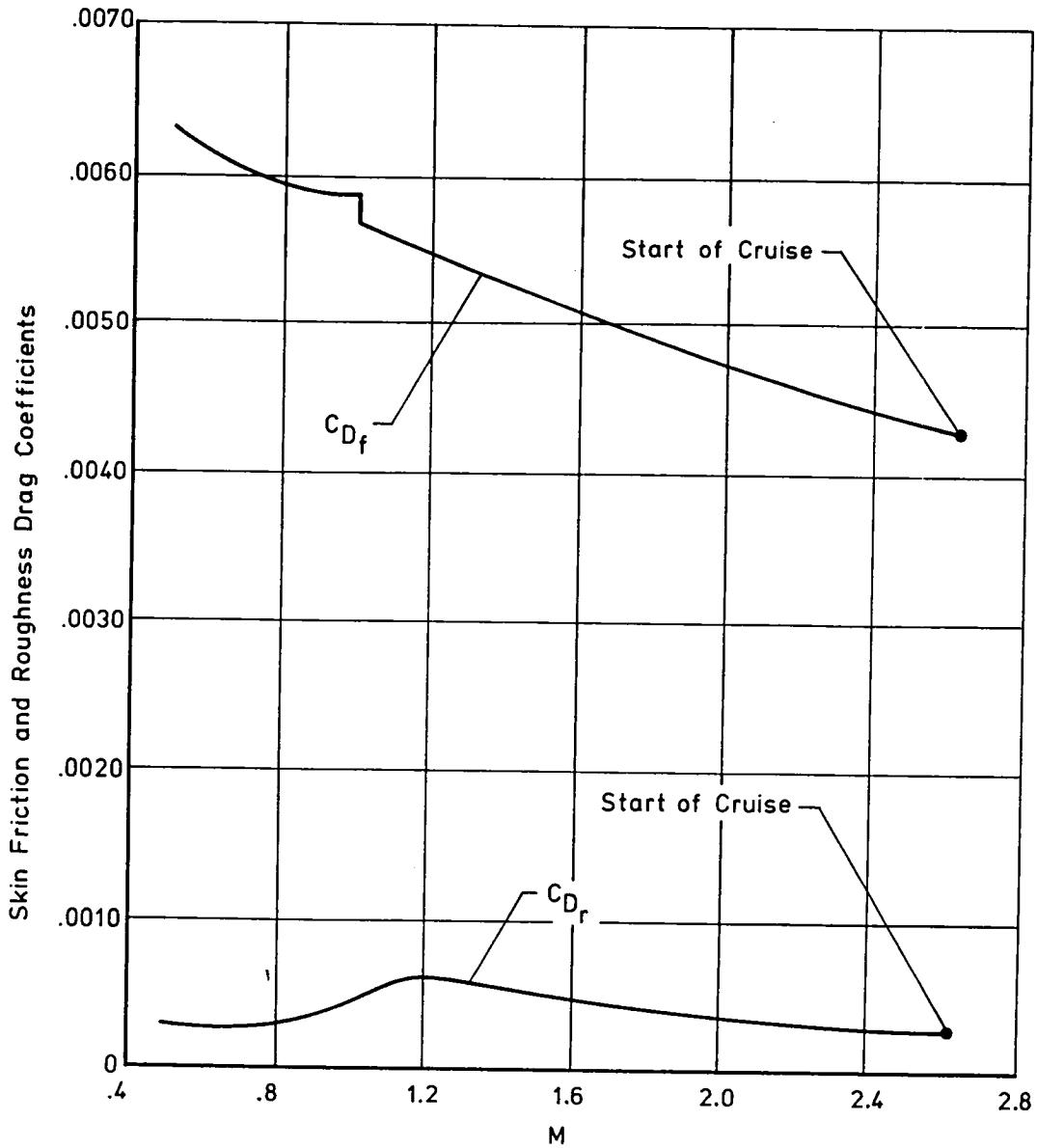

Figure 14.- Skin friction and roughness drag coefficient as a function of of Mach number for the design mission trajectory of figure 49.

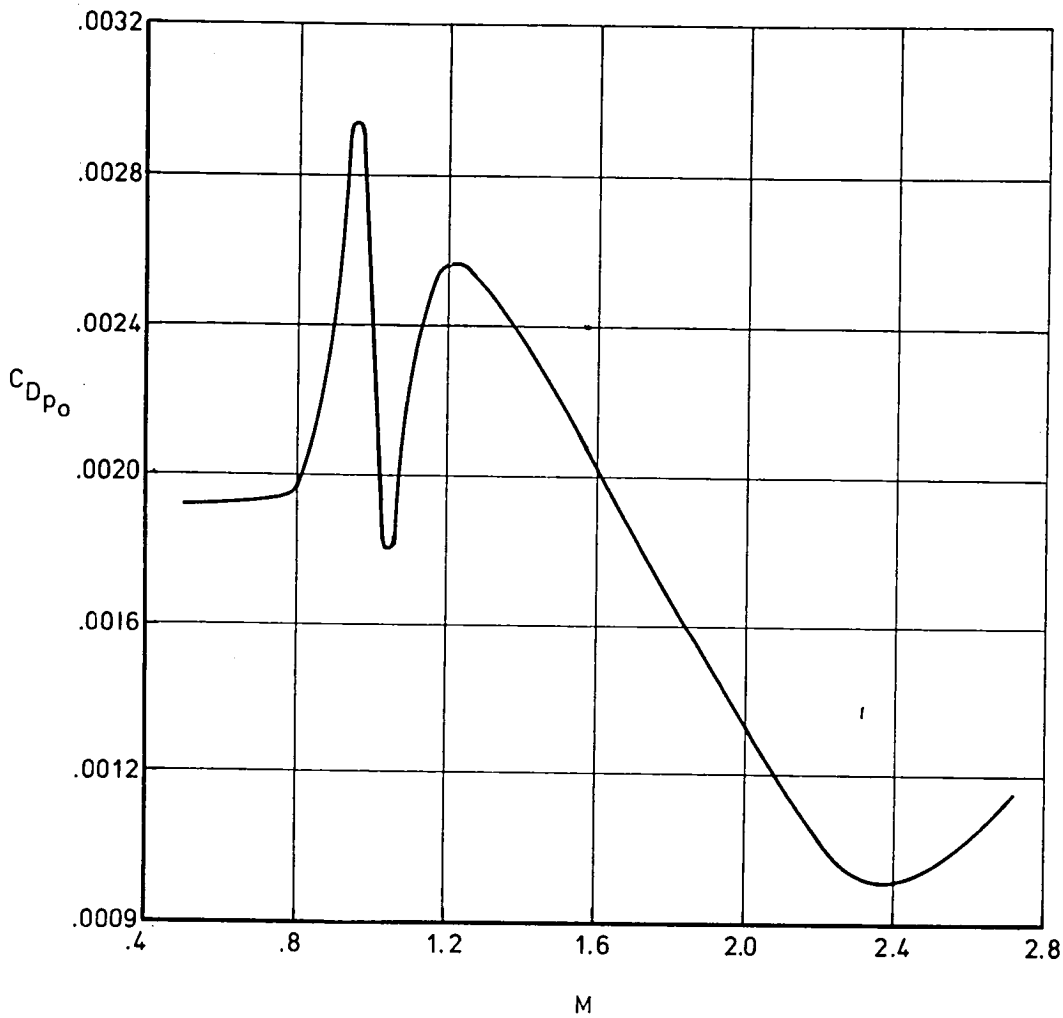

Figure 15.- Parasite drag coefficient as a function of Mach number.

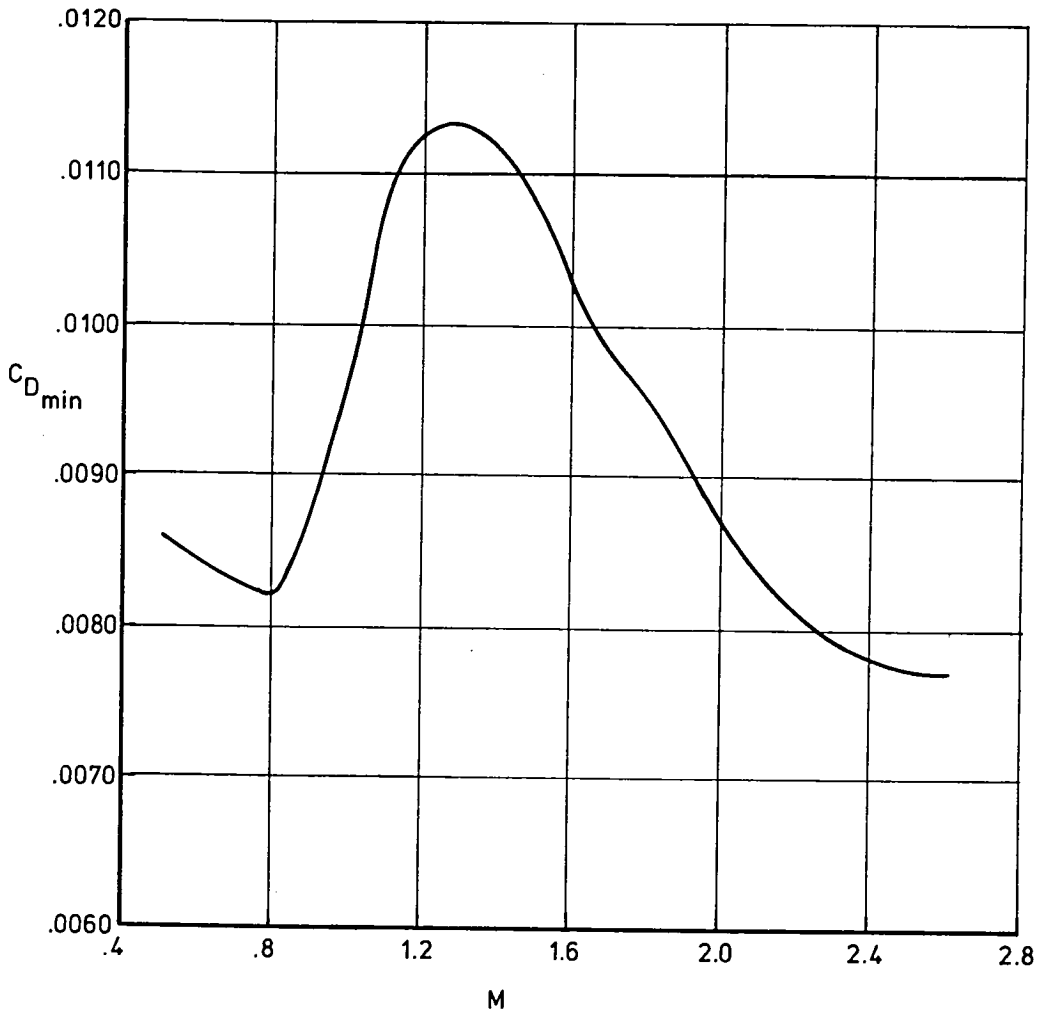

Figure 16.- Minimum drag coefficient as a function of Mach number.

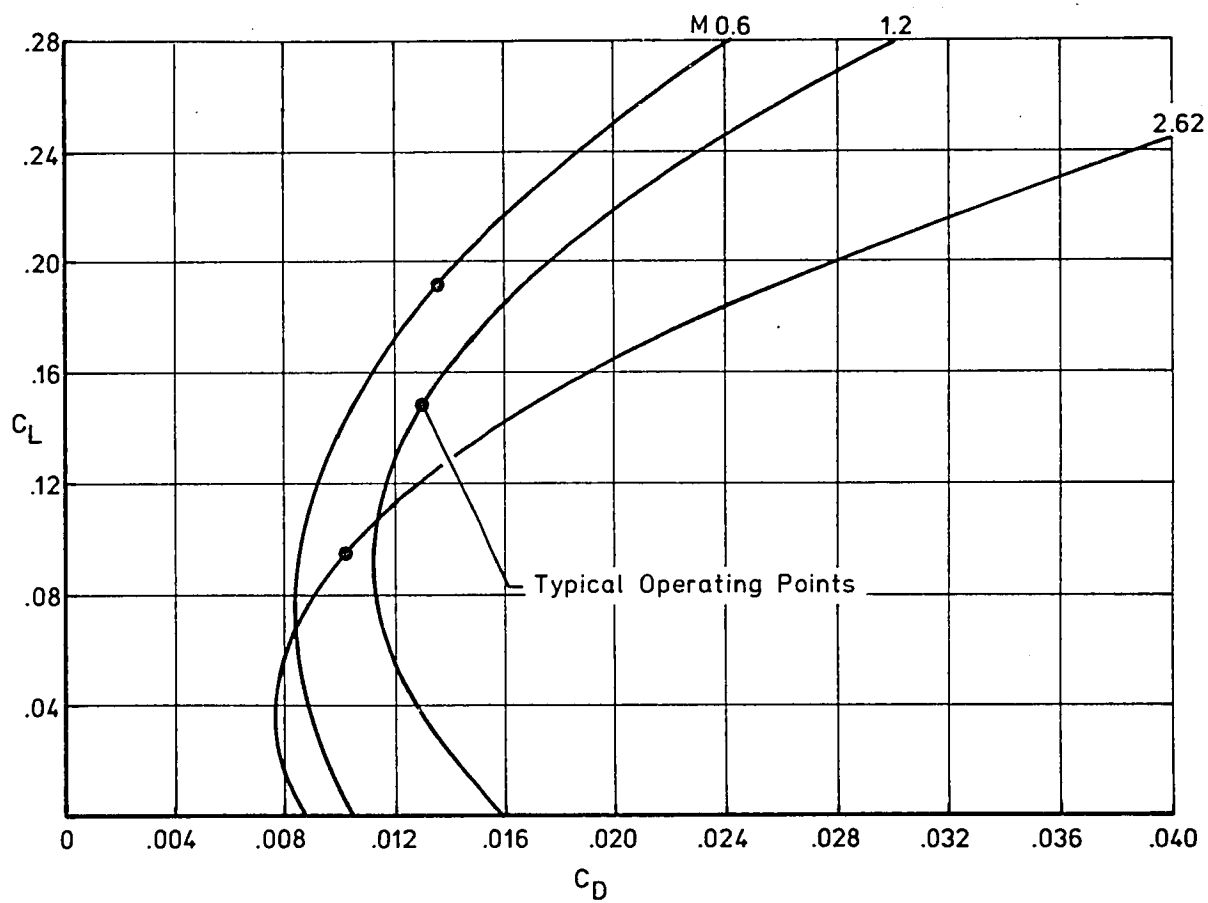

Figure 17.- Typical drag polars at several Mach numbers for the clean configuration.

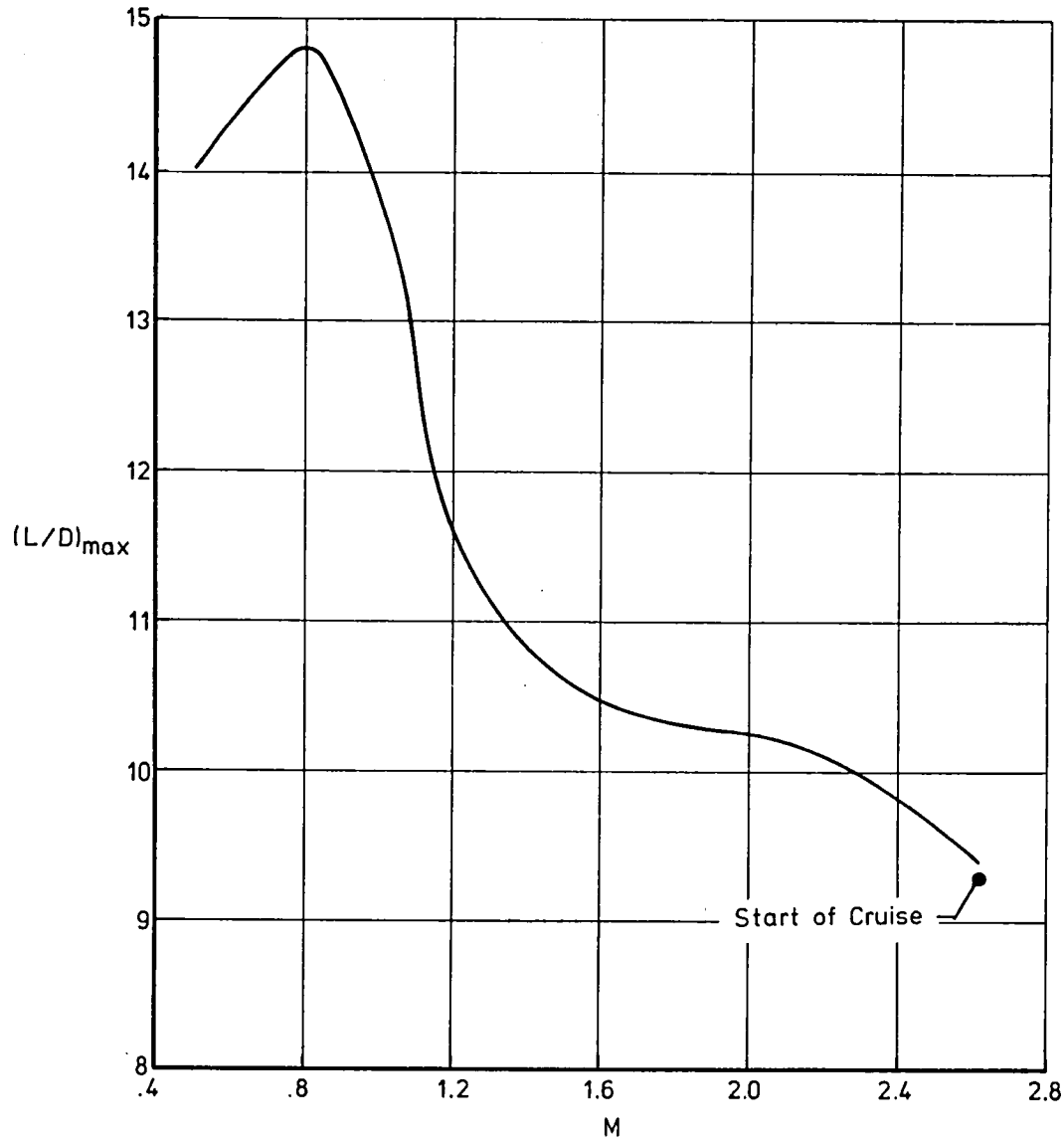

Figure 18.- Maximum lift-to-drag ratio as a function of Mach number.

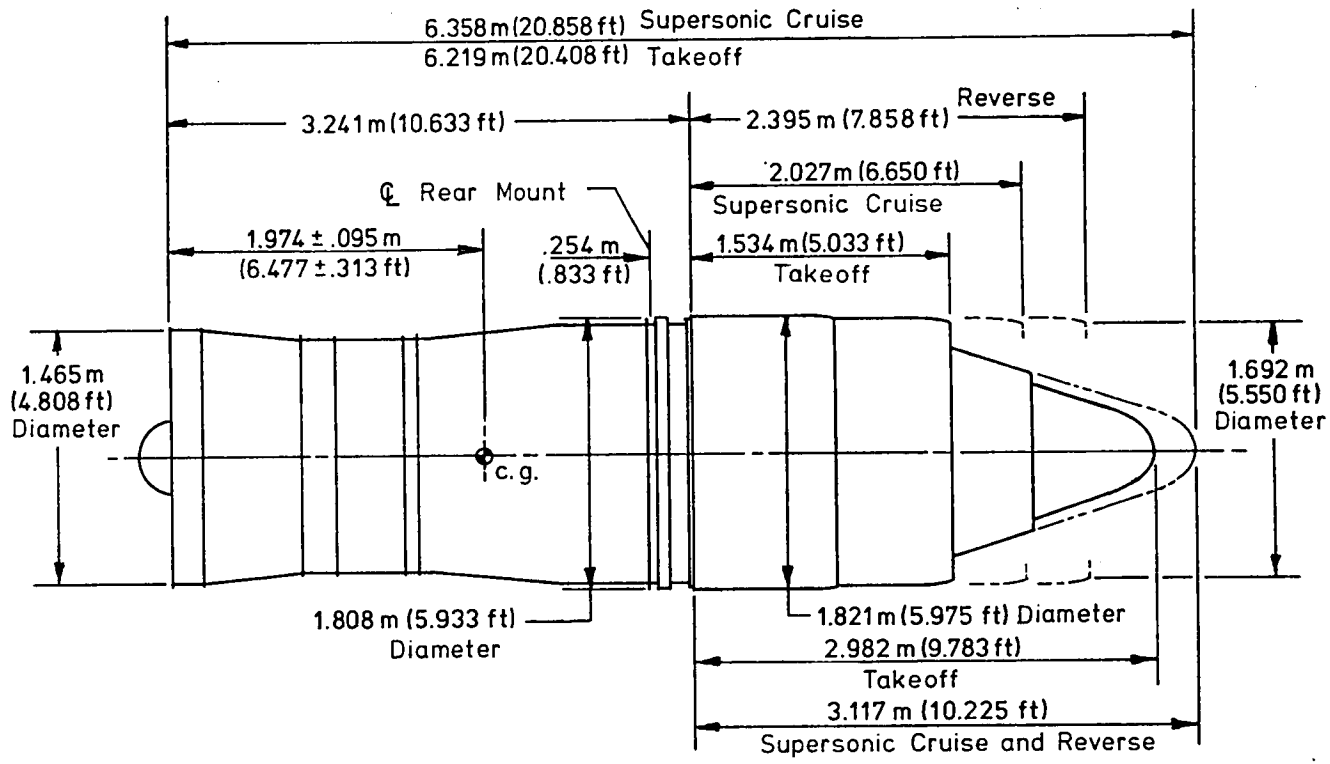

Figure 19.- The General Electric GE21/J10-B5 low-bypass ratio engine.

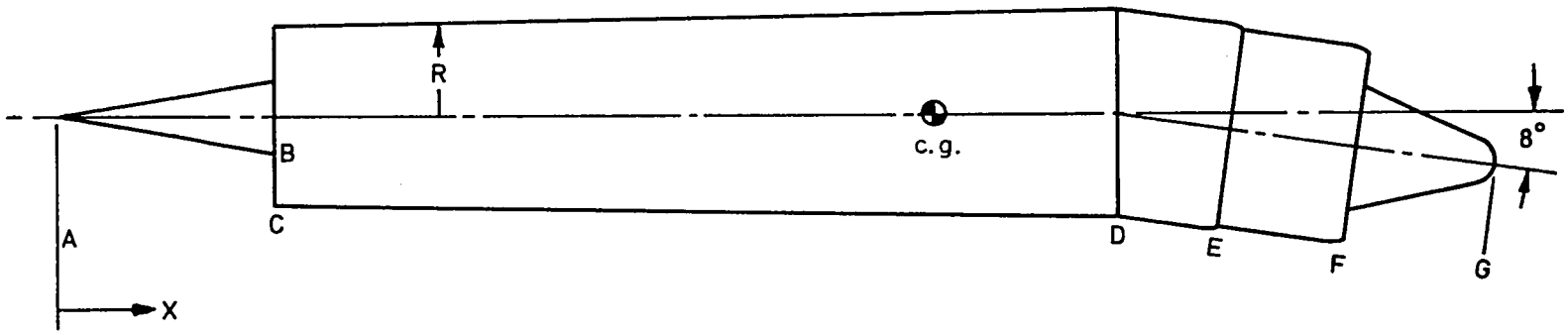

Station	X		R		Area	
	m	ft	m	ft	m^2	ft^2
A	0	0	0	0	0	0
B	1.948	6.391	.308	1.012	.299	3.217
C	1.948	6.391	.790	2.591	1.959	21.090
D	8.936	29.319	.911	2.988	2.606	28.049
E	9.933	32.588	.885	2.905	2.463	26.511
F	11.091	36.389	.846	2.775	2.248	24.192
G	12.181	39.964	0	0	0	0
c. g. (Engine)	7.666	25.152				

Figure 20.- GE21/J10-B5 engine nacelle.

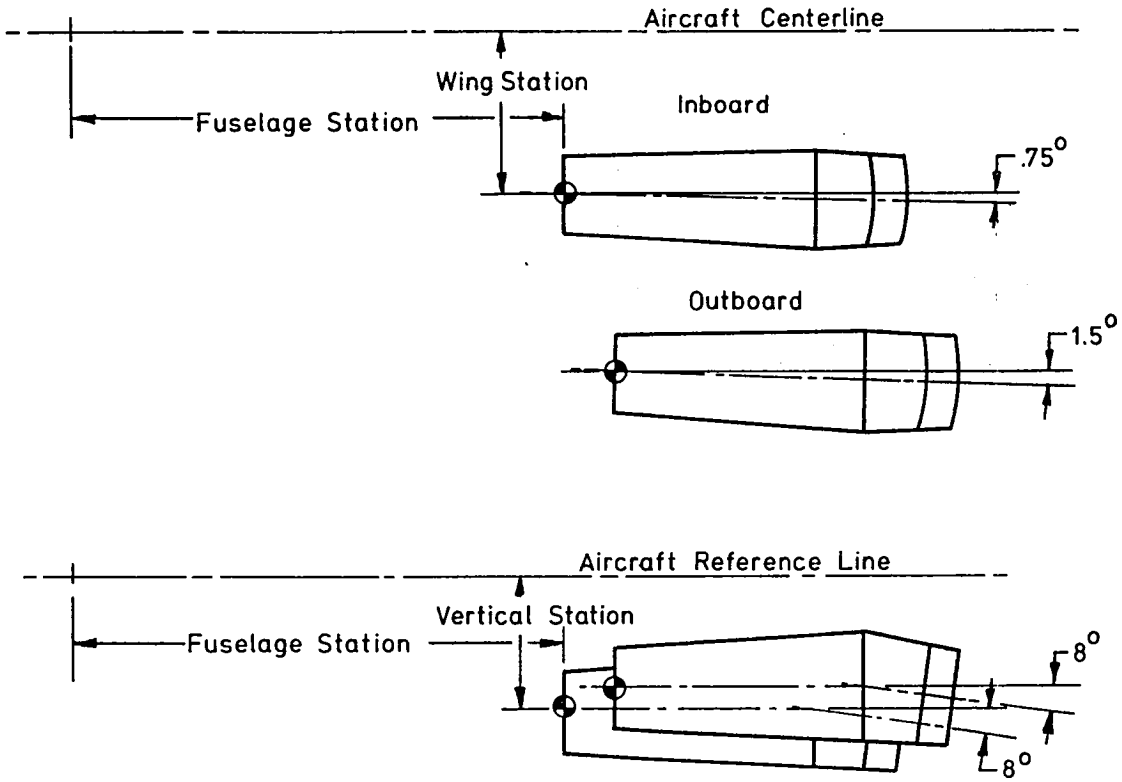

⊕ Inboard Nacelle	in	ft	m
Fuselage Station	2328.220	194.018	59.137
Wing Station	248.736	20.728	6.318
Vertical Station	-211.583	-17.632	-5.374
⊕ Outboard Nacelle			
Fuselage Station	2372.590	197.716	60.264
Wing Station	407.508	33.959	10.351
Vertical Station	-204.462	-17.038	-5.193

Figure 21.- Engine-nacelle location detail.

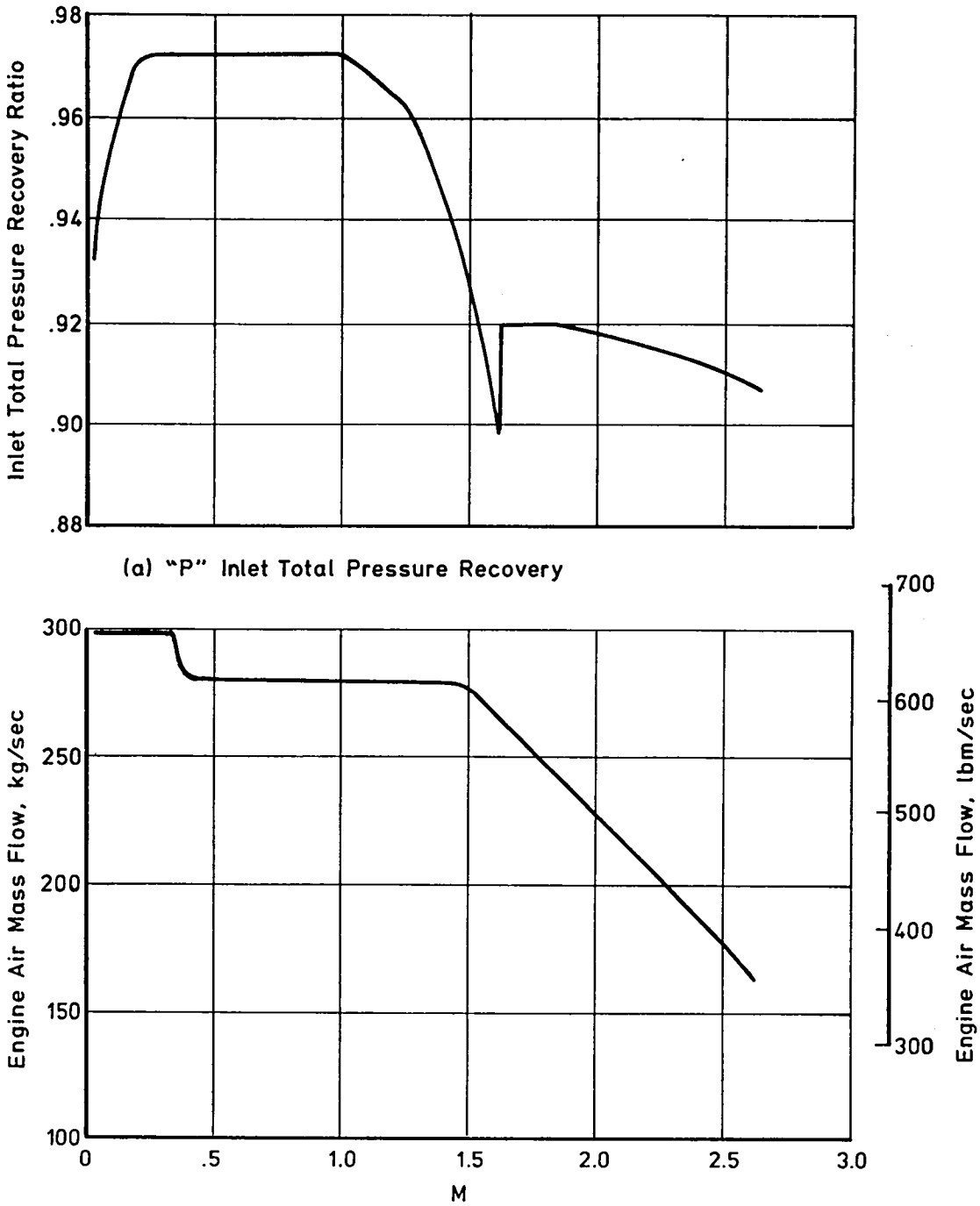

Figure 22.- NASA/Ames "P" inlet performance.

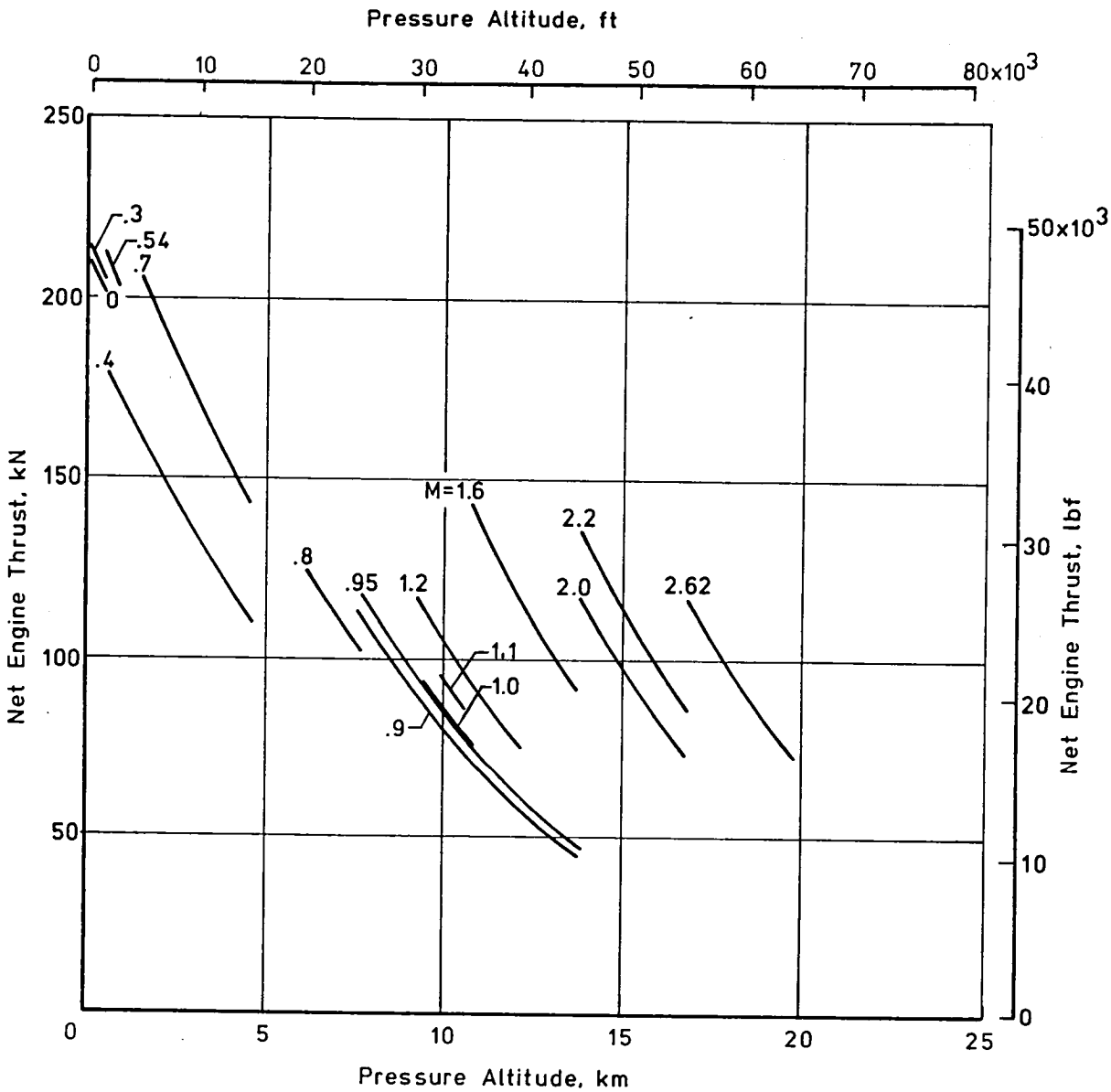

(a) Maximum Climb Power Setting

Figure 23 - GE21/J10-B5 installed net thrust at standard day plus eight degrees centigrade ambient temperature.

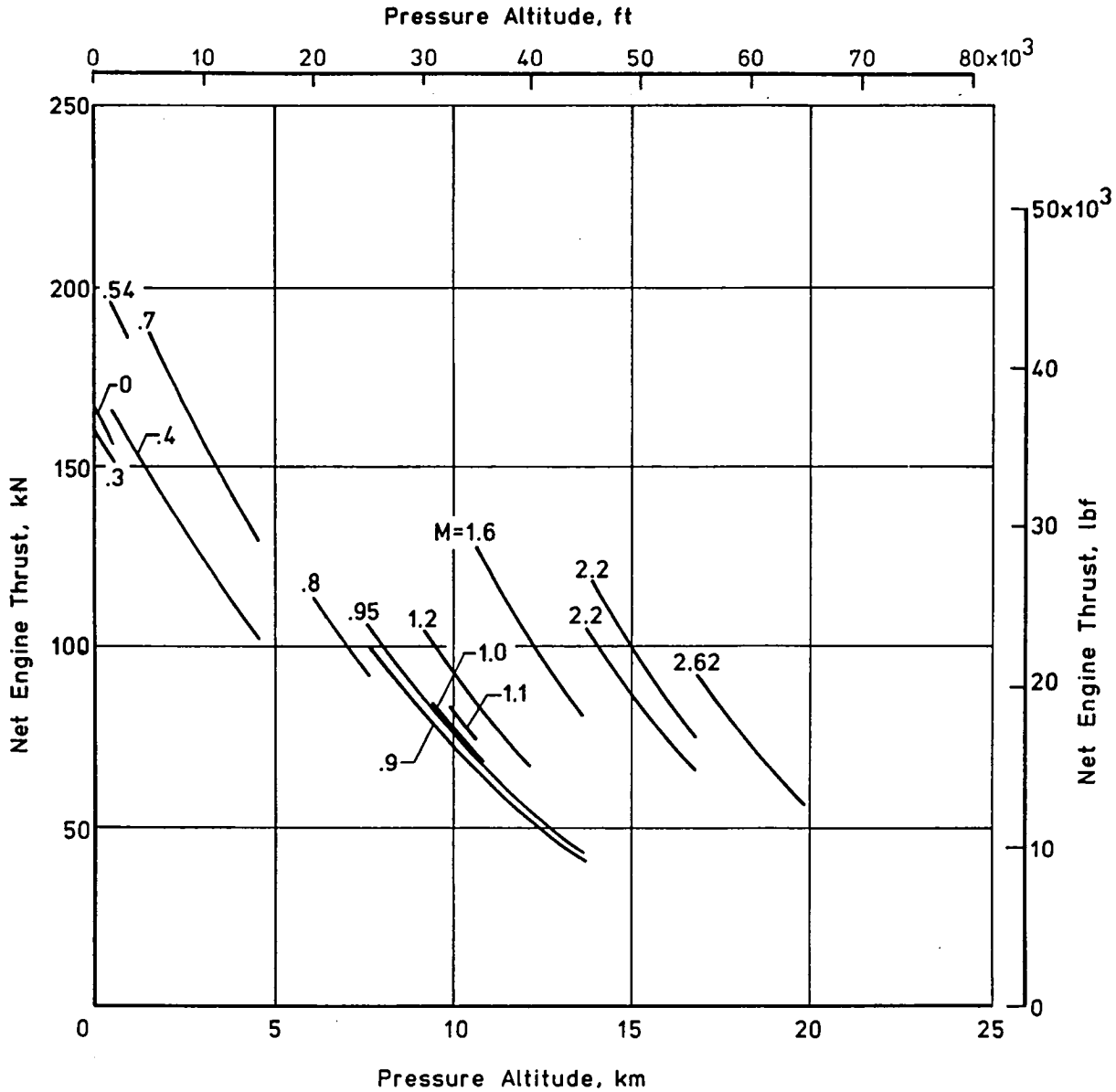

(b) Maximum Cruise Power Setting

Figure 23 - Concluded.

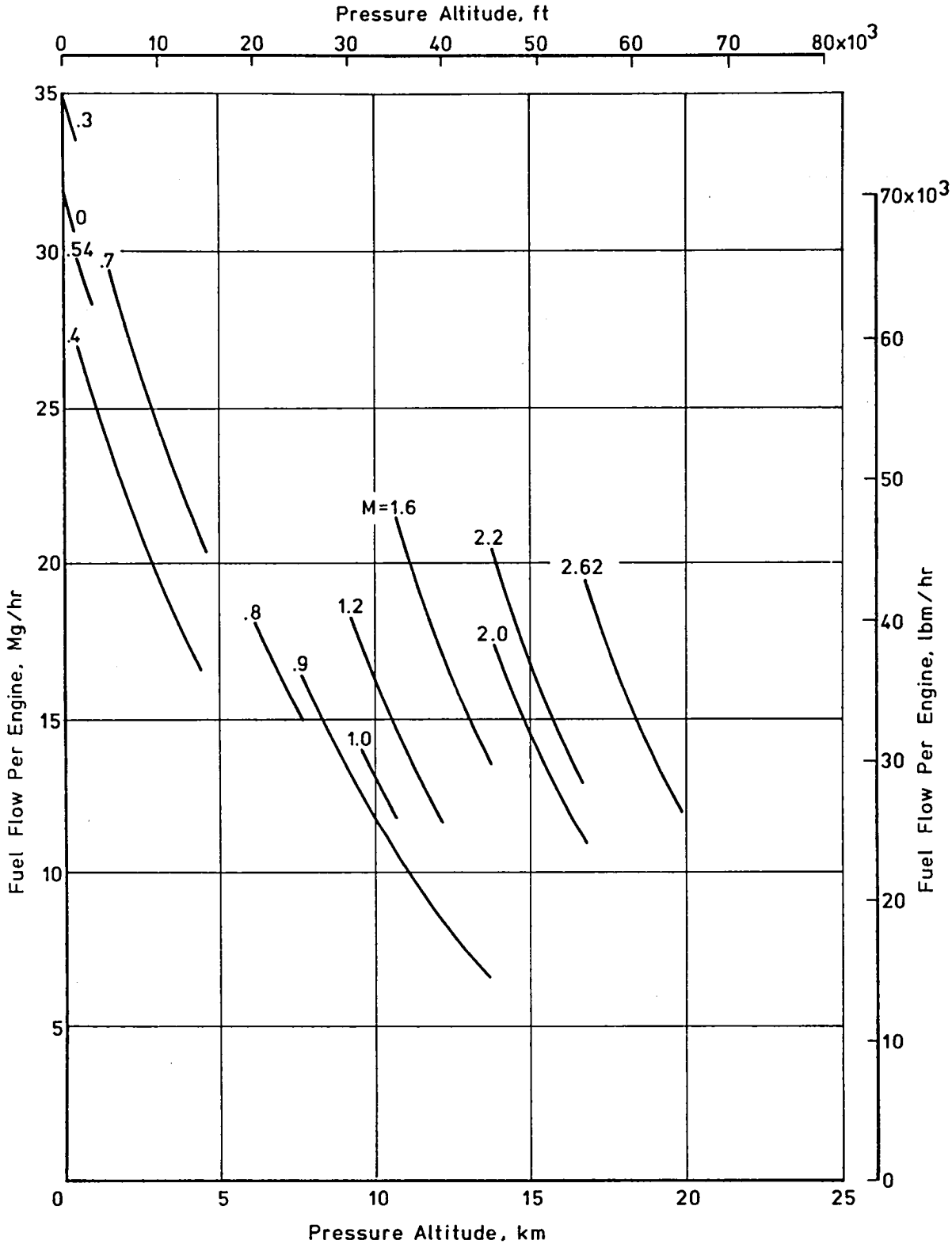

(a) Maximum Climb Power Setting

Figure 24 - GE21/J10-B5 installed fuel flow rate at a standard day plus eight degrees centigrade ambient temperature.

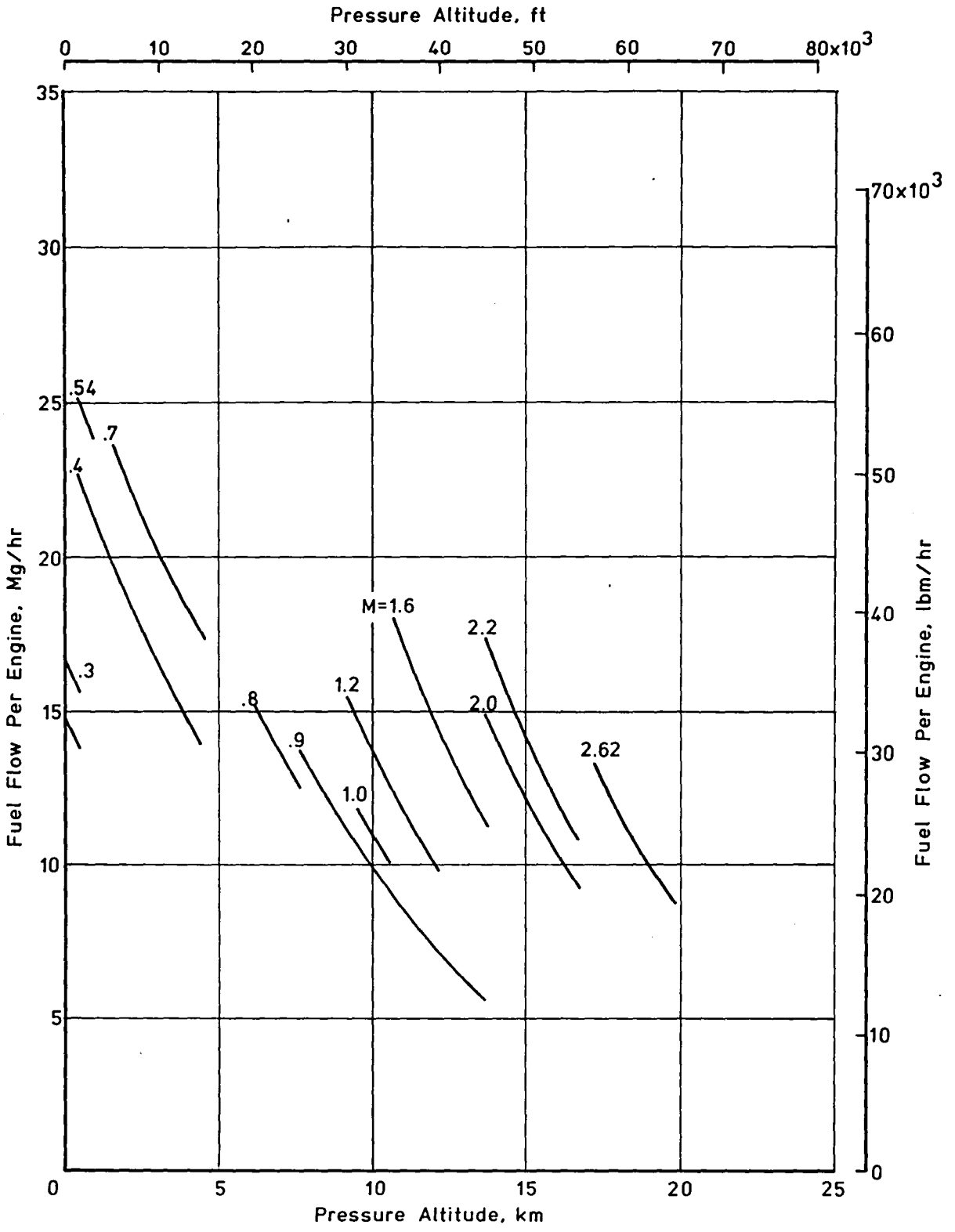

(b) Maximum Cruise Power Setting

Figure 24 - Concluded.

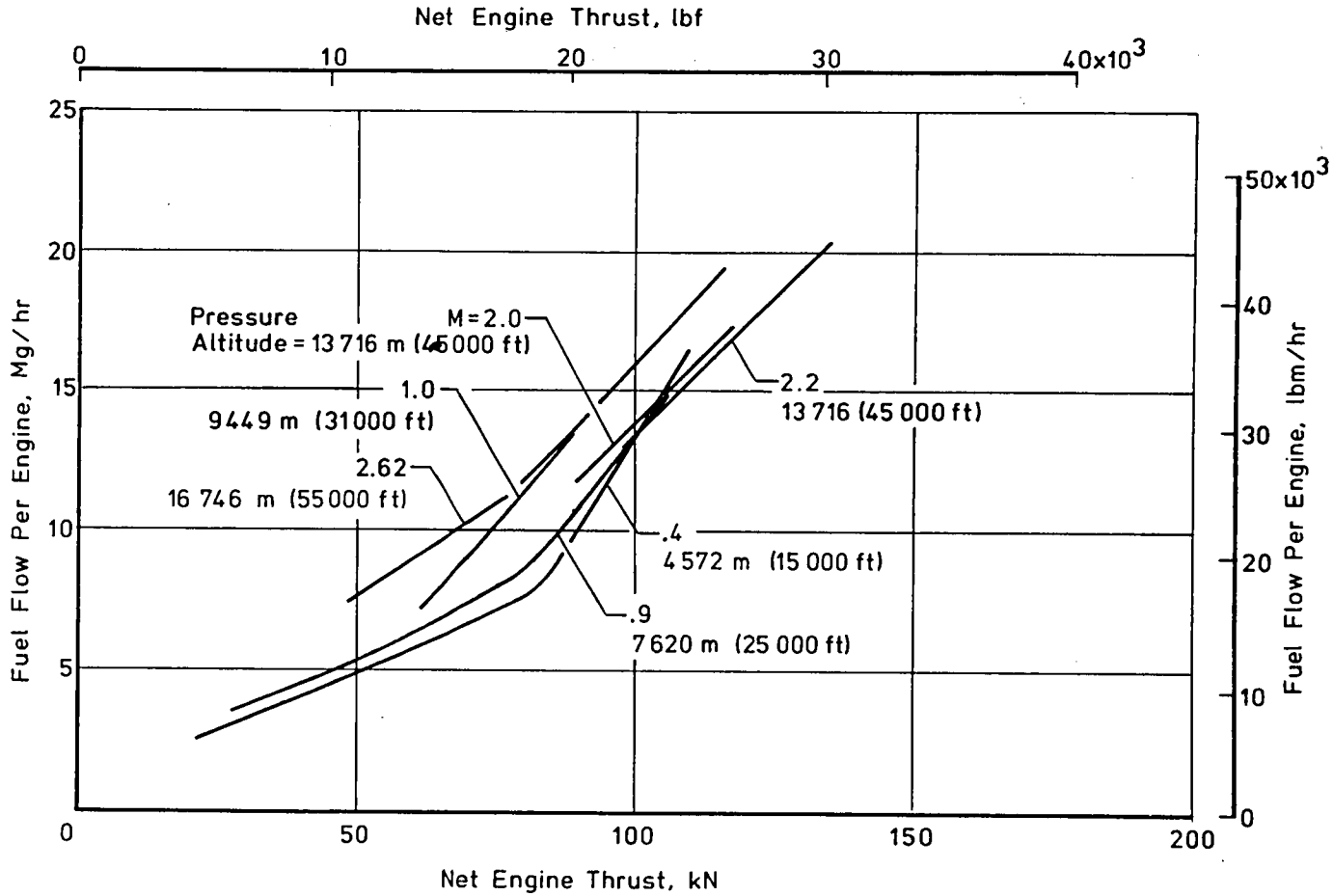

Figure 25.- Installed fuel flow for maximum and part power cruise at a standard day plus eight degree centigrade ambient temperature.

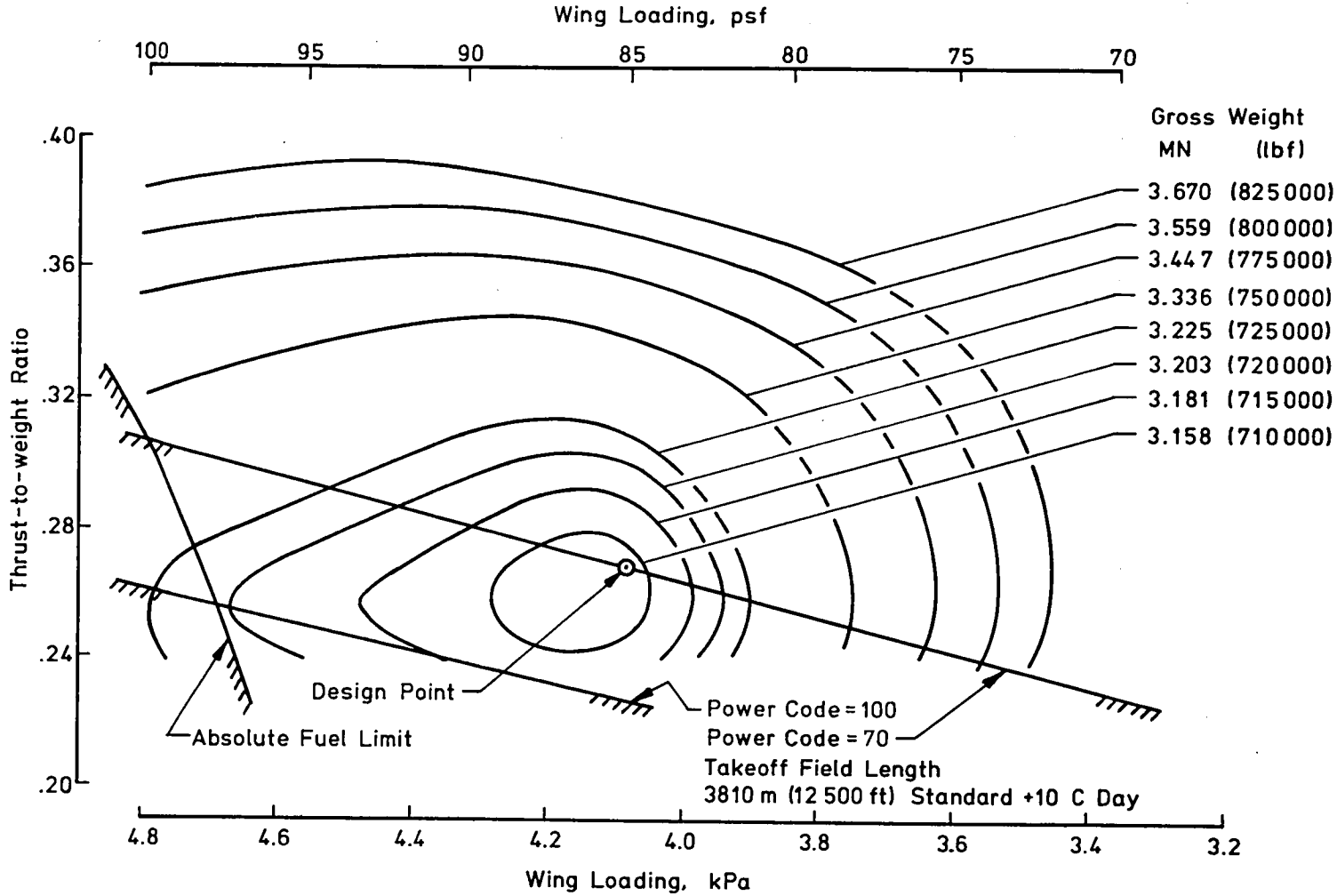

Figure 26 - Aircraft sizing "thumbprint" for the AST-107 carrying 273 passengers over a range of 8334 km (4500 n.mi.) at M = 2.62 hot day cruise conditions.

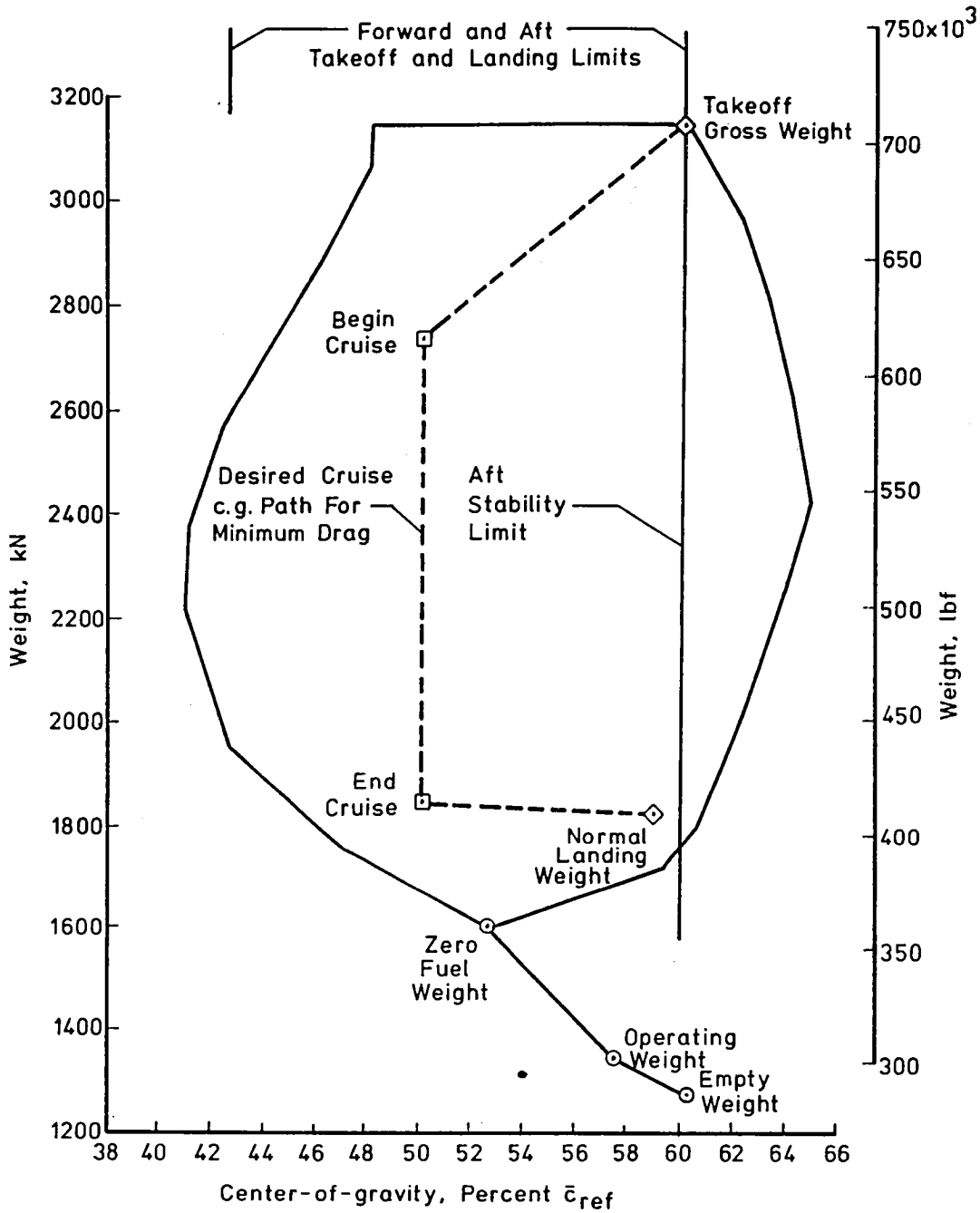

Figure 27. - Center-of-gravity travel diagram.

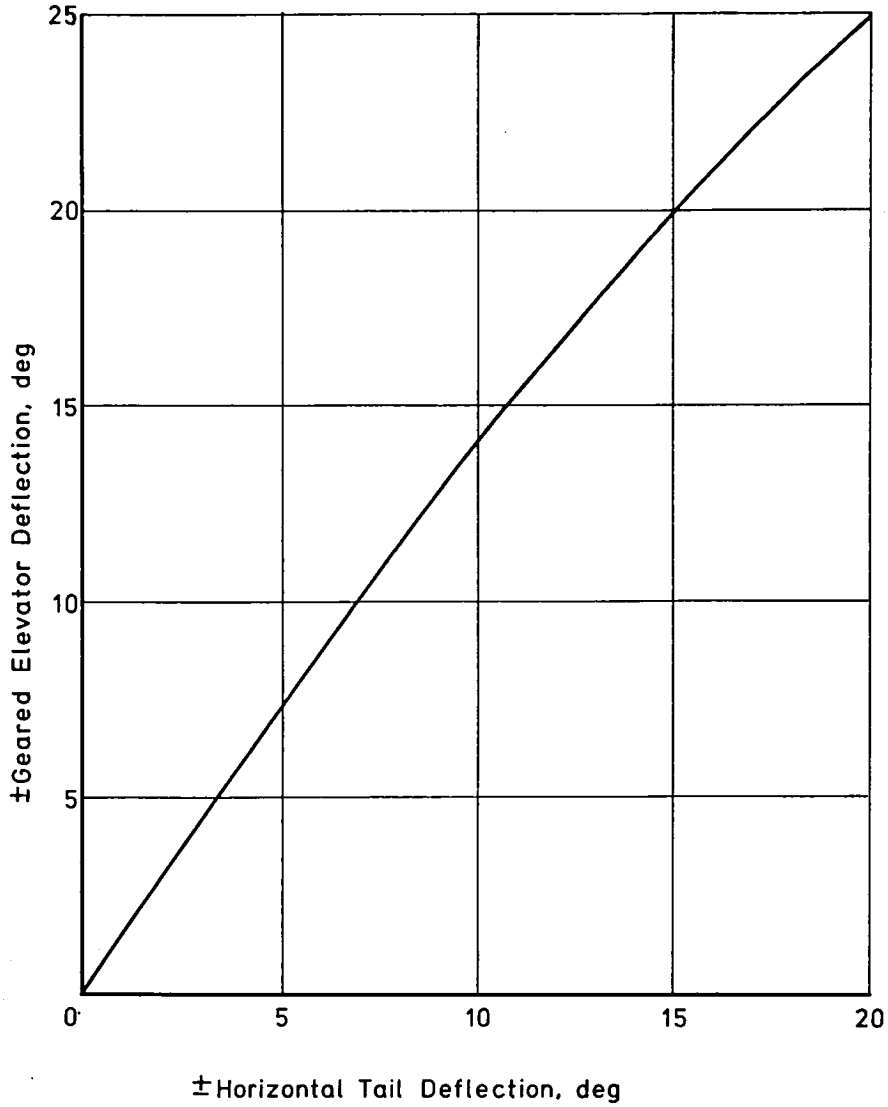

Figure 28. - Assumed horizontal tail/elevator deflection relationship.

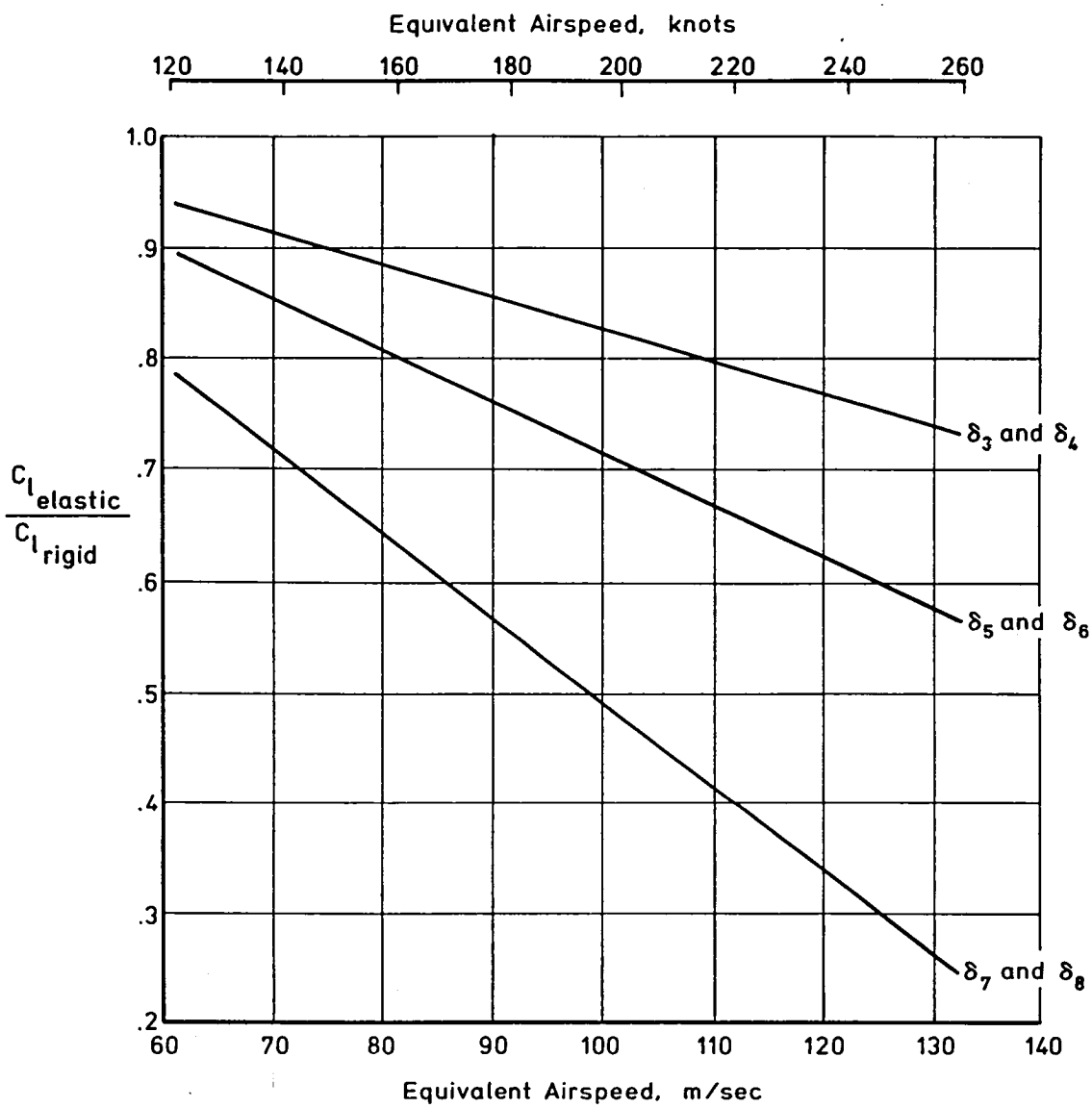

Figure 29. - Estimated lateral control flexibility factors.

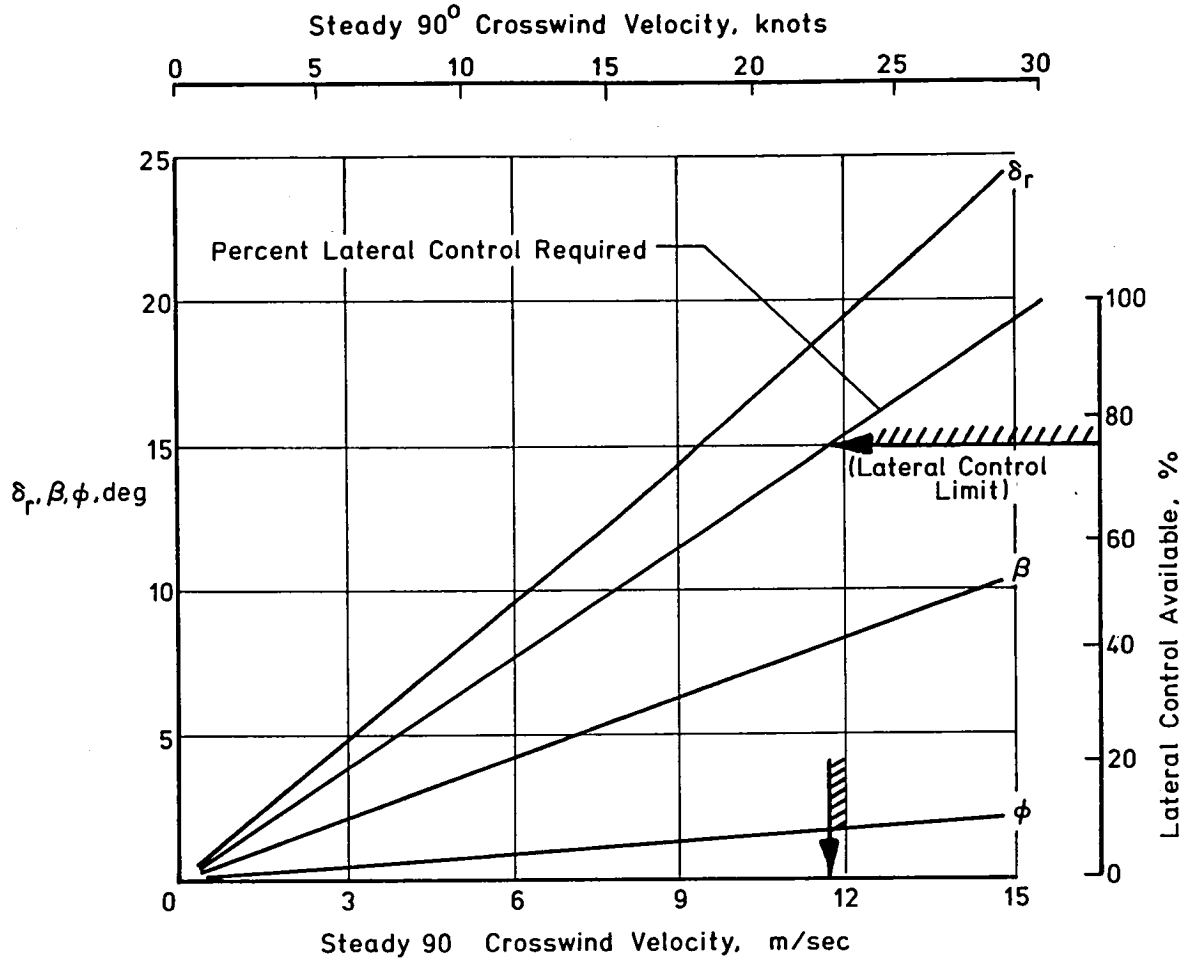

Figure 30. - Crosswind trim capability at an approach speed of 81.3 m/sec (158 knots).

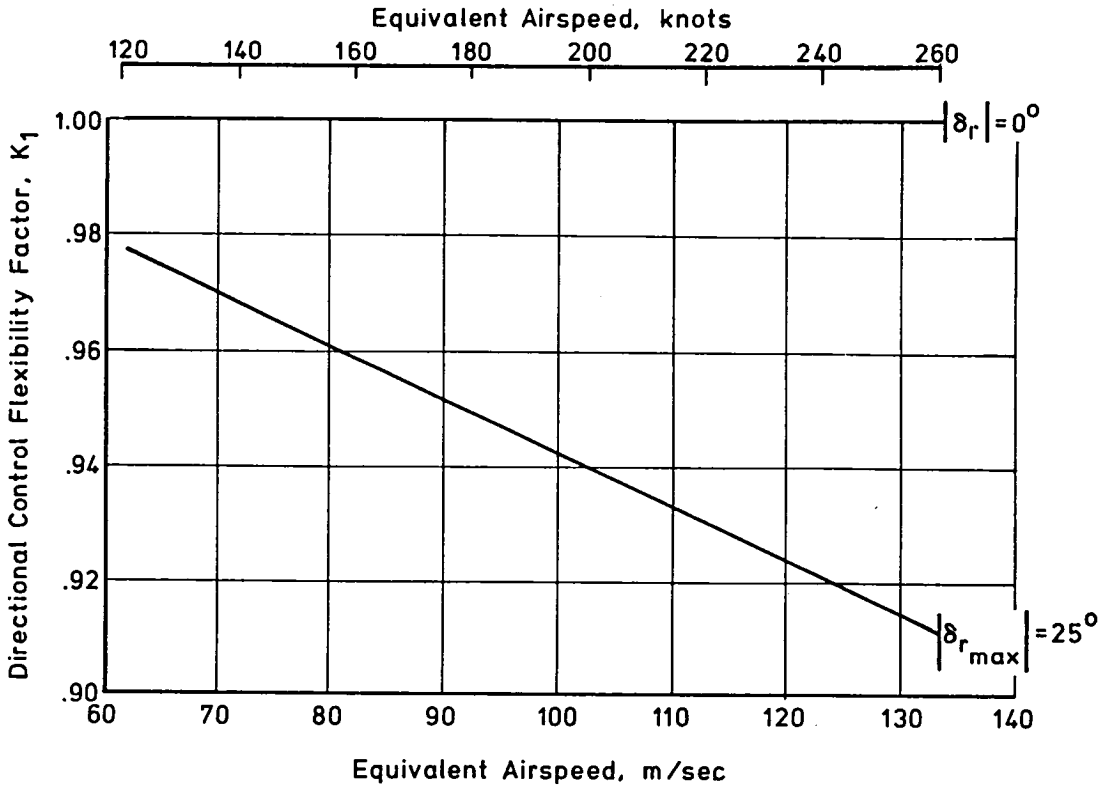

Figure 31. - Estimated directional control factors due to fuselage bending.

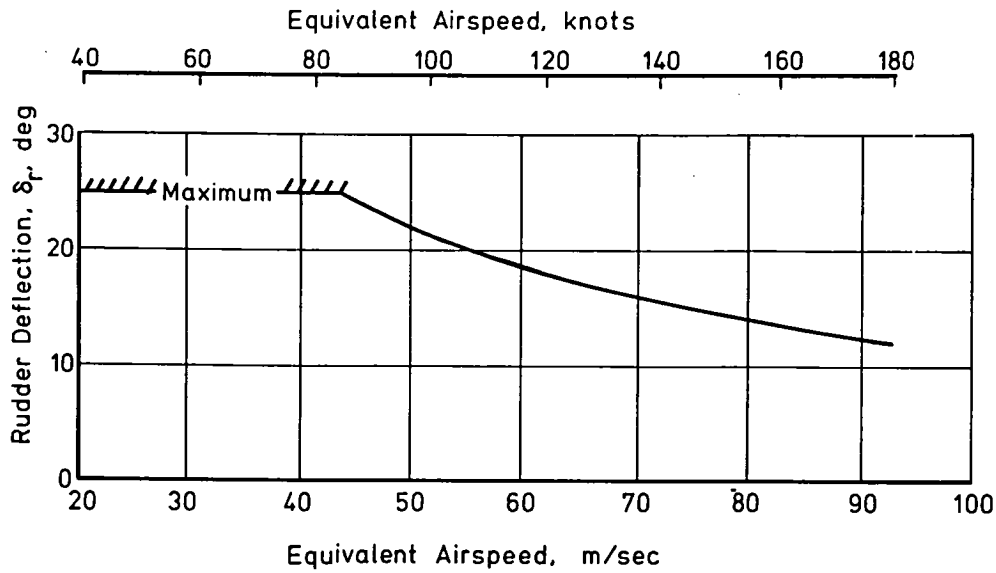

Figure 32. - Estimated directional control factors due to fuselage bending.

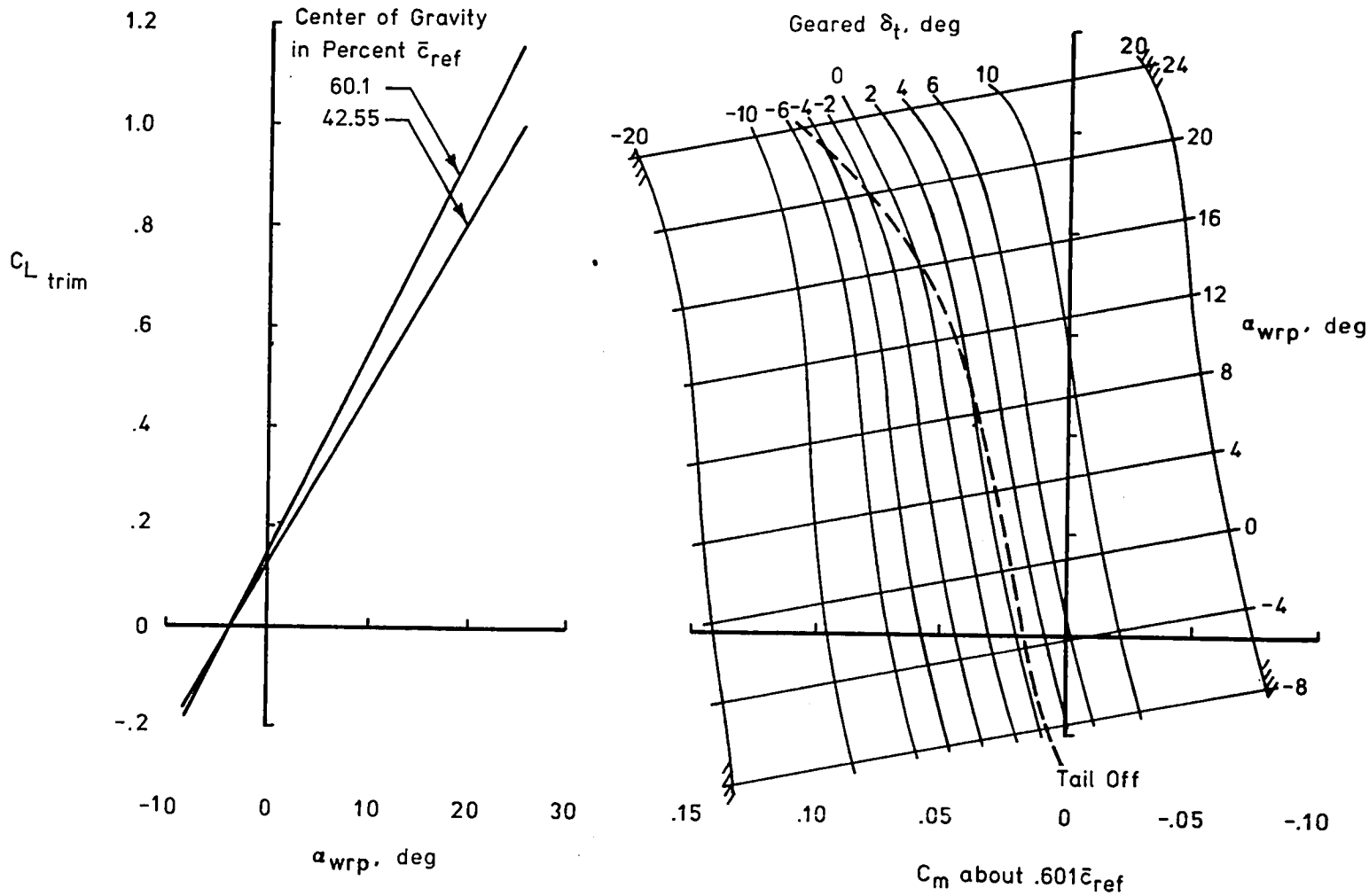

Figure 33. - Directional trim required in 90-degree crosswind at maximum gross weight for an angle of attack of the wing reference plane of -5^{0} and a crosswind velocity of 11.58 m/sec (22.5 knot).

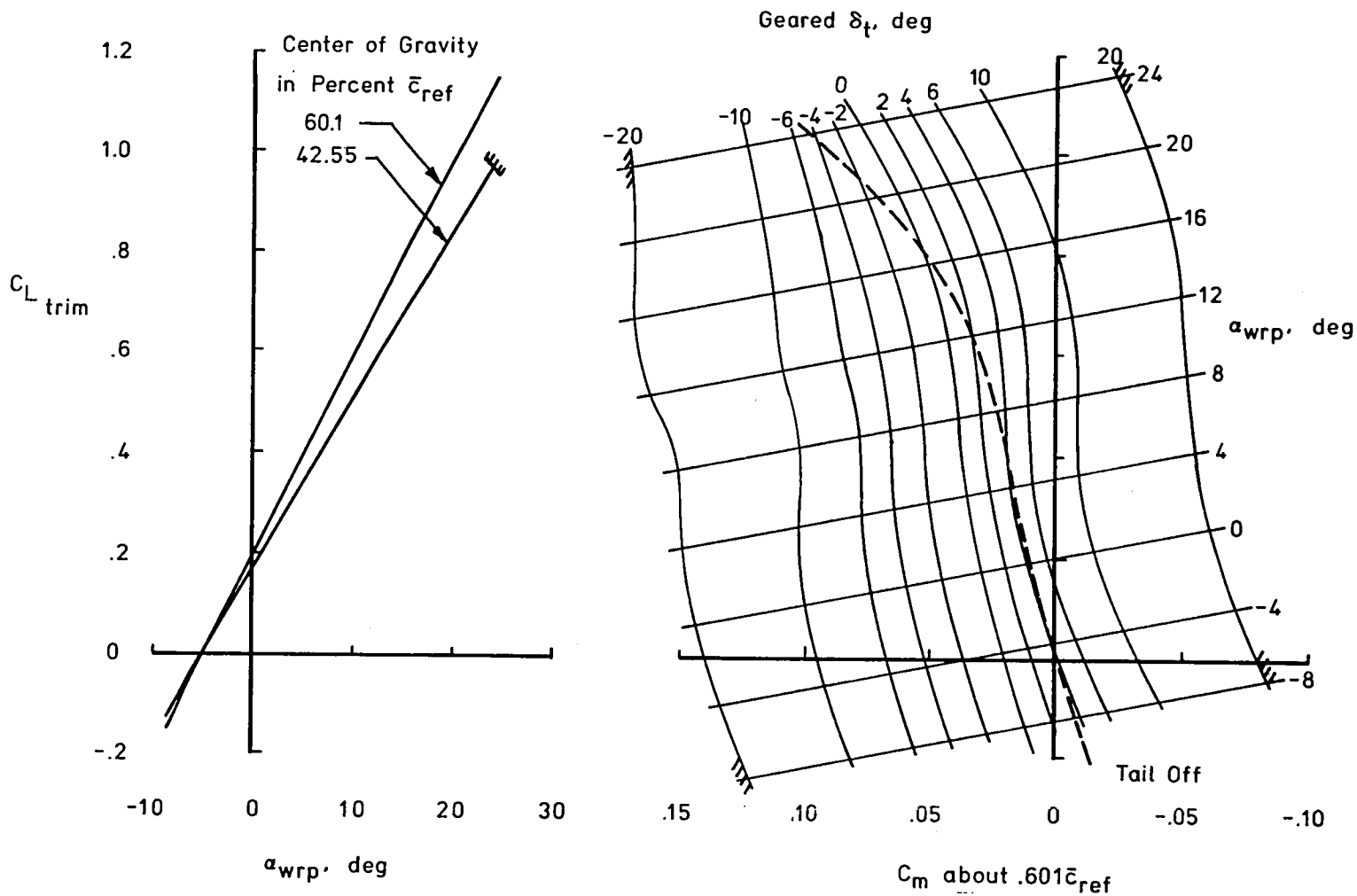

Figure 34. - High-lift trim and stability (out of ground effect), with power off, $\delta_5 = \delta_6 = \delta_7 = \delta_8 = 30^o$, $\delta_1 = \delta_2 = \delta_3 = \delta_4 = 20^o$.

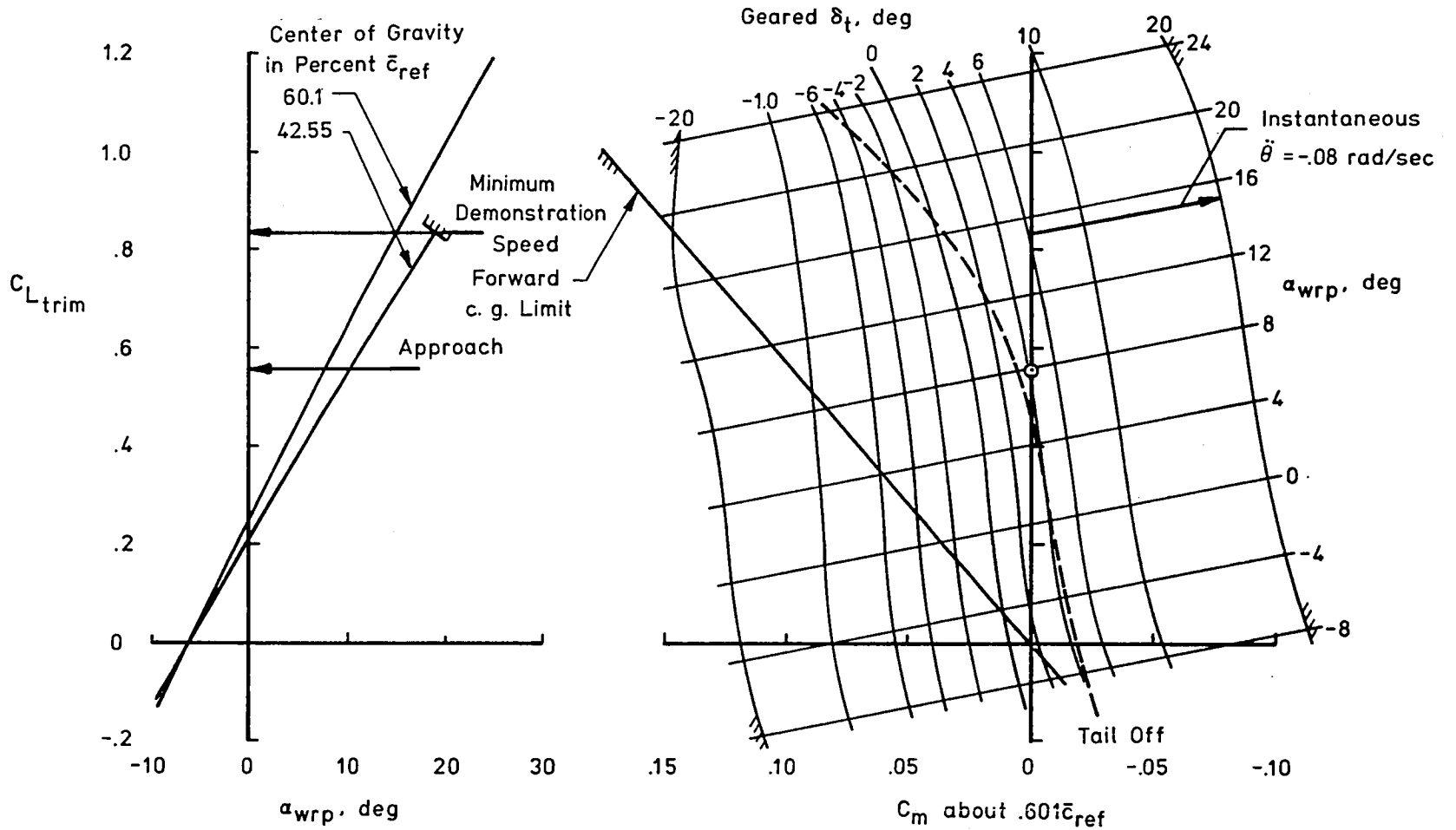

Figure 35. - High-lift trim and stability (out of ground effect), with power off, $\delta_9 = \delta_{10} = \delta_{11} = \delta_{12} = 30^0$, $\delta_{13} = \delta_{14} = 45^0$, $\delta_5 = \delta_6 = \delta_7 = \delta_8 = 5^0$, $\delta_1 = \delta_2 = \delta_3 = \delta_4 = 20^0$.

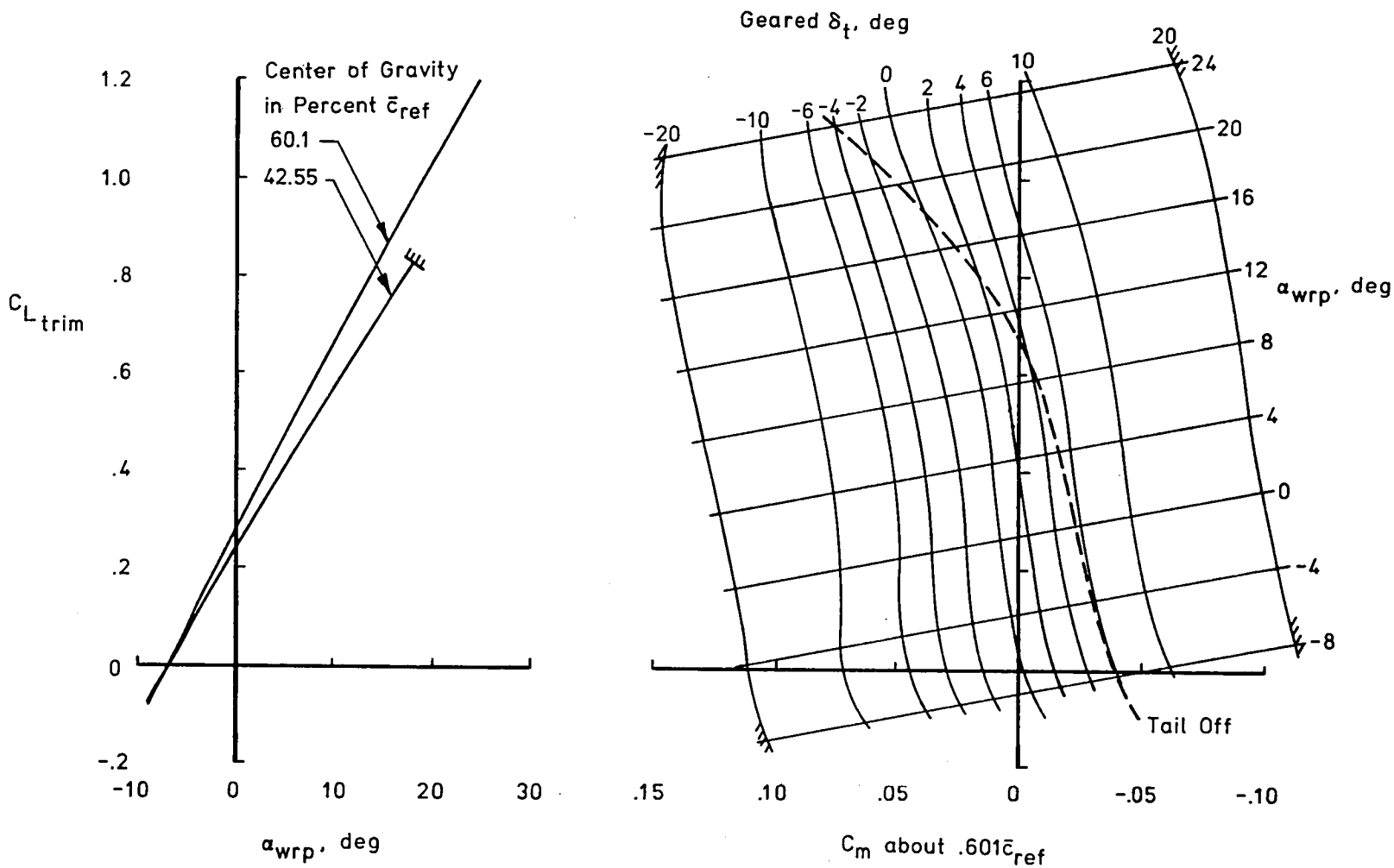

Figure 36. - High-lift trim and stability at thirty degrees (out of ground effect), with power off, $\delta_9 = \delta_{10} = \delta_{11} = \delta_{12} = 30^o$, $\delta_{13} = \delta_{14} = 45^o$, $\delta_1 = \delta_2 = \delta_3 = \delta_4 = 30^o$.

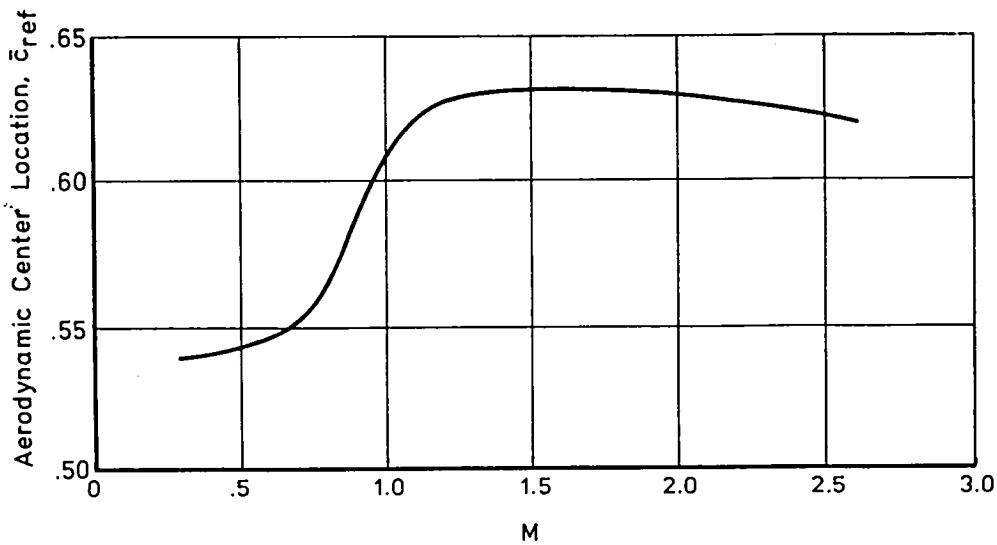

Figure 37. - Flexible airplane aerodynamic center location variation with Mach number with all flaps undeflected except $\delta_{13} = \delta_{14} = 20^{0}$ at Mach numbers less than 1.2.

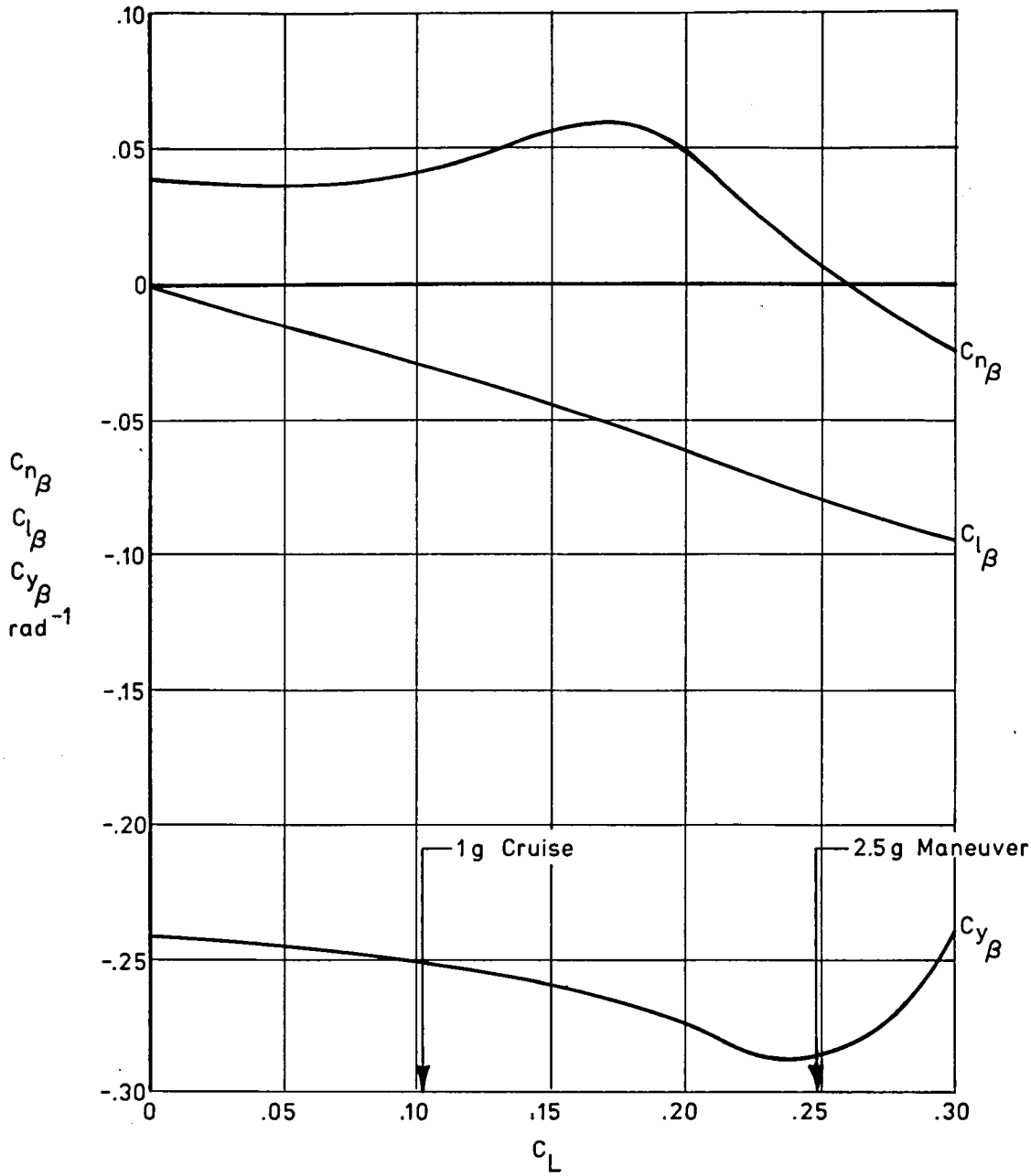

Figure 38. - Flexible static lateral-directional stability at M = 2.62.

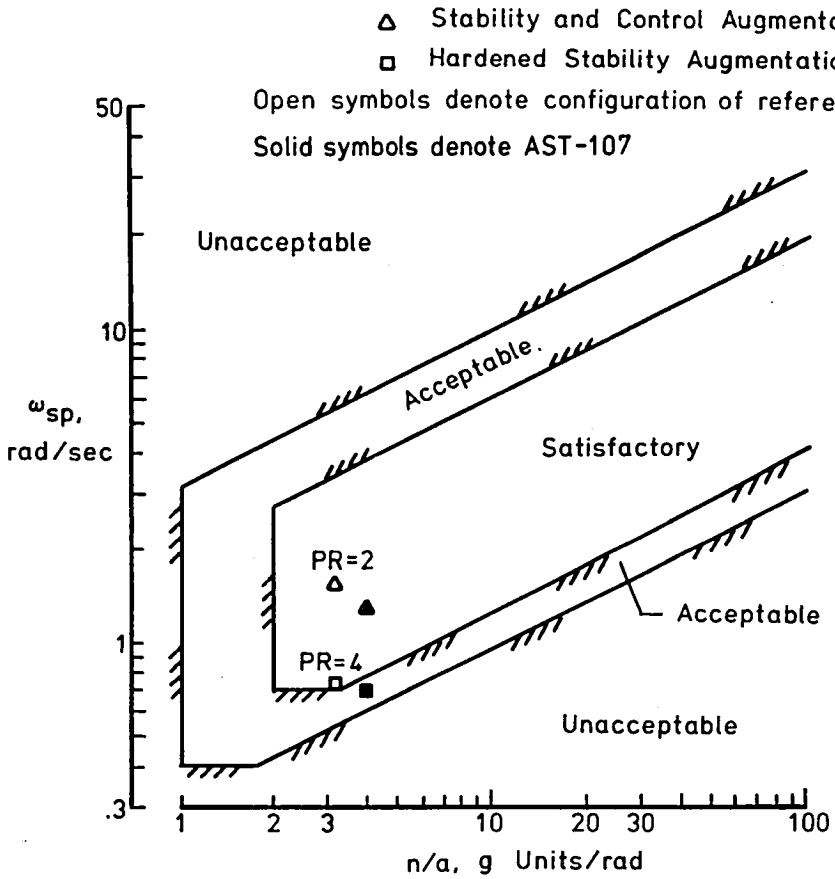

(a) Longitudinal short-period frequency requirements of reference 12

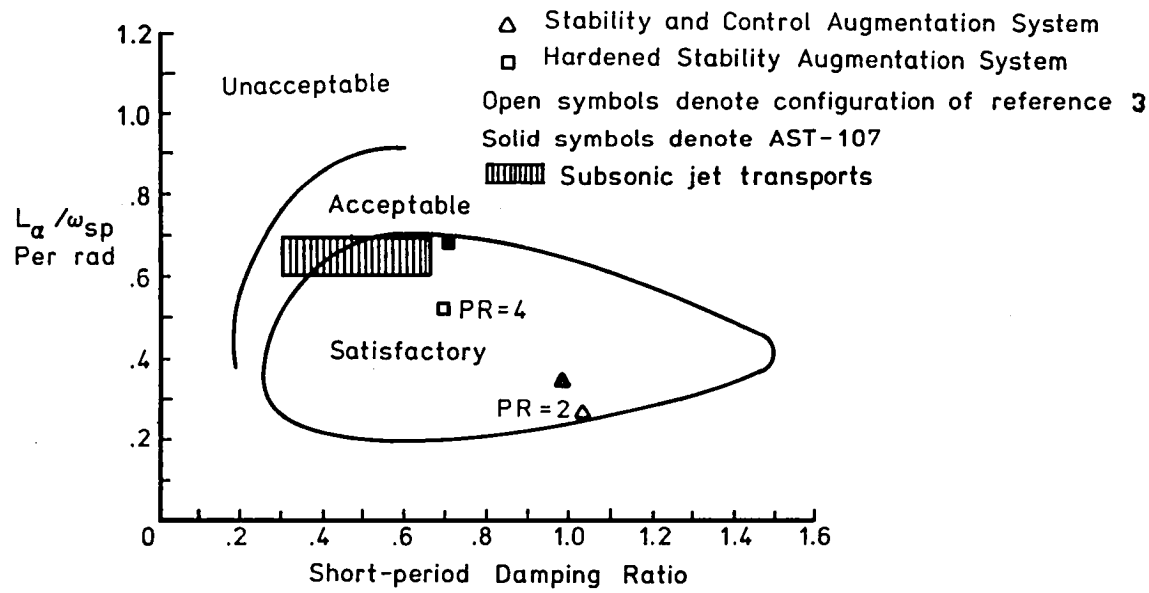

(b) Shomber-Gertsen longitudinal handling qualities criteria of reference 23

Figure 39.- Comparison of longitudinal short-period characteristics with handling qualities criteria.

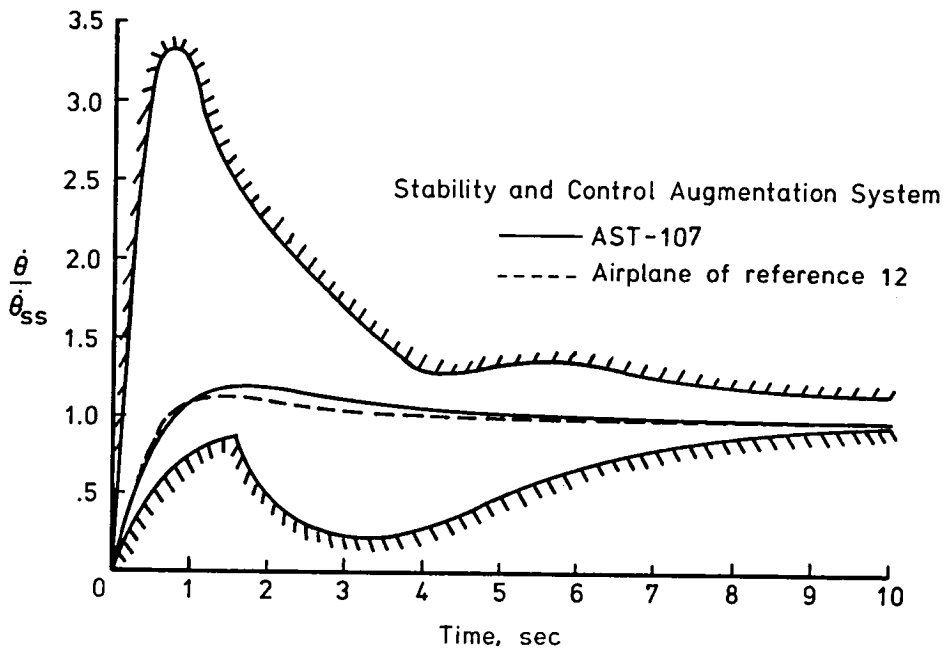

Figure 40.- Comparison of low-speed pitch rate response using the stability and control augmentation system criteria from reference 24.

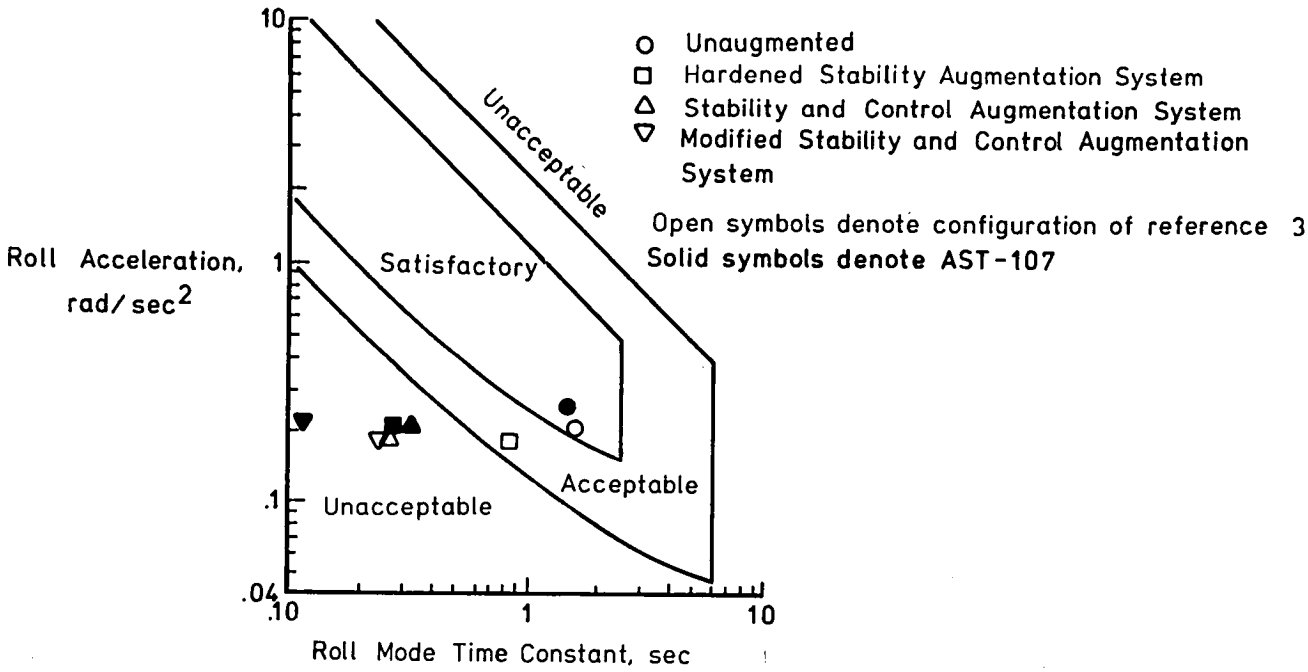

(a) Roll acceleration response boundaries for large aircraft. Boundaries from reference 24

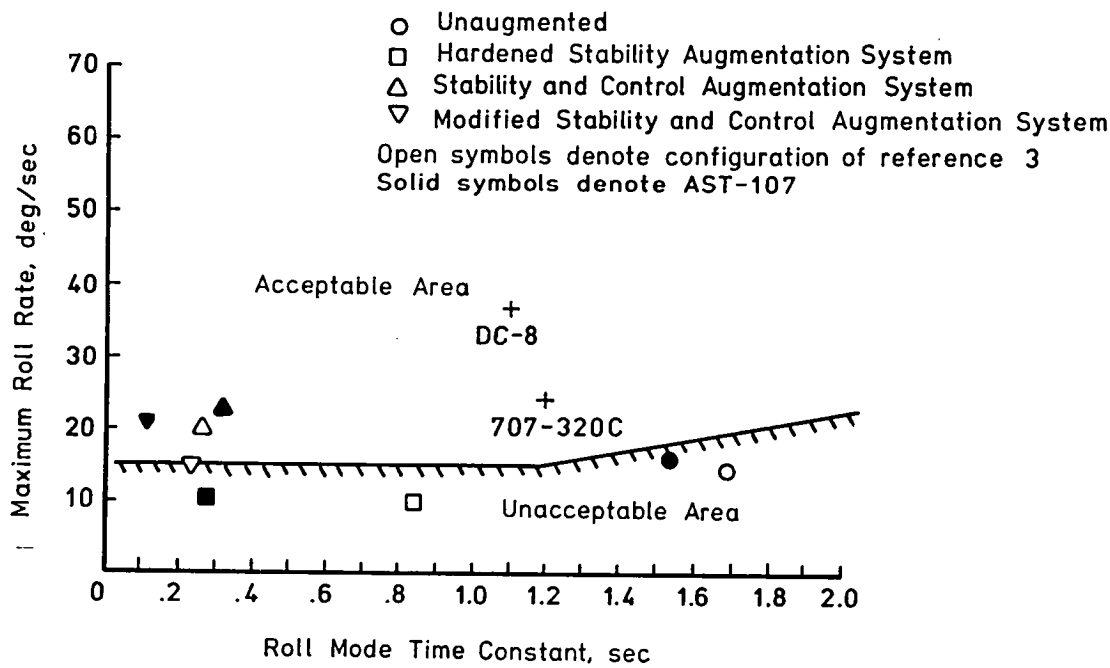

(b) Roll-rate capability criterion for transport aircraft. Boundaries from reference 25

Figure 41.- Comparison of roll response with criteria boundaries.

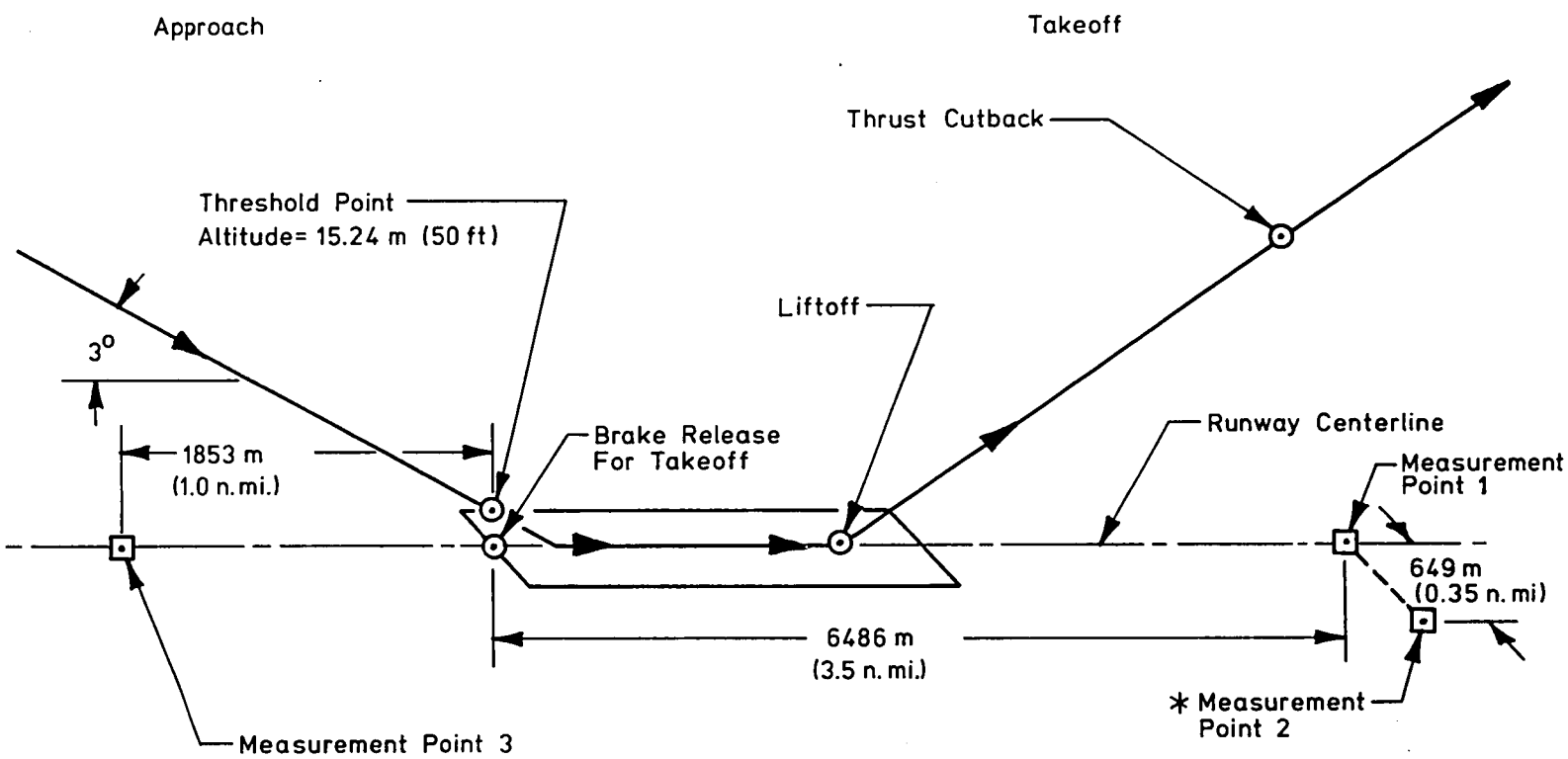

*NOTE: Sideline noise is measured where noise level after liftoff is greatest.

Figure 42.- Noise measurement locations prescribed in reference 26 for approach and takeoff.

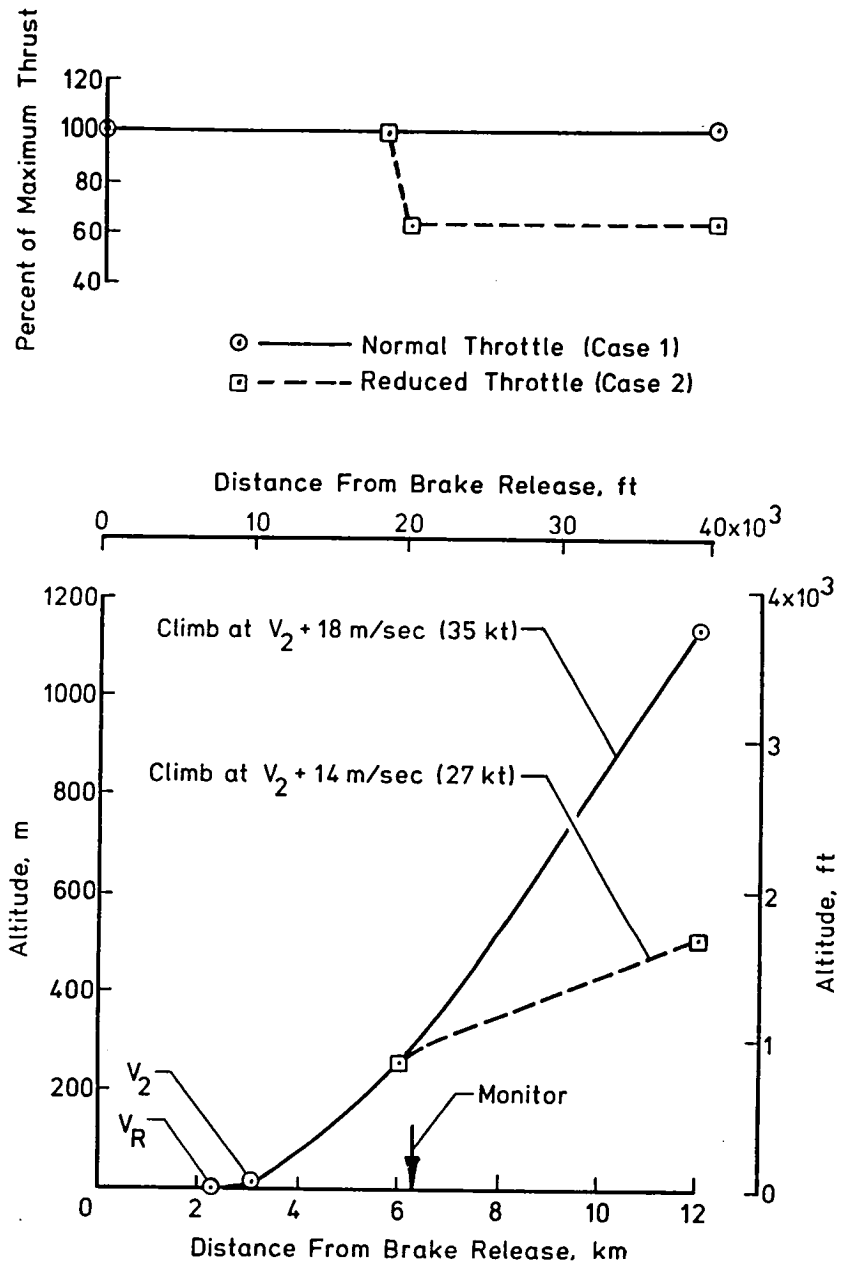

Figure 43.- Comparison of normal throttle and reduced throttle takeoff procedures.

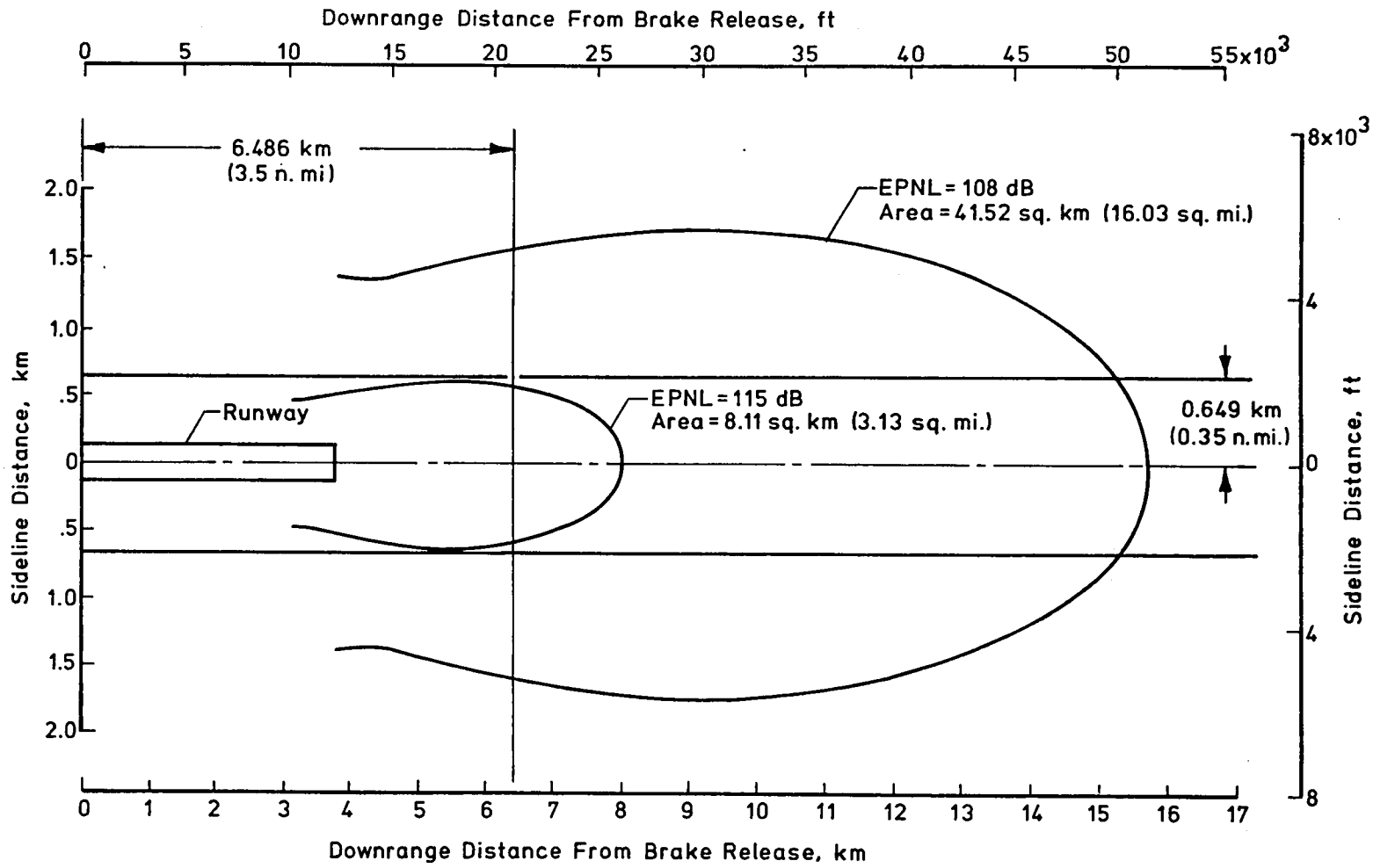

Figure 44.- Noise contours for Case 1 type takeoff (jet noise only).

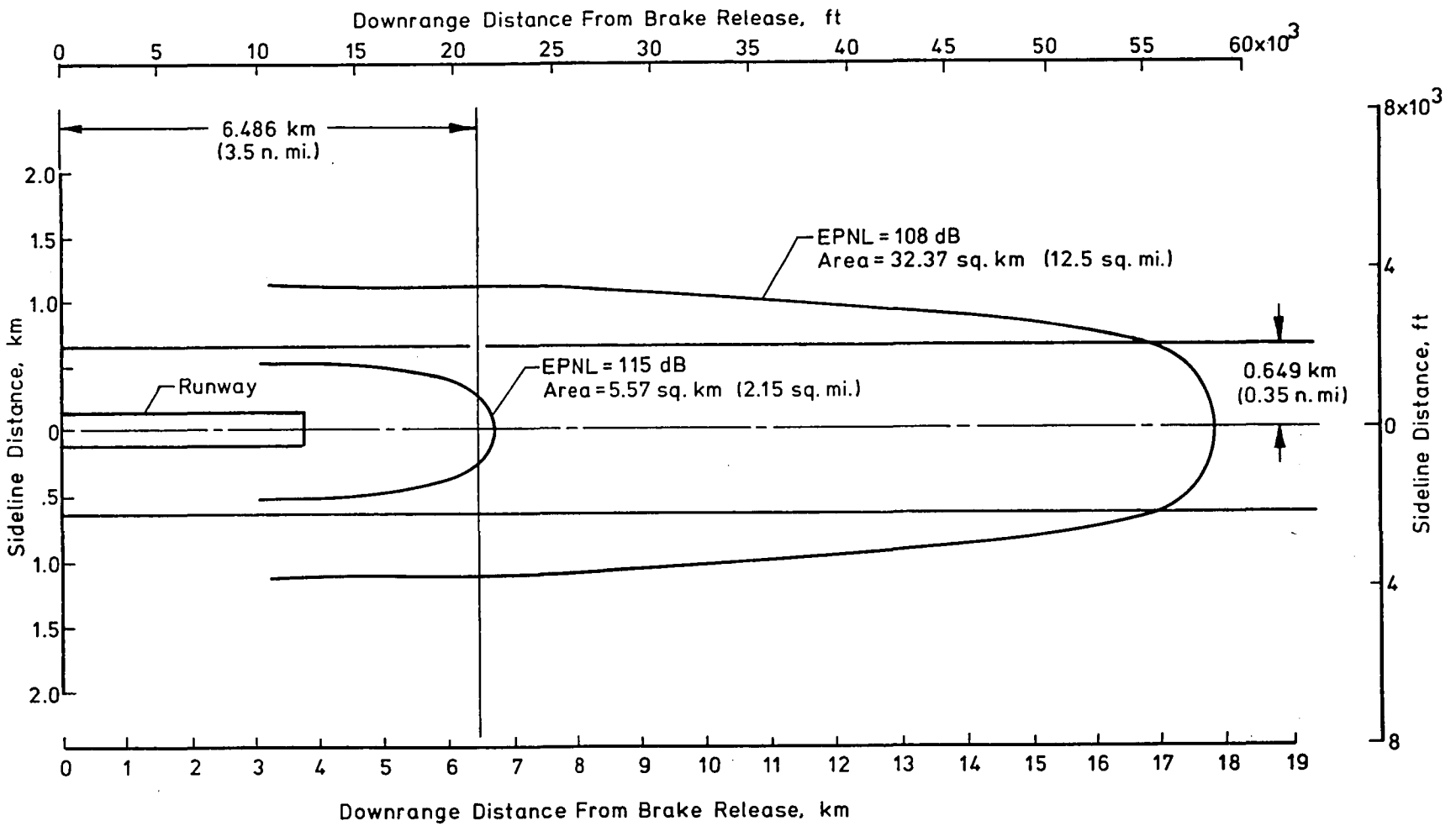

Figure 45.- Noise contours for Case 2 type takeoff (jet noise only).

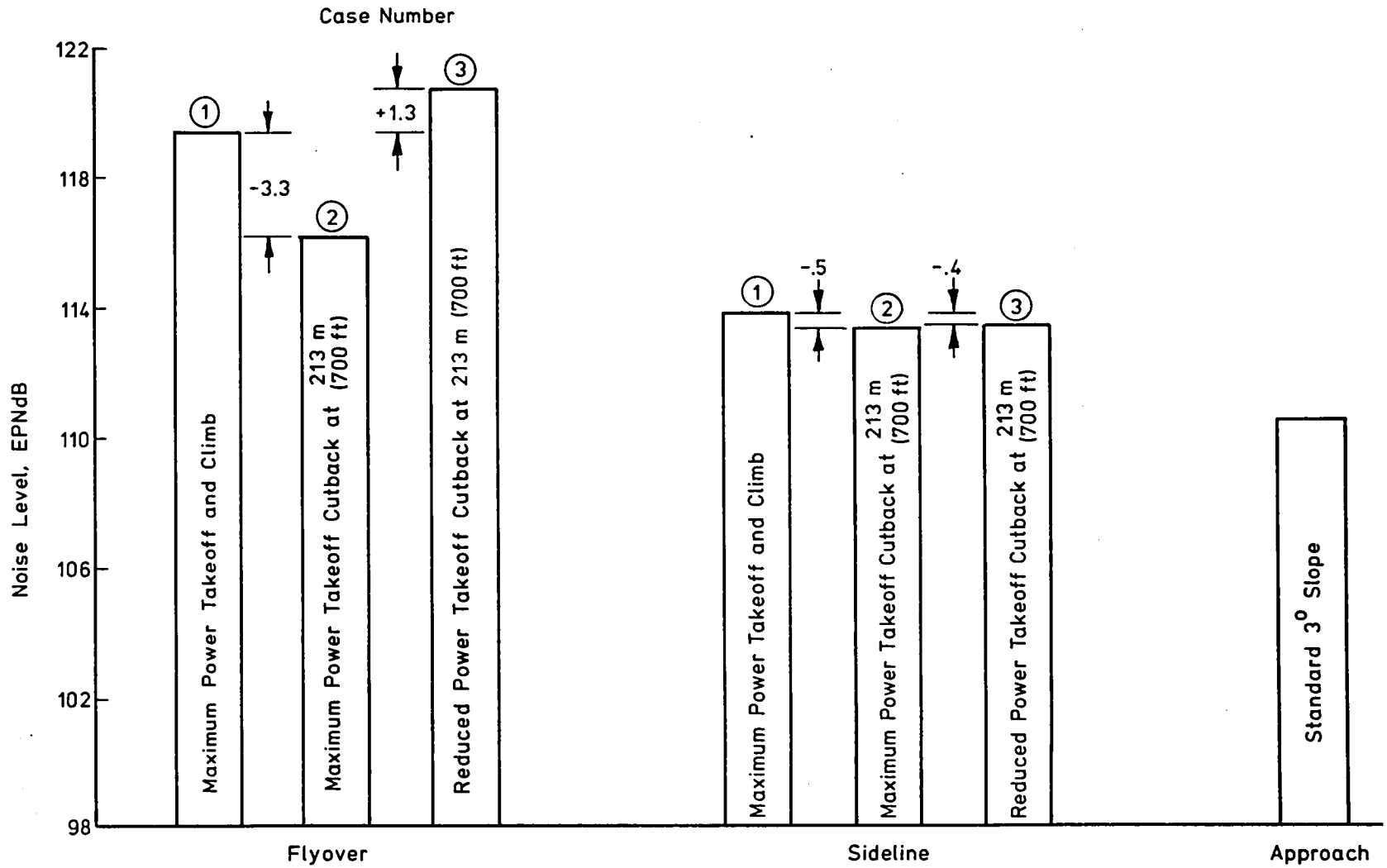

Figure 46.- Comparison of noise results (jet noise only) for the different takeoff procedures.

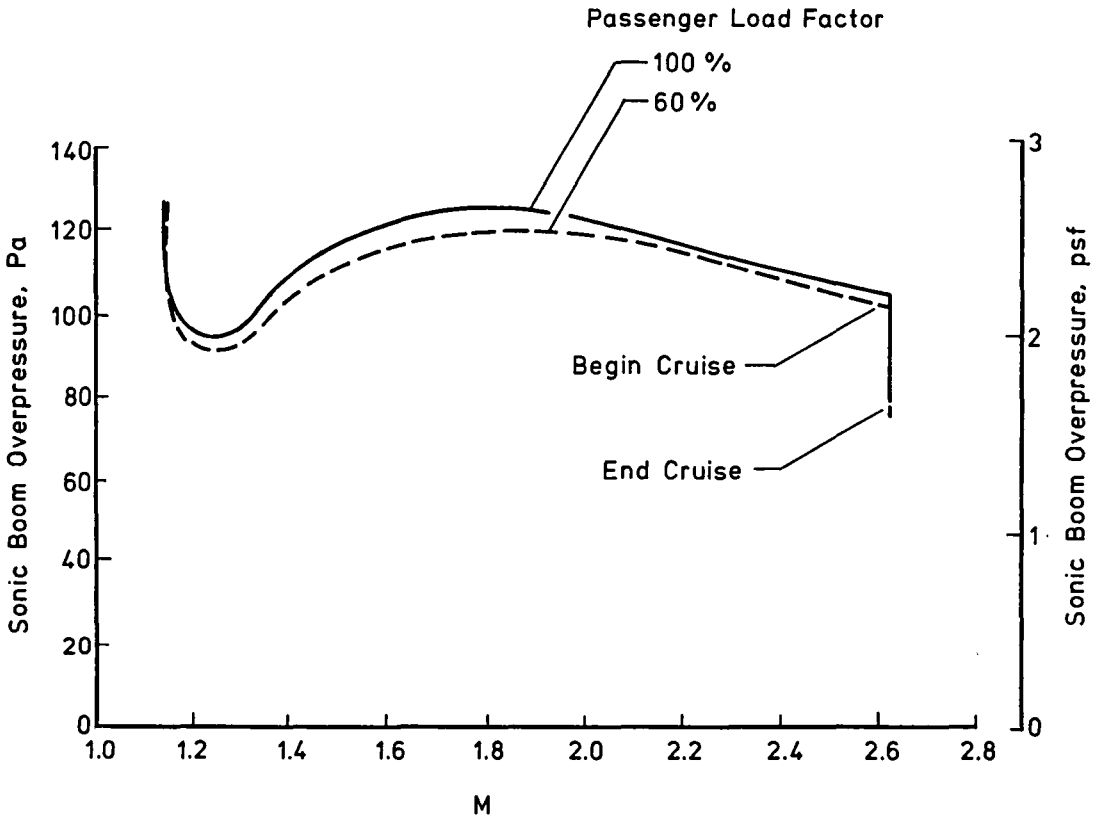

Figure 47.- Maximum over-pressure during climb and cruise.

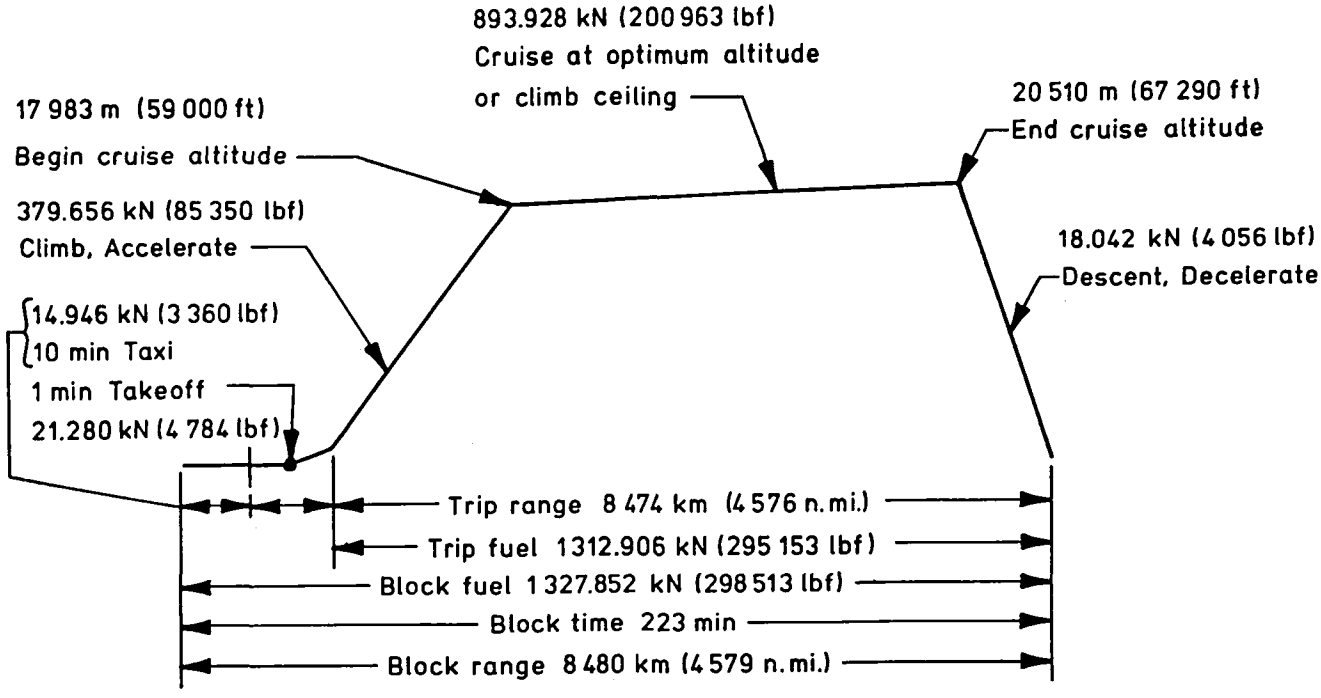

NOTE: Civil Aeronautics Board Range = Trip range minus traffic allowance as specified for supersonic aircraft.

(a) Primary Mission

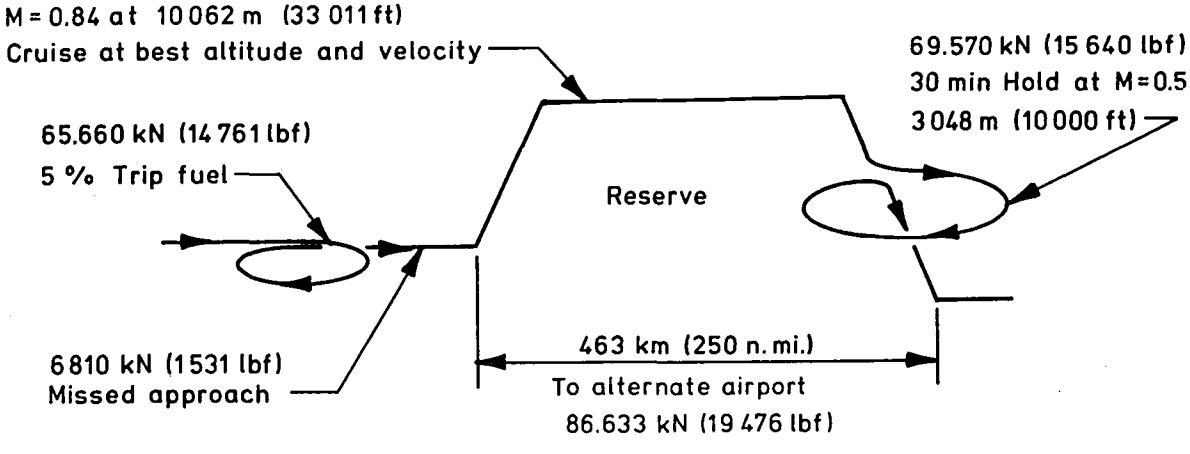

(b) Reserve Allowance Mission

Figure 48.- Mission profile and fuel weights associated with each profile segment to indicate the fuel burned during that segment.

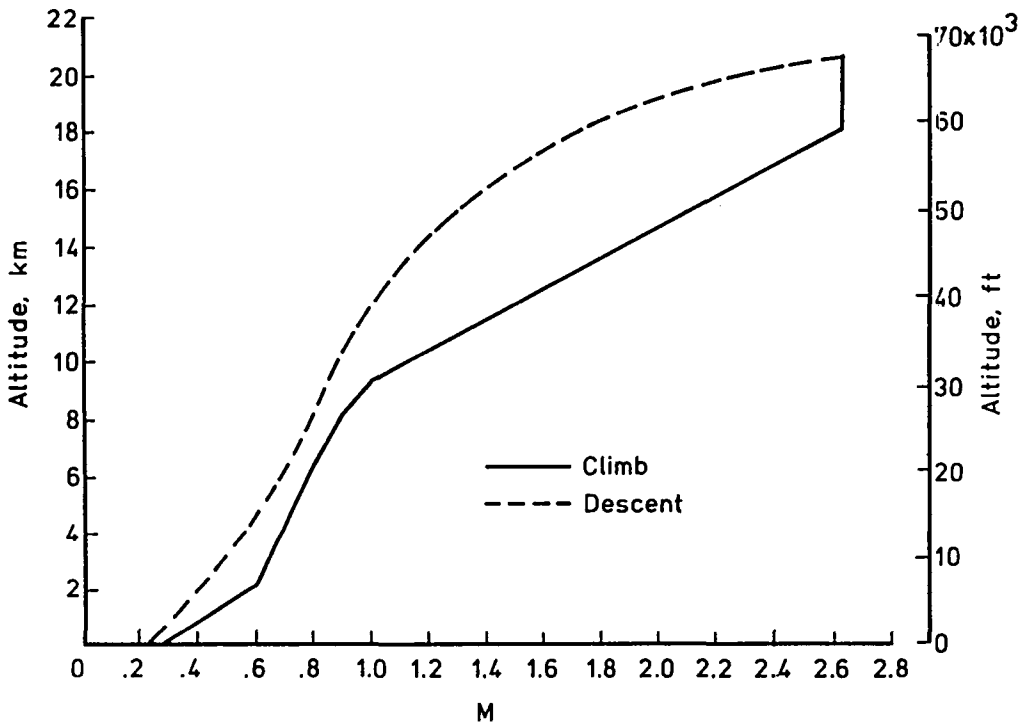

Figure 49.- Climb and descent schedule as a function of Mach number for a standard day plus 8 degree centigrade ambient temperature atmosphere.

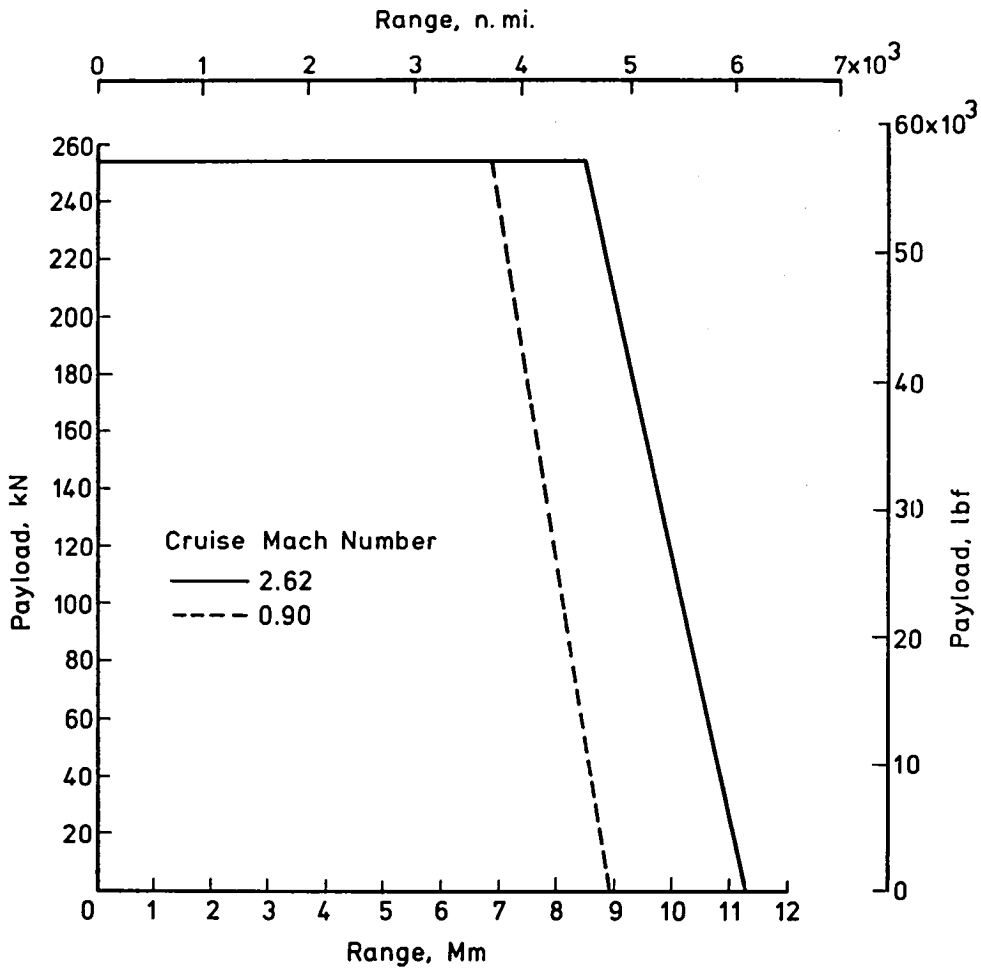

Figure 50.- Payload-range capability variation with cruise Mach number.

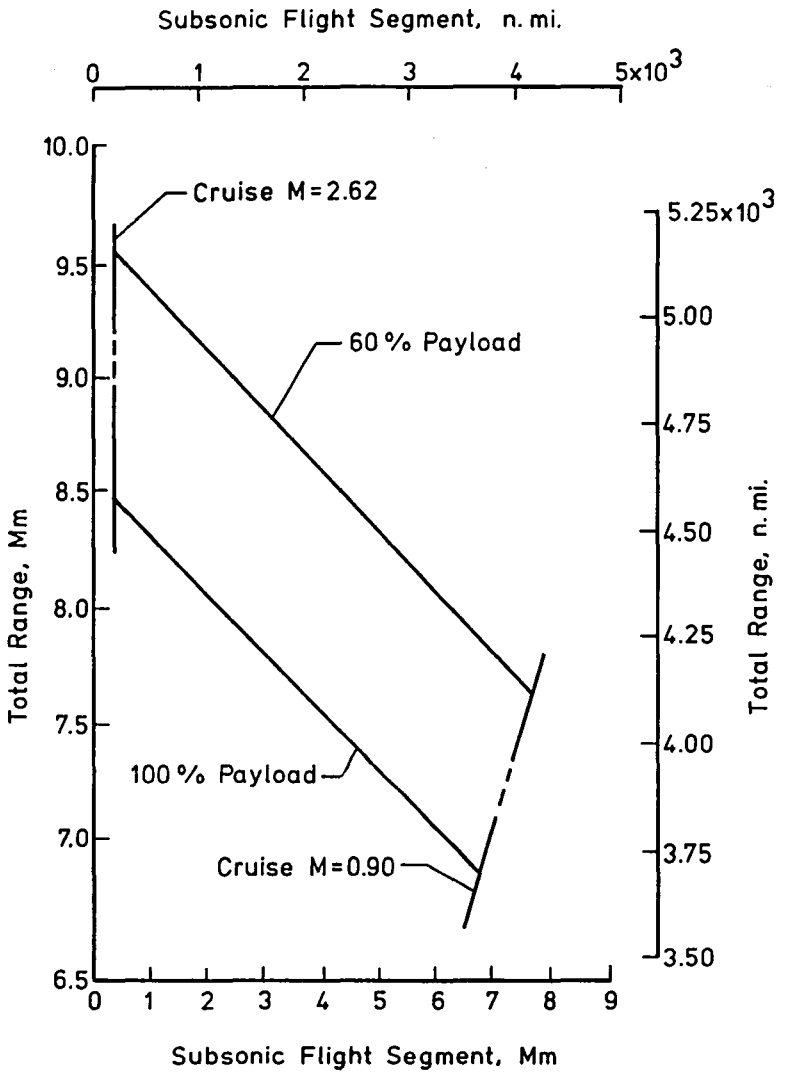

Figure 51.- Total range as a function of subsonic flight segment and passenger load factor.

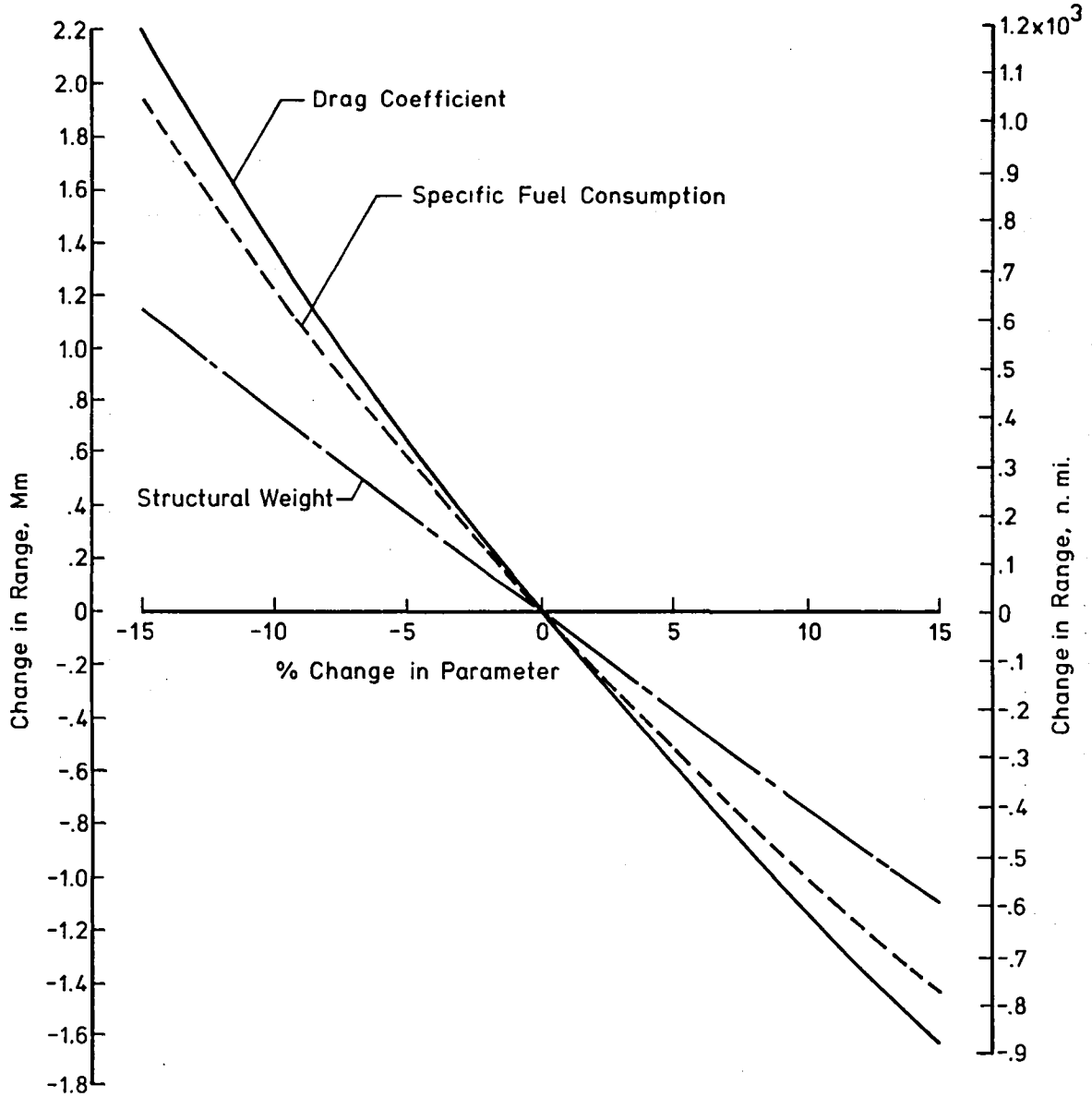

Figure 52.- Range sensitivity to changes in drag, structural weight, and specific fuel consumption.

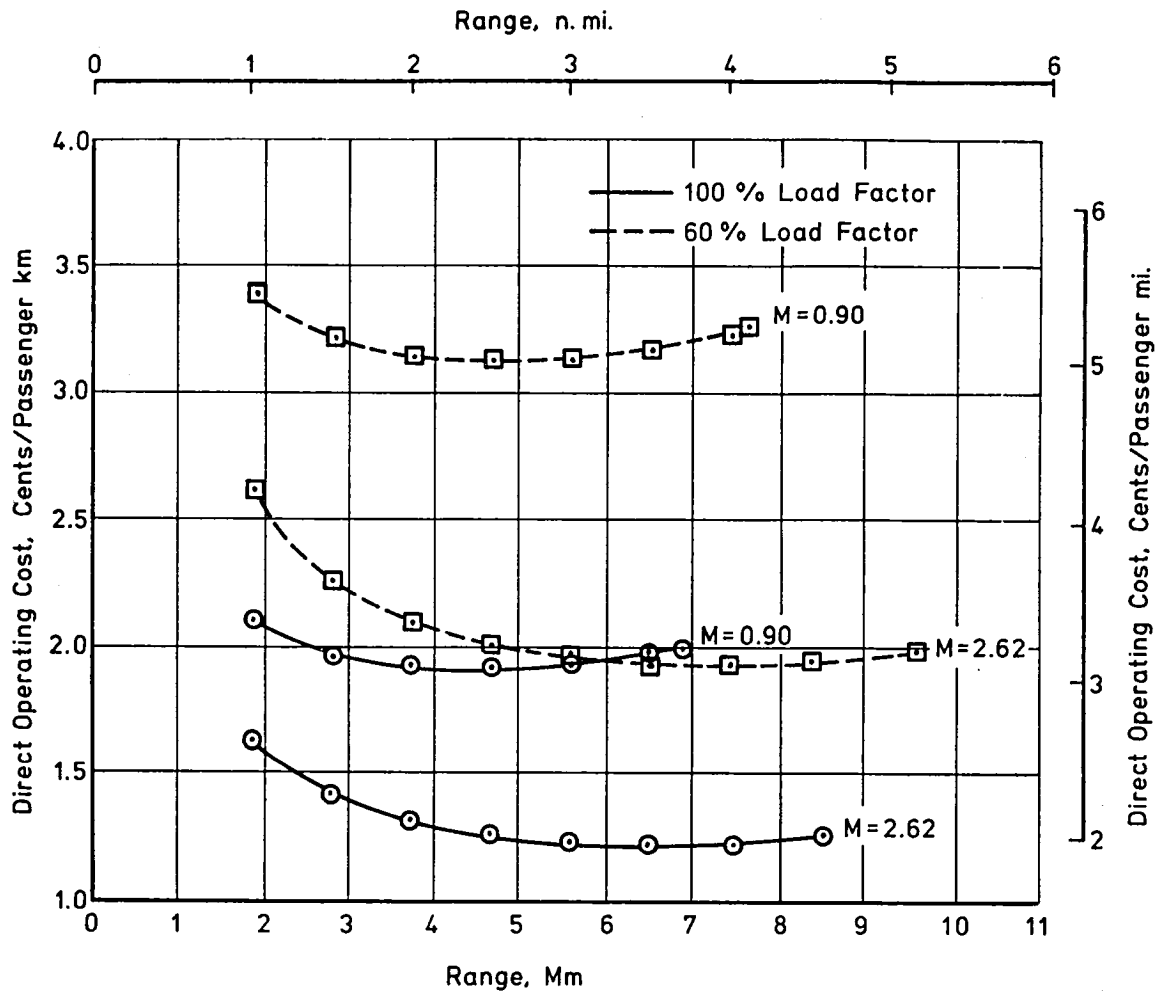

Figure 53.- Effect of passenger load factor and cruise speed on direct operating cost.

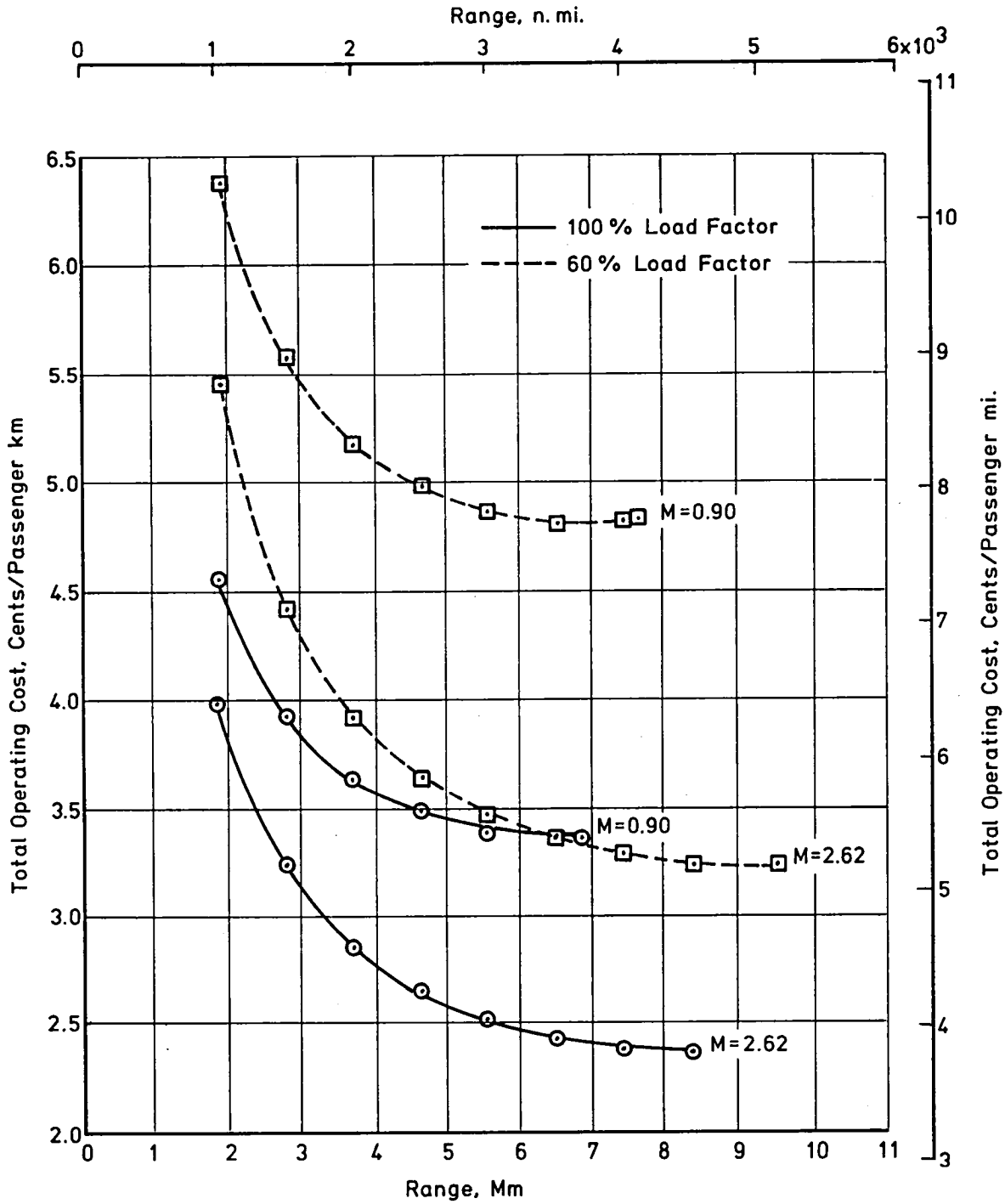

Figure 54.- Effect of passenger load factor and cruise speed on total operating cost.

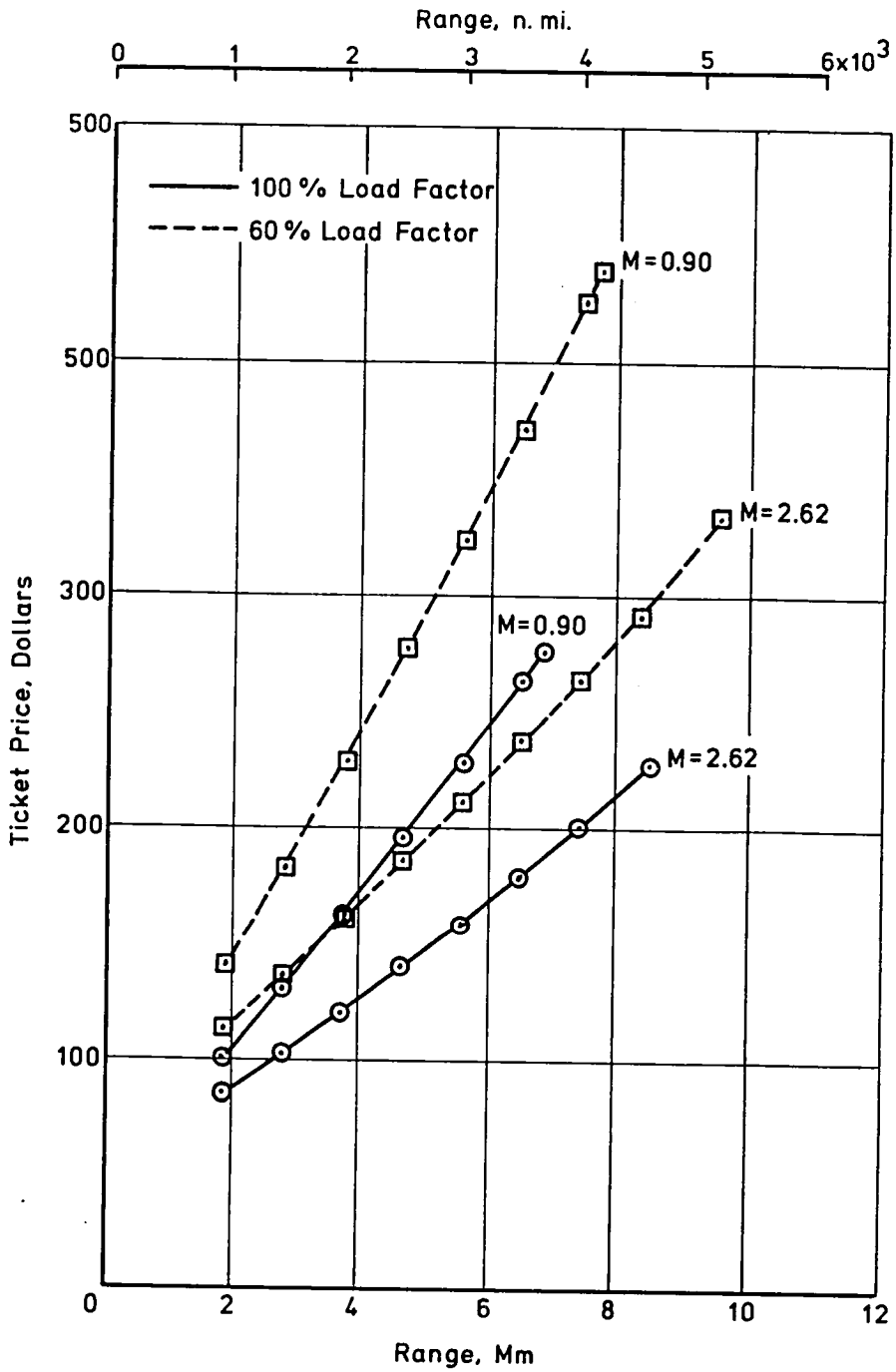

Figure 55.- Effect of passenger load factor and cruise speed on ticket cost.

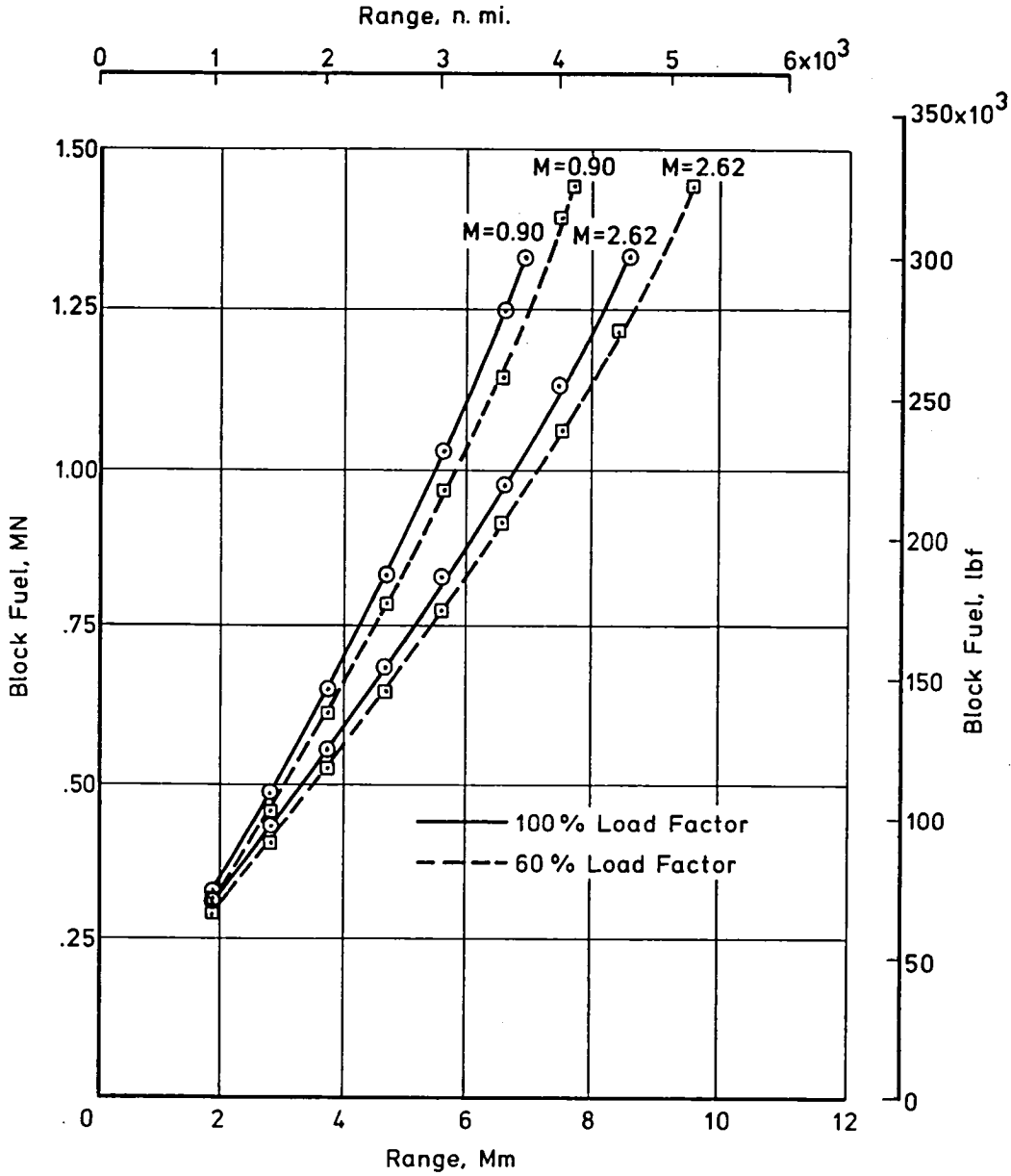

Figure 56.- Effect of passenger load factor and cruise speed on block fuel.

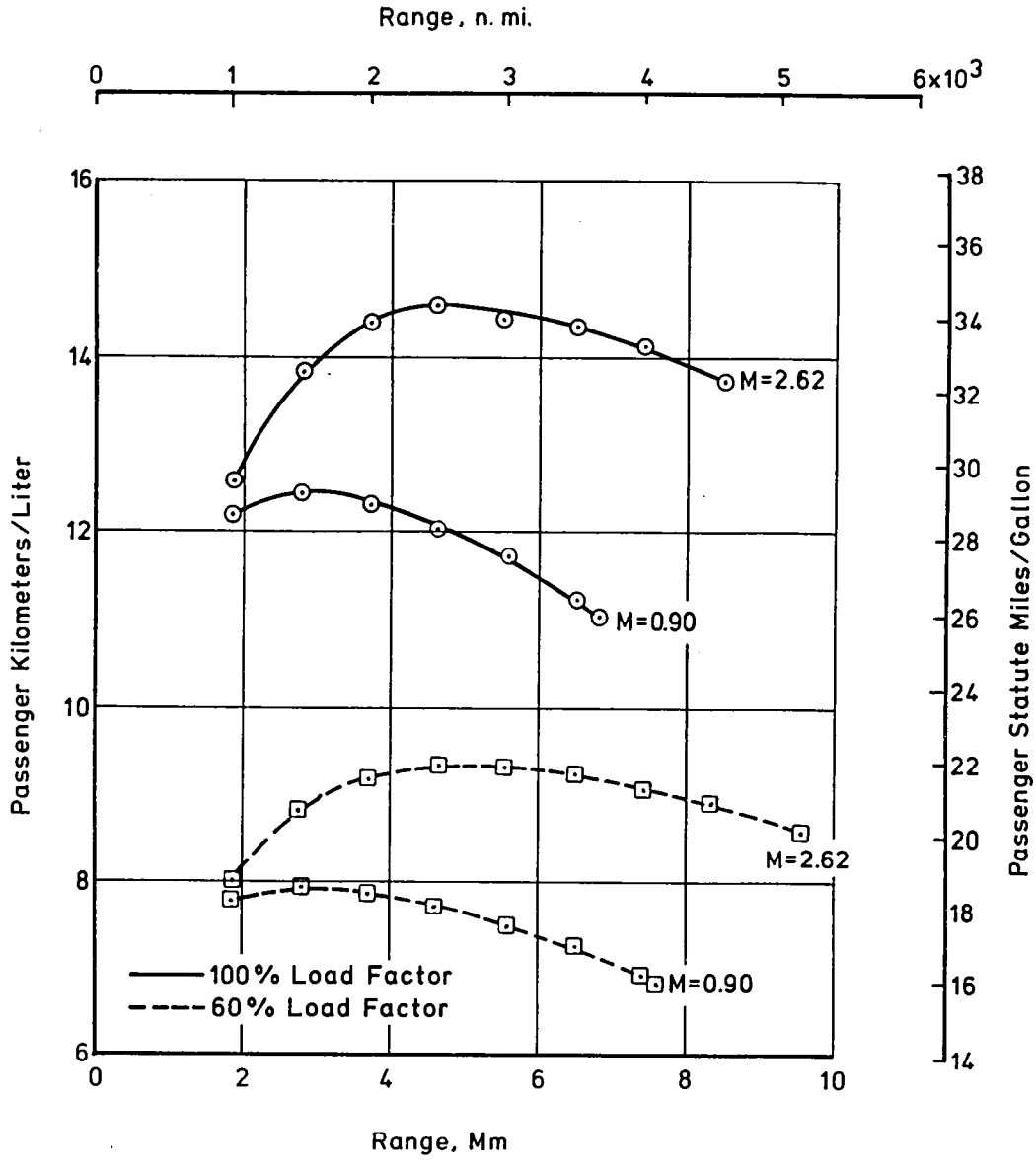

Figure 57.- Effect of passenger load factor and cruise speed on passenger statute-miles per gallon.

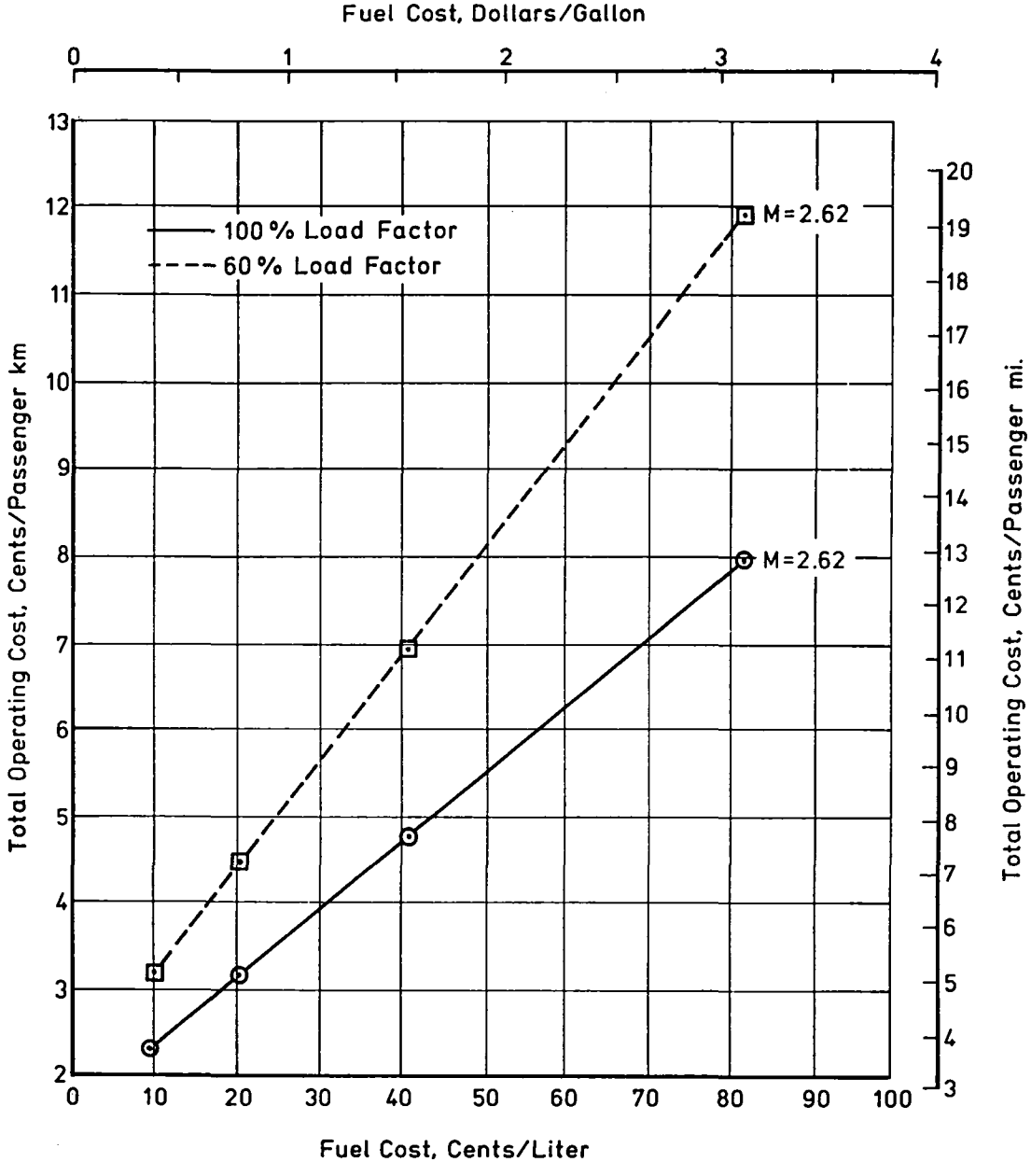

Figure 58.- Sensitivity of total operating cost to variation in fuel cost, 1976 dollars.

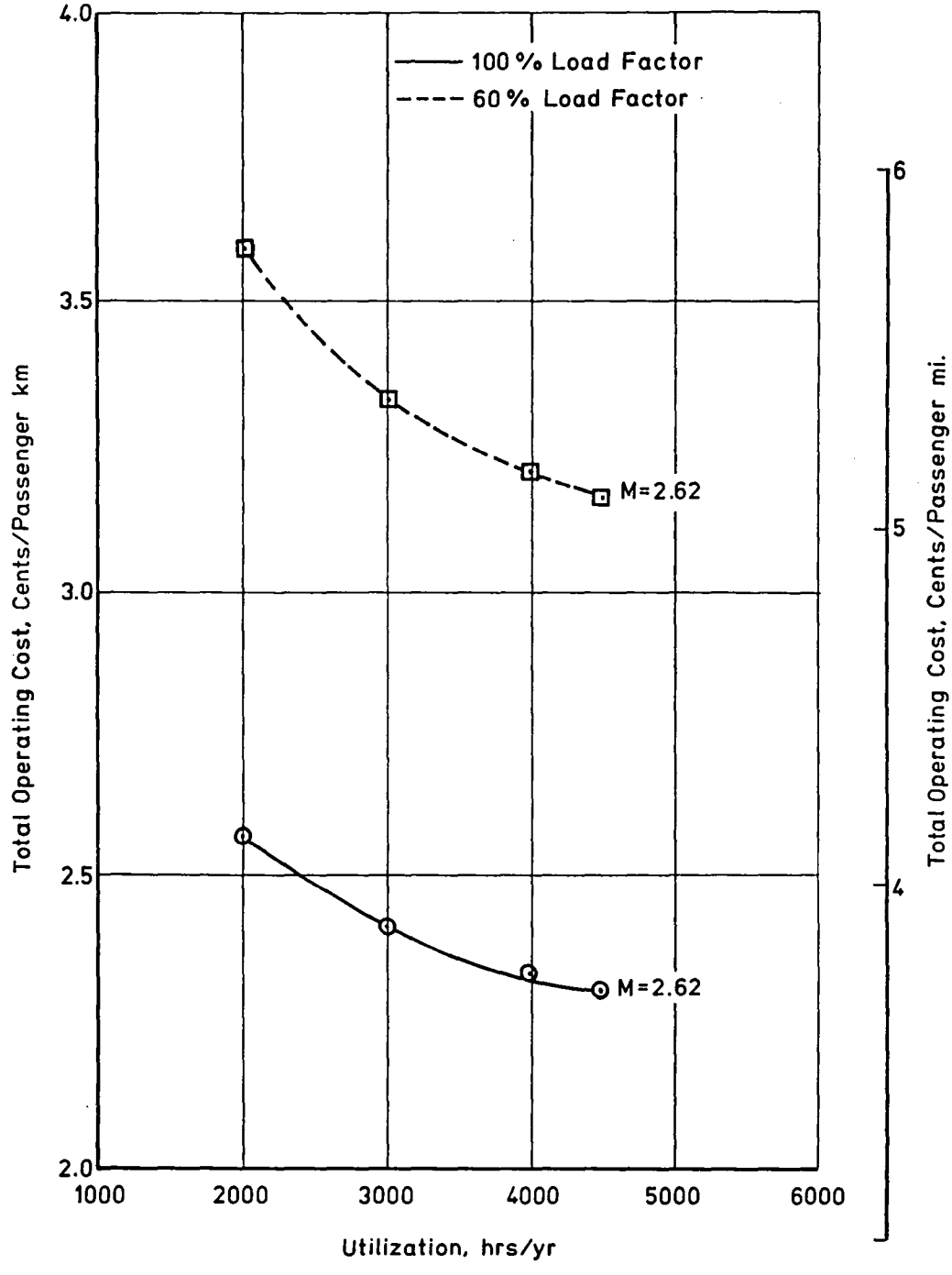

Figure 59.- Sensitivity of total operating cost (TOC) to variation in aircraft utilization per year.

1. Report No.	2. Government Accession No.	3. Recipient's Catalog No.
NASA TM-81872		

4. Title and Subtitle	5. Report Date
CONCEPTUAL STUDY OF AN ADVANCED SUPERSONIC TECHNOLOGY TRANSPORT (AST-107) FOR TRANSPACIFIC RANGE USING LOW-BYPASS-RATIO TURBOFAN ENGINES	September 1980
	6. Performing Organization Code
7. Author(s)	8. Performing Organization Report No.
Shelby J. Morris, Jr.; Willard E. Foss, Jr. and Milton J. Neubauer, Jr.	
9. Performing Organization Name and Address	10. Work Unit No.
NASA Langley Research Center Hampton, Virginia 23665	517-53-43-01
	11. Contract or Grant No.
12. Sponsoring Agency Name and Address	13. Type of Report and Period Covered
National Aeronautics and Space Administration Washington, DC 20546	Technical Memorandum
	14. Sponsoring Agency Code

15. Supplementary Notes

This paper is partially based on unpublished memoranda by R.A. DaCosta, G.J. Espil, W.A. Lovell, J. W. Russell, P.M. Smith, E.E. Swanson and K.B. Walkley of the Hampton Technical Center of Kentron International under contract NAS1-16000.

16. Abstract

A new advanced supersonic technology configuration concept designated the AST-107, using a low bypass-ratio-turbofan engine, is described and analyzed. The aircraft had provisions for 273 passengers arranged five abreast. The cruise Mach number was 2.62. The mission range for the AST-107 was 8.48 Mm (4576 n.mi.) and an average lift-drag ratio of 9.15 during cruise was achieved. The available lateral control was not sufficient for the required 15.4 m/s (30 kt) crosswind landing condition, and a crosswind landing gear or a significant reduction in dihedral effect would be necessary to meet this requirement. The lowest computed noise levels, including a mechanical suppressor noise reduction of 3 EPNdB at the flyover and sideline monitoring stations, were 110.3 EPNdB (sideline noise, 113.1 EPNdB (centerline noise) and 110.5 EPNdB (approach noise).

17. Key Words (Suggested by Author(s))	18. Distribution Statement
Aerodynamics; Aircraft Design, Testing, and Performance; Aircraft Propulsion and Power; Aircraft Stability and Control; Advanced Supersonic Transport; Aircraft Noise; Sonic Boom	Star Category 01 Unclassified - Unlimited

19. Security Classif. (of this report)	20. Security Classif. (of this page)	21. No. of Pages	22. Price*
UNCLASSIFIED	UNCLASSIFIED	94	A05

For sale by the National Technical Information Service, Springfield, Virginia 22161